

Electronic Supplementary Information

**Non-conventional Synthesis and Photophysical Studies of Platinum(II)
Complexes with Methylene Bridged 2,2'-Dipyridylamine Derivatives**

Evgeny Bulatov and Matti Haukka*

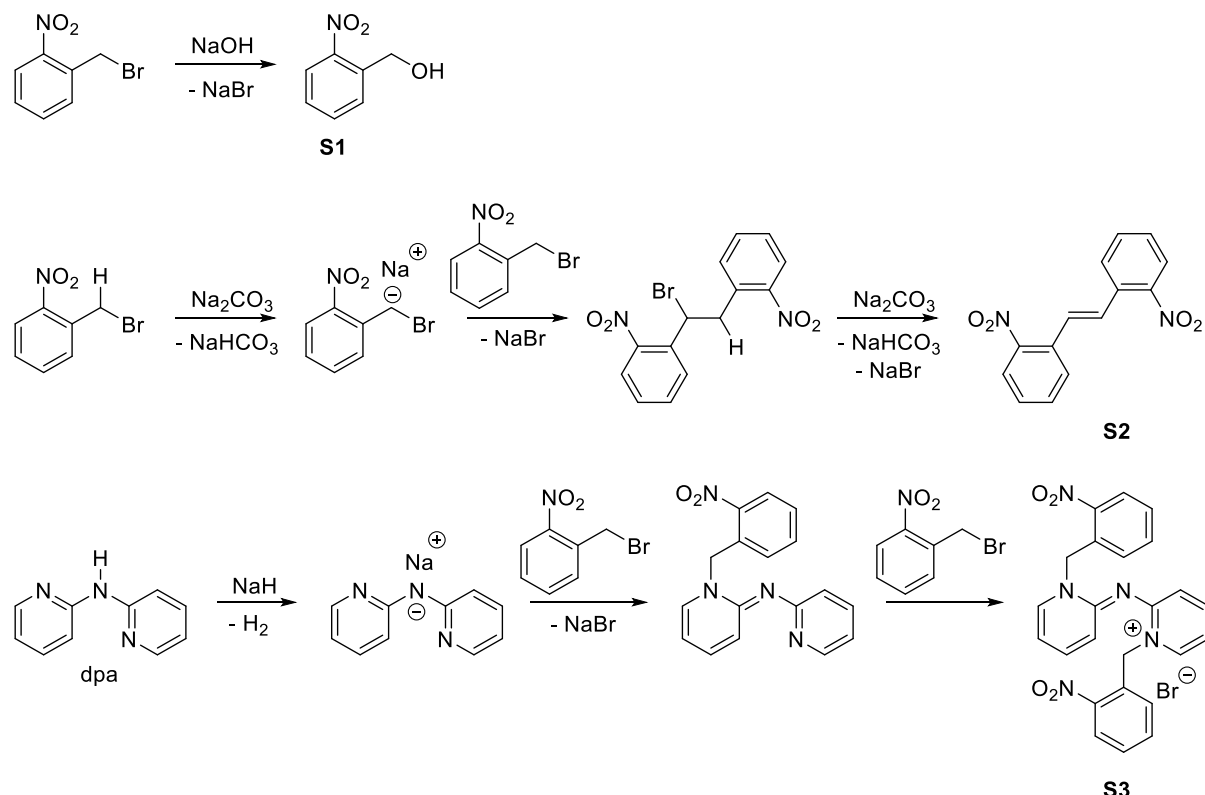
Department of Chemistry, University of Jyväskylä, P.O. Box 35, FI-40014 Jyväskylä, Finland.
E-mail: matti.o.haukka@jyu.fi

Table of contents

S1. Side reactions in synthesis of 2-nitrobenzyldi(2-pyridyl)amine (3)	2
S2. Side product dibromo(2-cyanobenzyldi(2-pyridyl)amine)platinum(II) (S4).....	4
S3. Absorption, luminescence, and photocyclization of ligands 1-3 in solution	5
S4. Phosphorescence of complexes [7-10]·Br₂ at low temperatures	7
S5. ¹ H NMR spectra of 1-10 and S3-S4	38
S6. Crystallographic data for 1-10 and S2-S4	62
S7. Cited literature.....	65

S1. Side reactions in synthesis of 2-nitrobenzyldi(2-pyridyl)amine (3)

Various side products obtained and identified in attempts of synthesis of 2-nitrobenzyldi(2-pyridyl)amine **3** and corresponding side reactions are summarized in Scheme S1.



Scheme S1 Side reactions in synthesis of 2-nitrobenzyldi(2-pyridyl)amine **3**.

All attempts of reacting dpa with 2-nitrobenzyl bromide in presence of NaOH in DMF (similarly to synthesis of **1** and **2** according to published procedure¹) resulted in unreacted dpa and *o*-nitrobenzyl alcohol **S1** (¹H NMR spectrum matched the published one²). This indicates, that the bromide is reactive towards hydroxide ions, presumably *via* S_N2 mechanism, since hydrolysis is accelerated by electron withdrawing group (no major hydrolysis under same conditions was observed in case of unsubstituted and 2-iodo substituted benzyl bromides).

Hydrolysis of the bromide was prevented by using dry DMF and less nucleophilic base (Na₂CO₃); however, unreacted dpa was again recovered. This time, *trans*-2,2'-dinitrostilbene **S2** was crystallized as minor product from the reaction mixture (crystal structure is presented in Fig. S1, ¹H NMR spectrum matched the published one³). Its formation is known³ and ascribed to deprotonation of the methylene group followed by its nucleophilic attack on another 2-nitrobenzyl bromide molecule. These observations allow to conclude, that the electron withdrawing property of the nitro group hinders formation of the target 2-nitrobenzyldi(2-pyridyl)amine by accelerating hydrolysis and deprotonation of the electrophile.

In order to avoid the aforementioned side reactions, different synthetic route was employed, involving complete deprotonation of dpa with NaH prior to addition of the electrophile.⁴ In this way, the target product **3** was obtained in low yield (9%) along with a significant amount of side product **S3**, in which

the pyridine nitrogen atoms of dpa have been subjected to benzylation (crystal structure is presented in Fig. S1).

Side product **S3** was obtained as white precipitate upon adding chloroform to the evaporated reaction mixture. ^1H NMR (methanol-d4, 300 MHz): δ 8.15-8.10 (m, 2H), 8.08-7.95 (m, 4H), 7.52-7.40 (m, 6H), 7.05-6.99 (m, 2H), 6.71-6.66 (m, 2H), 5.63 (s, 4H, CH_2).

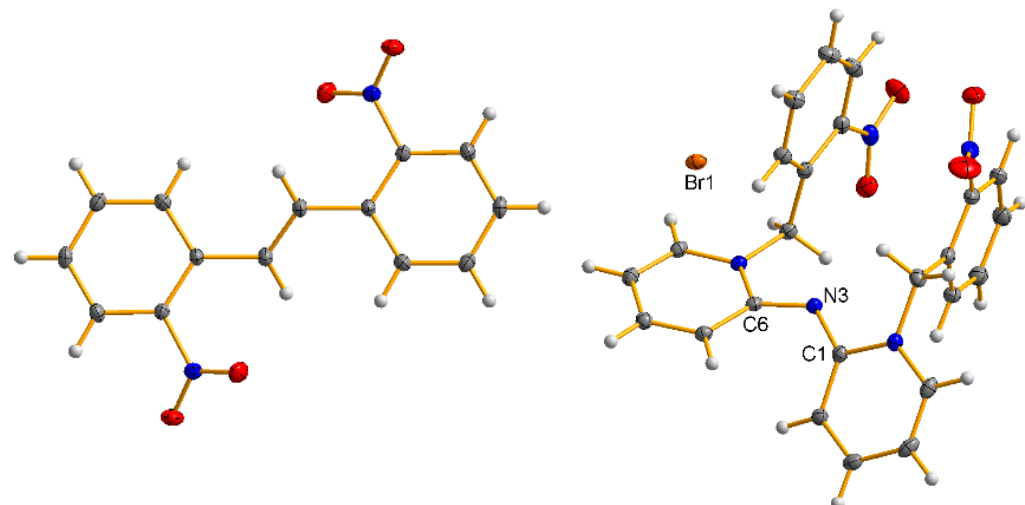


Fig. S1 Crystal structures of **S2** (left) and **S3** (right).

S2. Side product dibromo(2-cyanobenzylid(2-pyridyl)amine)platinum(II) (S4)

Dibromo(2-cyanobenzylid(2-pyridyl)amine)platinum(II) **S4** was obtained as a minor side product from synthesis of **[10]·Br₂** as undissolved yellow precipitate after dissolving the worked-up residue from the evaporated reaction mixture (see experimental part of the main article for details). We presume that this product could be formed from reaction between the 2-cyanobenzyl bromide and [Pt(dpa)I₂] or [Pt(dpa-H)I₂]⁻ complexes, which could be contained as impurities in the [Pt(dpa-H)₂] material. Observation of this product demonstrates that the proposed synthetic approach can also be utilized for complexes containing one methylene bridged dpa ligand along with other ligands.

Yield: 8 mg. Elemental analysis (%): C, 36.9; H, 0.3; N, 9.9. Calcd for C₁₈H₁₄N₄Br₂Pt: C, 33.7; H, 2.2; N, 8.7. ¹H NMR (THF-*d*8, 300 MHz): δ 9.31-9.14 (m, 2H, broad sidebands due to *J*_{Pt,H} = 45.0 Hz), 8.57 (d, 1H, *J* = 6.0 Hz), 7.99-7.91 (m, 2H), 7.73-7.65 (m, 2H), 7.46-7.35 (m, 3H), 7.18-7.12 (m, 2H), 5.66 (s, 2H, CH₂). ESI MS (m/z): 560.00 (calcd for [M-Br]⁺ 560.00), 601.03 (calcd for [M-Br⁺ACN]⁺ 601.03). Crystals suitable for X-ray diffraction analysis were obtained by slow evaporation of solution in THF. The obtained structure is presented in Fig. S2.

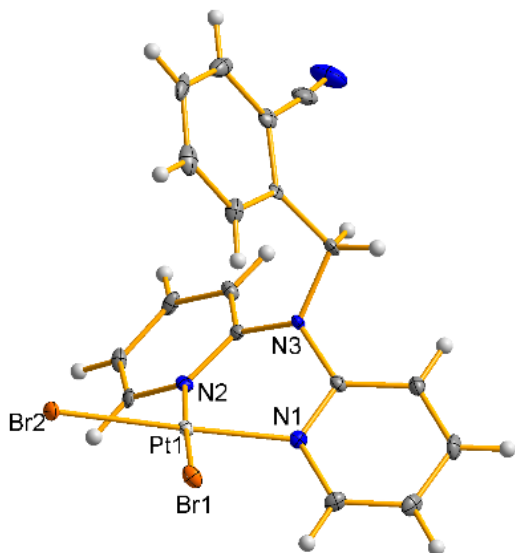


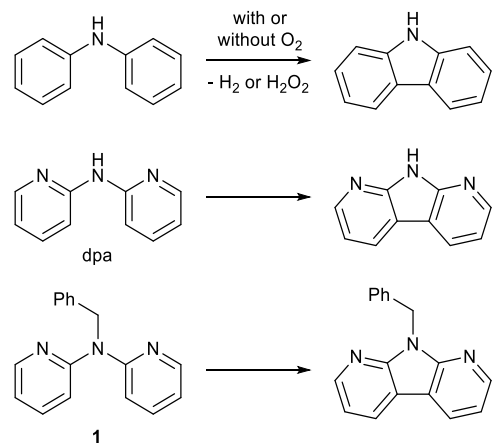
Fig. S2 Crystal structure of **S4**.

S3. Absorption, luminescence, and photocyclization of ligands 1-3 in solution

Table S1 Absorption properties of ligands **1-3** in methanol solution ($C = 50 \mu\text{M}$) at RT

Ligand	λ_{abs} , nm	$\epsilon \cdot 10^{-3}, \text{l} \cdot \text{mol}^{-1} \cdot \text{cm}^{-1}$
1	306	15.8
	278 (shoulder)	11.2
2	304	15.1
	277	11.8
3	302	16.3
	274	15.1

Conversion of diphenylamines into carbazoles under excitation with UV light has been known for more than 55 years.⁵ Analogous photocyclization of dpa into 1,8-diazacarbazole has been discovered in 1968⁶ and shortly after this reaction has been applied to benzylid(2-pyridyl)amine **1** (Scheme S2).⁷ Therefore the photocyclization reaction is well-established and yet often overlooked in more recent publications on photophysical properties of dpa derivatives.



Scheme S2 Photocyclization reactions of diphenylamine, dpa, and benzylid(2-pyridyl)amine **1**.

In this work, in course of optical measurements of THF and methanol solutions of **1**, continuously changing absorption and emission spectra were observed (Fig. S3). While the absorption spectrum remained without significant changes for relatively long (few minutes) irradiation times, changes in emission were fast enough, so that a reliable emission spectrum with defined λ_{em} value could not be obtained. Changes in the optical spectra were also accompanied by changes in ^1H NMR spectrum (Fig. S4). The obtained spectra indicate, that the photocyclization reaction under irradiation in spectrophotometer is rather slow, but luminescence of the product is much stronger compared to **1**, preventing reliable measurement of emission spectrum of the latter. Trial measurement of the emission of **1** in methanol/ethanol mixture (1:4, v/v) at 77 K revealed both fluorescence and phosphorescence emissions (Fig. S5), but since the appearance of the spectra was changing continuously during the measurement, no numerical data was extracted. Similar changes in emission (measured only at room temperature) upon irradiation with UV light were also observed for the substituted derivatives **2** and **3**.

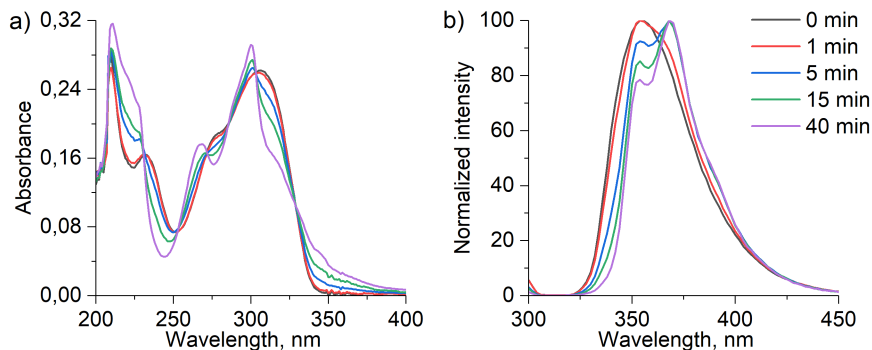


Fig. S3 Changes in absorption (a) and normalized emission (b) spectra of **1** in THF ($C = 20 \mu\text{M}$) under 254 nm lamp irradiation for variable time (the legend applies to both sets of spectra).

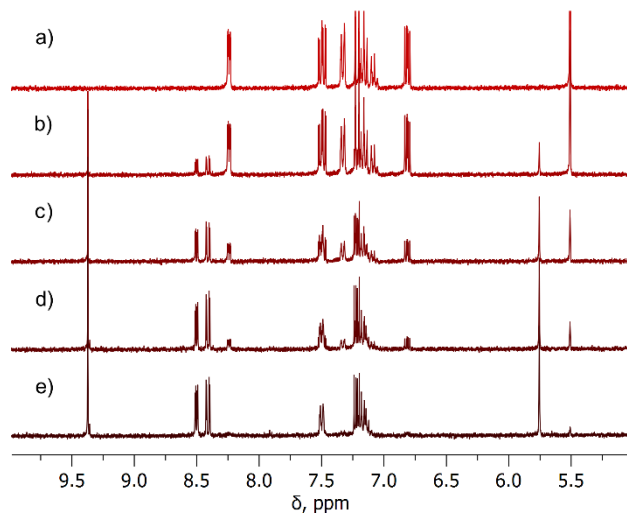


Fig. S4 ^1H NMR (300 MHz, $\text{THF}-d_8$) spectrum of 1mM solution of **1**: fresh (a), after 2 days on ambient light (b), and after 40 min (c), 80 min (d), and 3 h (e) irradiation by UV lamp (254 nm).

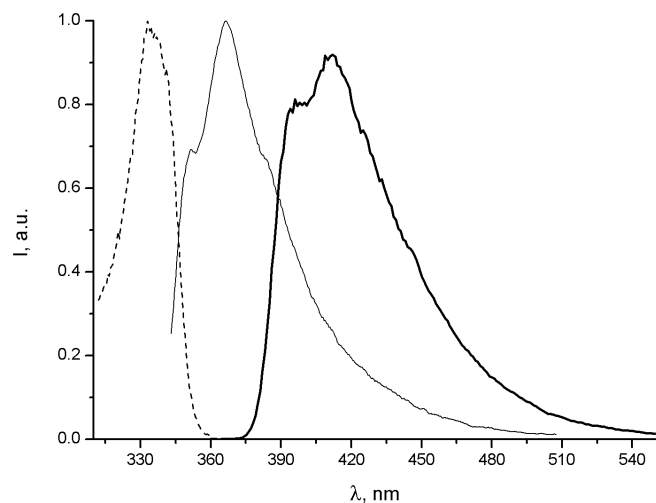


Fig. S5 Normalized excitation (dashed line) and emission (solid line – fluorescence, bold line – phosphorescence) spectra of **1** in methanol/ethanol mixture (1:4, v/v) at 77 K. Note: the spectra were changing in shape and intensity during the measurements.

S4. Phosphorescence of complexes [7-10]·Br₂ at low temperatures

Excitation spectra of [7,8,10]·Br₂ in methanol/ethanol glass at 77 K, presented in Fig. S6, were obtained using Varian Cary Eclipse Fluorescence spectrophotometer equipped with Oxford Optistat cryostat using cryogenic 1 cm quartz luminescence cuvette (FireflySci). Due to the fact that the shortest available delay time on this instrument is 100 μ s, the weak and fast decaying emission of [9]·Br₂ could not be detected.

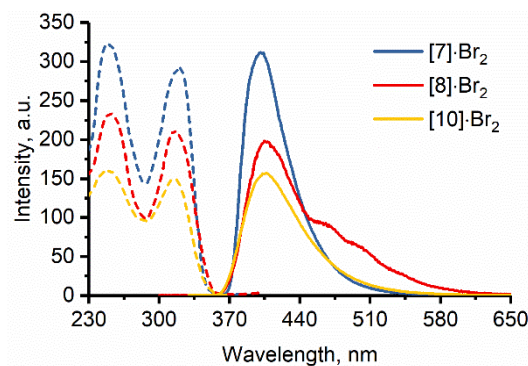


Fig. S6 Phosphorescence excitation ($\lambda_{\text{em}} = 405$ nm) and emission ($\lambda_{\text{ex}} = 320$ nm) spectra of [7,8,10]·Br₂ in methanol/ethanol glass (77 K, C = 20 μ M, delay time 0.1 ms, gate time 5 ms).

Time resolved phosphorescence emission spectra of [7-10]·Br₂ were obtained using pulsed excitation and gated detection technique, as described in the experimental section of the main article. The obtained raw spectra were processed using OriginPro software. Compounds [8,10]·Br₂ in methanol/ethanol glass at 80 K both displayed broad emission bands with multiple peaks, but their time dependences appeared substantially different, as demonstrated in Figs. S7 and S8.

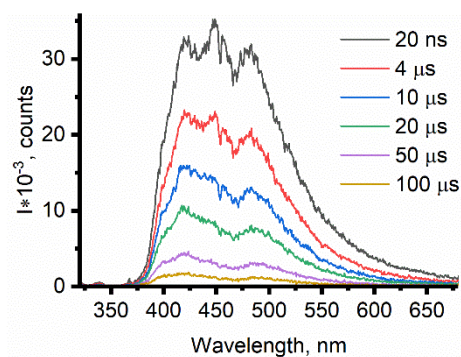


Fig. S7 Phosphorescence emission spectra of [10]·Br₂ in methanol/ethanol glass at variable delay times (80 K, C = 20 μ M, $\lambda_{\text{ex}} = 320$ nm, gate time 10 μ s). Only six spectra at selected delay times are presented for clarity; the full set of measured spectra are presented in Fig. S21.

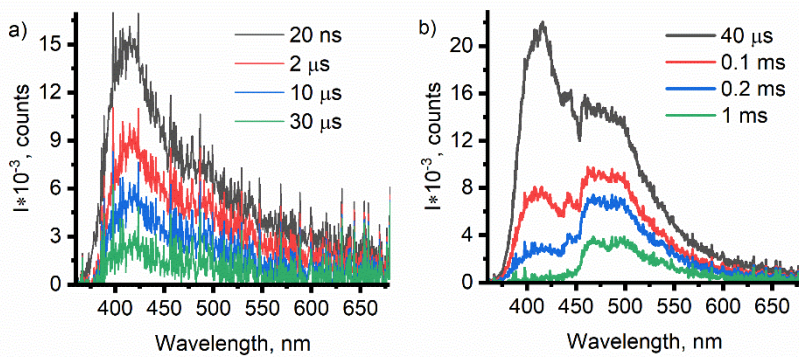


Fig. S8 Phosphorescence emission spectra of **[8]·Br₂** in methanol/ethanol glass at variable delay times (80 K, C = 20 µM, λ_{ex} = 320 nm, gate times: 1 µs (a), 100 µs (b)). Only four spectra at selected delay times are presented in each case for clarity; the full sets of measured spectra are presented in Figs. S11 and S13.

The phosphorescence lifetimes were determined from the series of emission spectra at variable delay and constant gate times. Emission decay curves were obtained from the spectra by averaging values of emission intensity in the range of $\lambda_{\text{max}} \pm 5$ nm. The emission lifetimes were determined as slopes of fitted linear functions in $\ln(I)$ vs. t plots according equations S1 and S2:

$$I = I_0 * e^{-\frac{t}{\tau}} \quad (\text{S1})$$

$$\ln(I) = \ln(I_0) - \left(\frac{1}{\tau}\right) * t \quad (\text{S2})$$

Full sets of the obtained spectra, emission decays, $\ln(I)$ vs. t plots, and fitted linear functions with the obtained parameters at variable temperatures, as well as temperature dependences of emission spectra and lifetimes are presented in Figs. S9–10 (**[7]·Br₂**), S11–14 (**[8]·Br₂** at C = 20 µM), S15–18 (**[8]·Br₂** at C = 2 µM), S19–20 (**[9]·Br₂**), and S21–22 (**[10]·Br₂**).

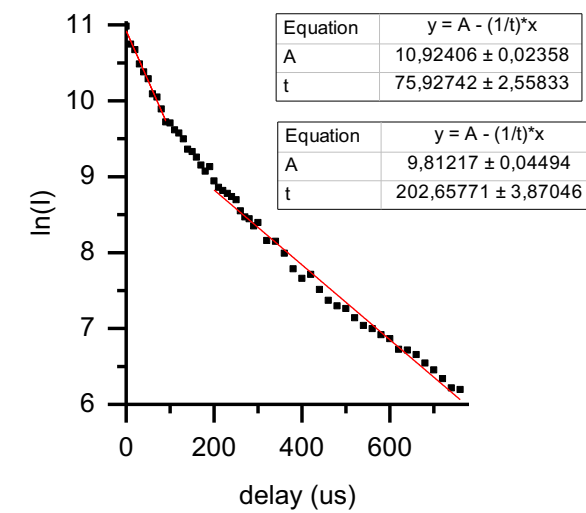
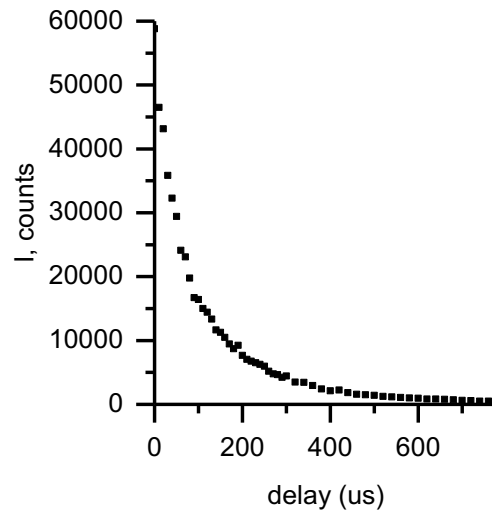
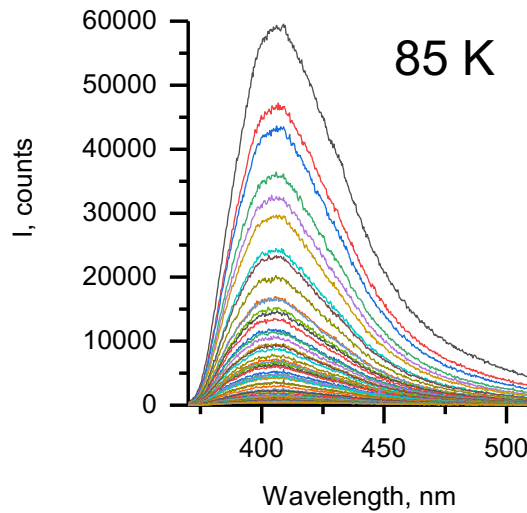
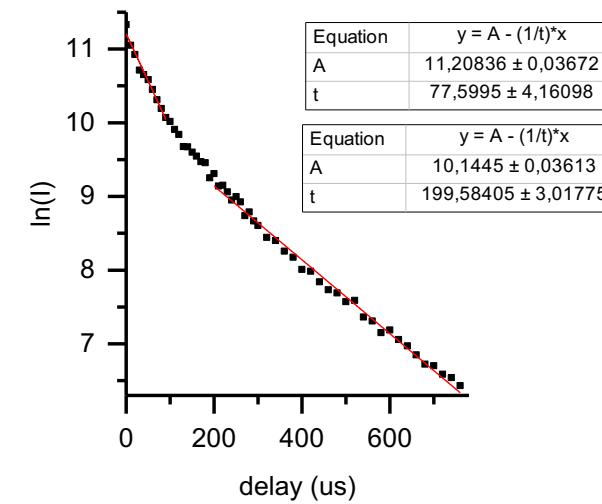
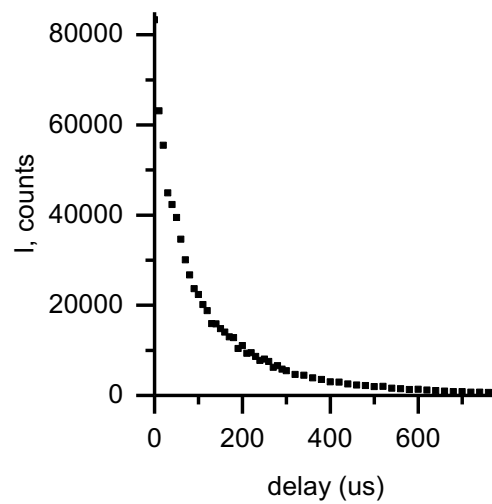
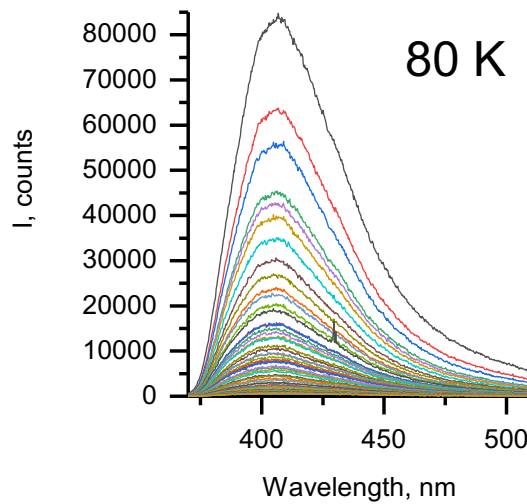


Fig. S9 Phosphorescence emission spectra at increasing delays, emission intensity decays, and $\ln(I)$ vs. delay time plots with fitted linear functions for **[7]·Br₂** in methanol/ethanol mixture (C = 20 μ M) at variable temperatures ($\lambda_{\text{ex}} = 320$ nm, gate = 10 μ s).

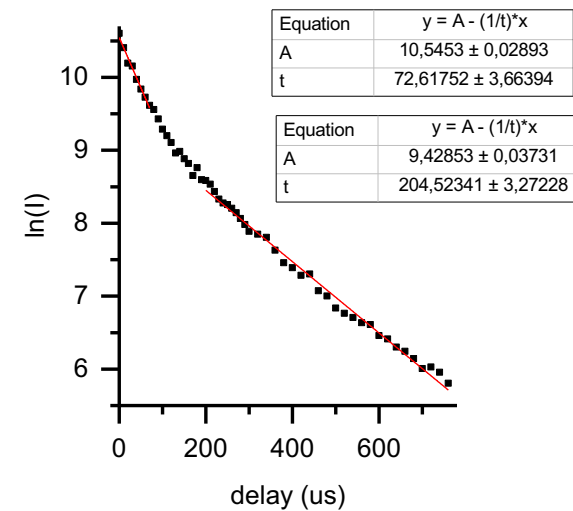
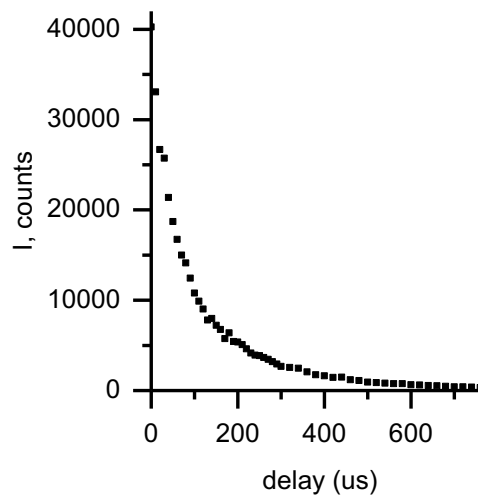
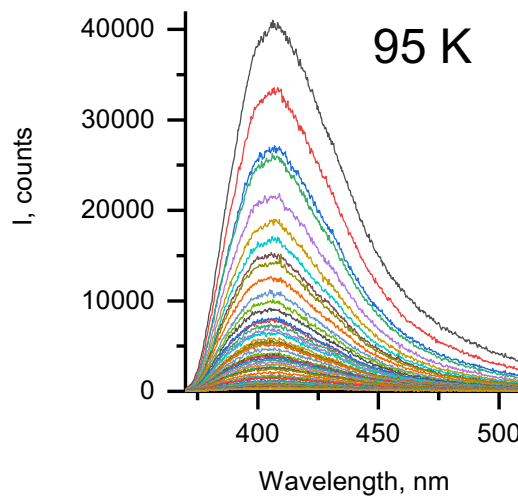
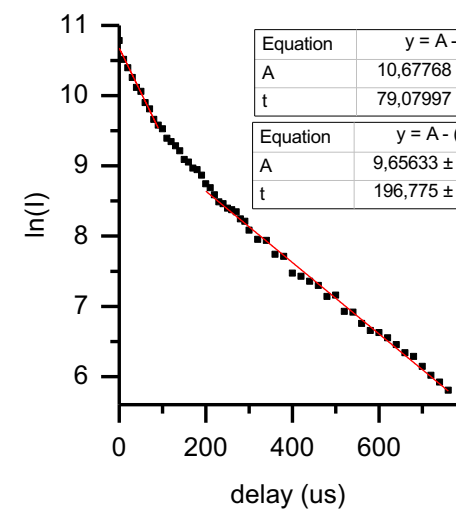
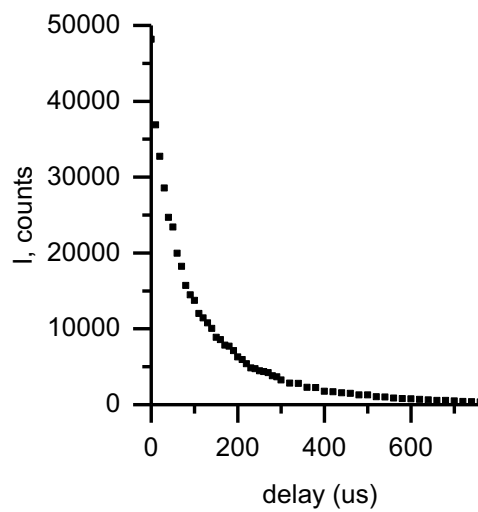
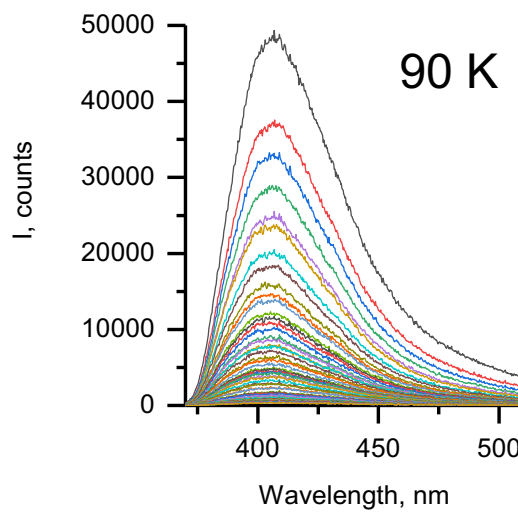


Fig. S9 (continued) Phosphorescence emission spectra at increasing delays, emission intensity decays, and $\ln(I)$ vs. delay time plots with fitted linear functions for $[7]\cdot\text{Br}_2$ in methanol/ethanol mixture ($C = 20 \mu\text{M}$) at variable temperatures ($\lambda_{\text{ex}} = 320 \text{ nm}$, gate = $10 \mu\text{s}$).

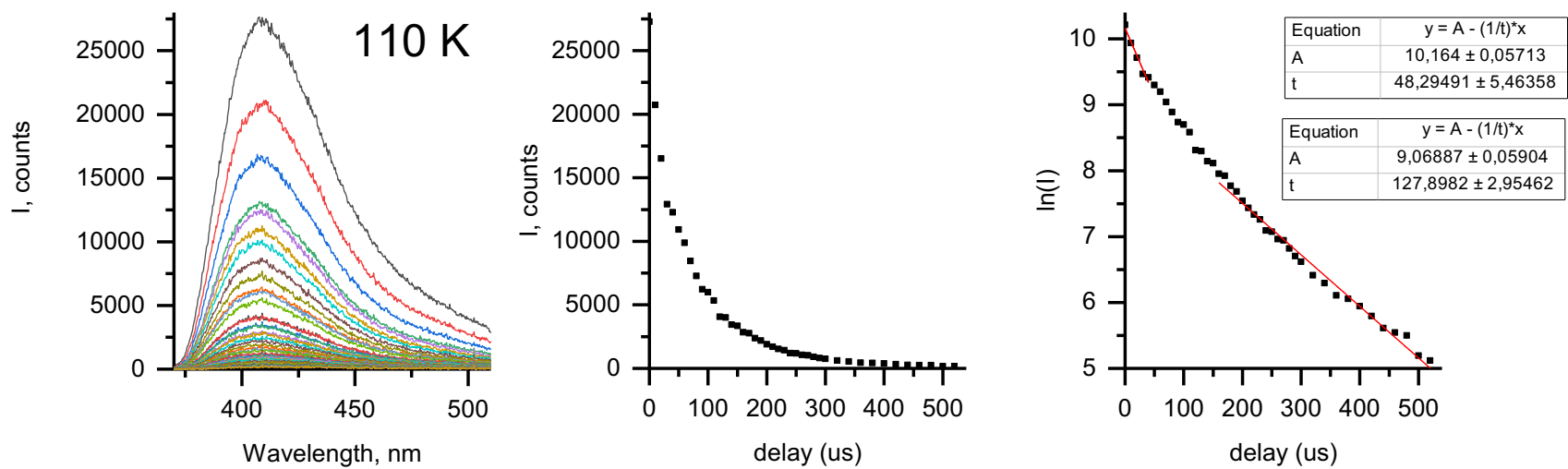
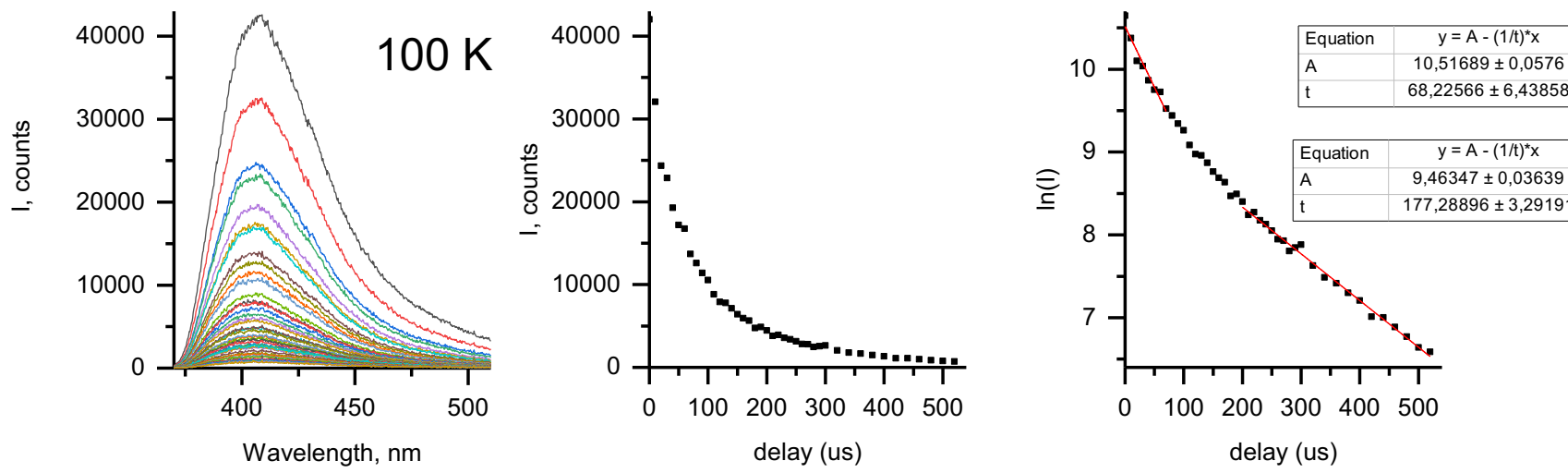


Fig. S9 (continued) Phosphorescence emission spectra at increasing delays, emission intensity decays, and $\ln(I)$ vs. delay time plots with fitted linear functions for **[7]·Br₂** in methanol/ethanol mixture ($C = 20 \mu\text{M}$) at variable temperatures ($\lambda_{\text{ex}} = 320 \text{ nm}$, gate = 10 μs).

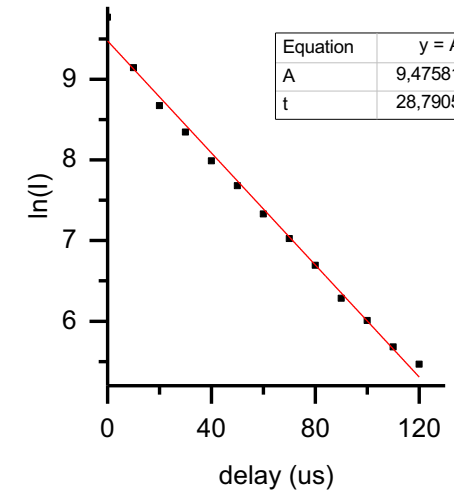
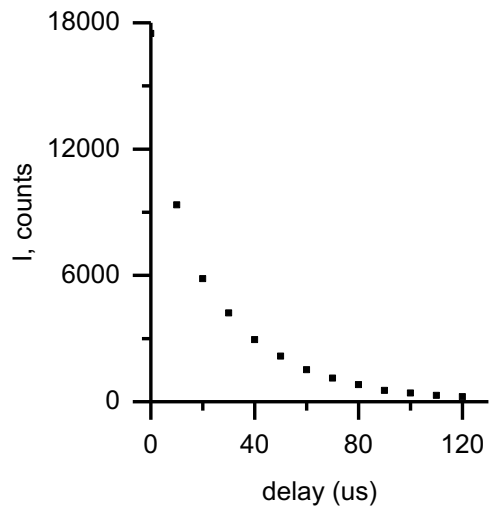
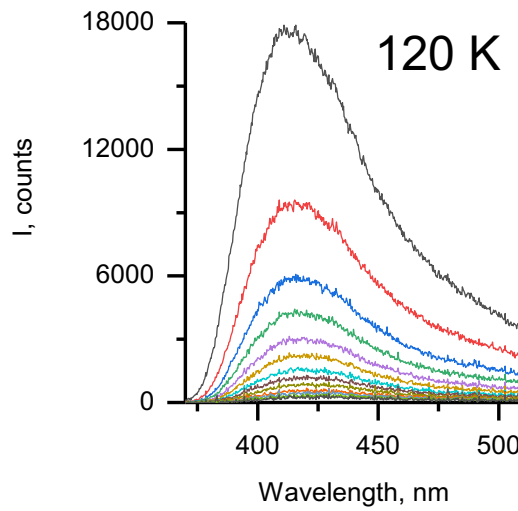
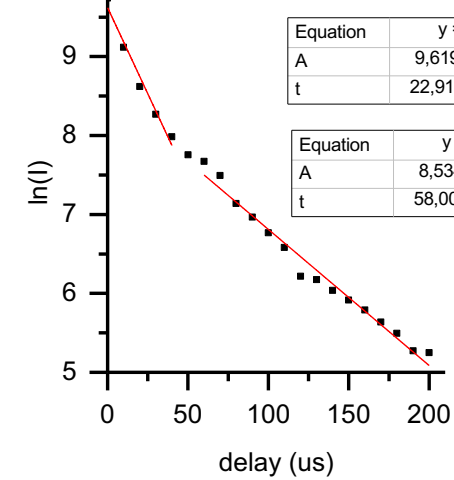
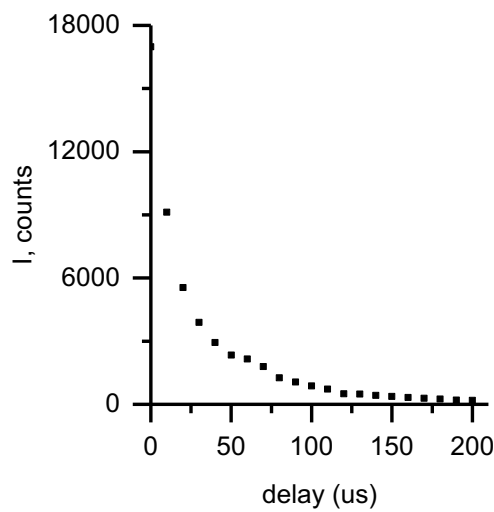
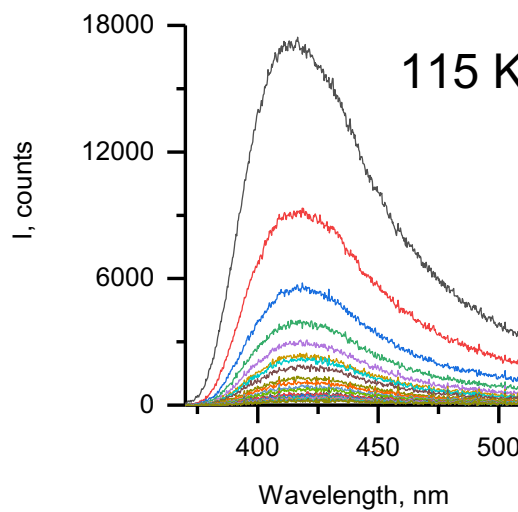


Fig. S9 (continued) Phosphorescence emission spectra at increasing delays, emission intensity decays, and $\ln(I)$ vs. delay time plots with fitted linear functions for [7]·Br₂ in methanol/ethanol mixture (C = 20 μ M) at variable temperatures ($\lambda_{\text{ex}} = 320$ nm, gate = 10 μ s).

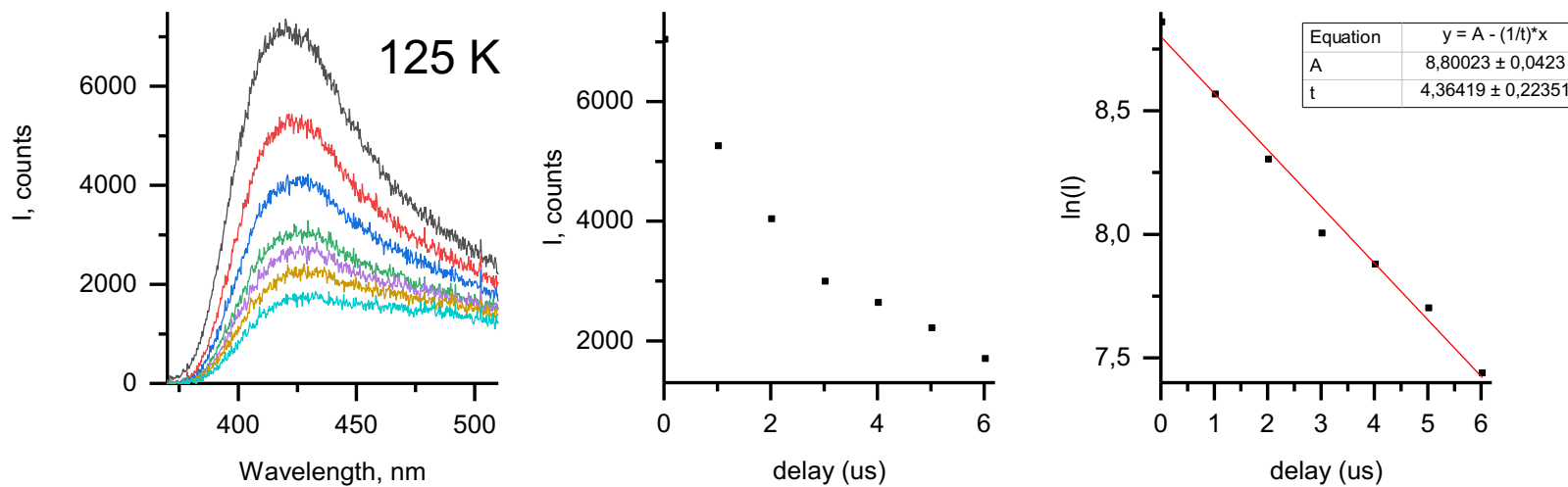


Fig. S9 (continued) Phosphorescence emission spectra at increasing delays, emission intensity decays, and $\ln(I)$ vs. delay time plots with fitted linear functions for $[7]\cdot\text{Br}_2$ in methanol/ethanol mixture ($C = 20 \mu\text{M}$) at variable temperatures ($\lambda_{\text{ex}} = 320 \text{ nm}$, gate = 10 μs).

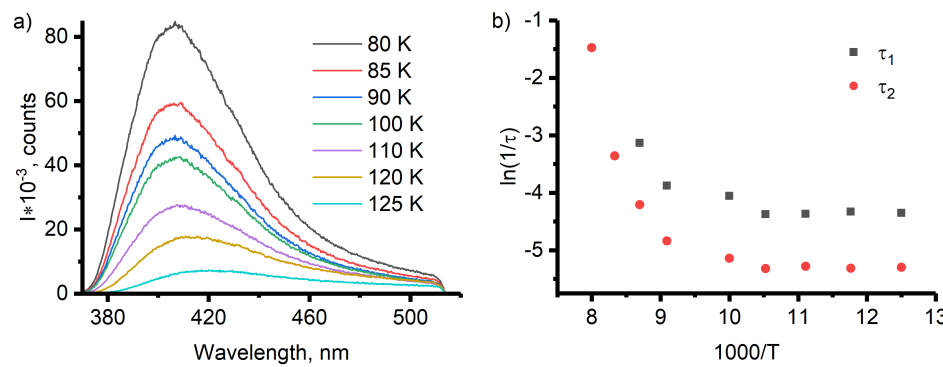


Fig. S10 Phosphorescence emission spectra of $[7]\cdot\text{Br}_2$ at variable temperatures (delay = 20 ns, gate = 10 μs , a) and Arrhenius plots of $\ln(1/\tau)$ vs. $1/T$ (b) in methanol/ethanol mixture ($C = 20 \mu\text{M}$, $\lambda_{\text{ex}} = 320 \text{ nm}$).

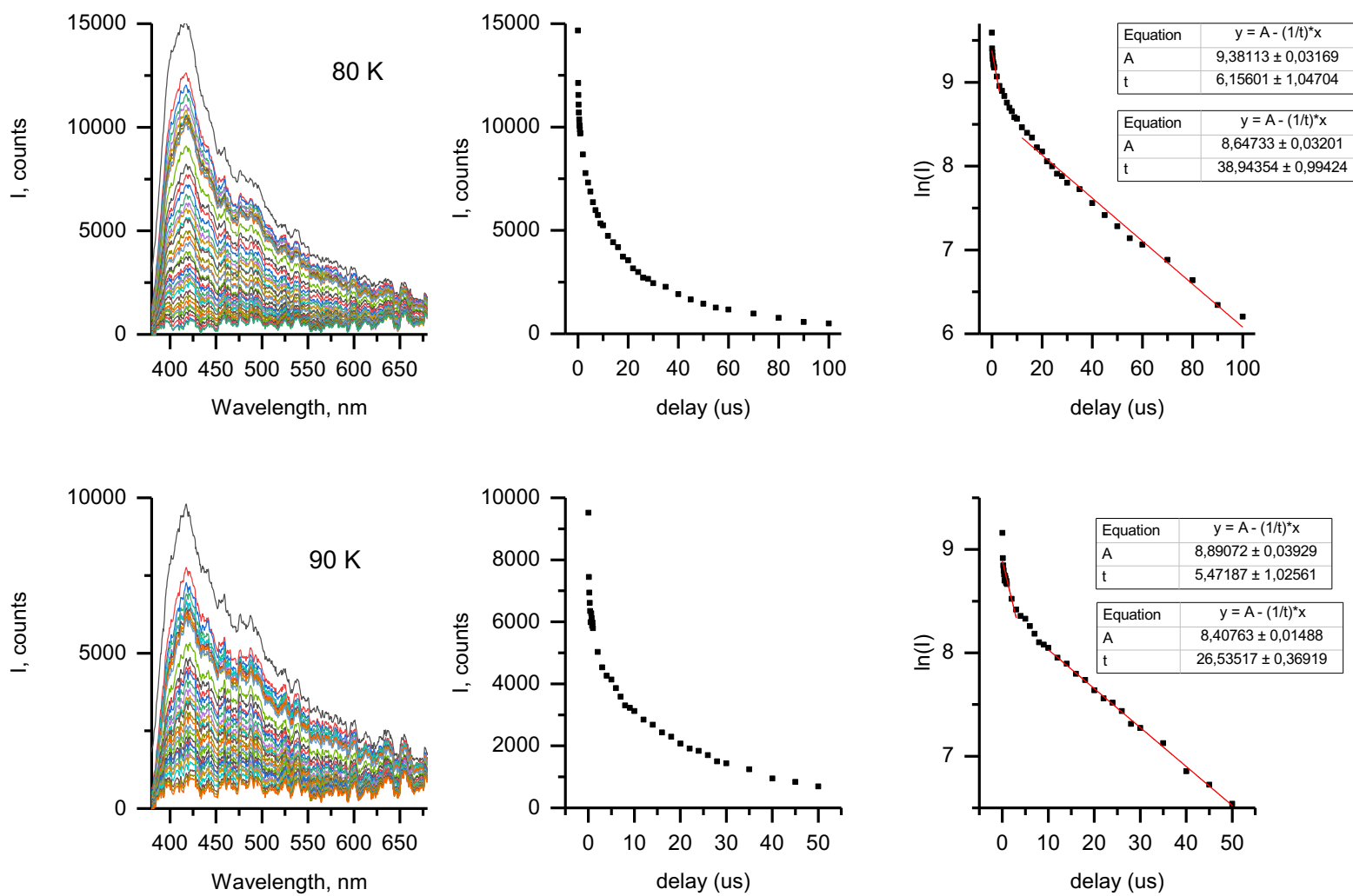


Fig. S11 Phosphorescence emission spectra at variable delays, emission intensity decays, and $\ln(I)$ vs. delay time plots with fitted linear functions for the fast decaying emission ($\lambda_{\text{em}} = 417$ nm) of **[8]·Br₂** in methanol/ethanol mixture (C = 20 μM) at variable temperatures ($\lambda_{\text{ex}} = 320$ nm, gate = 1 μs).

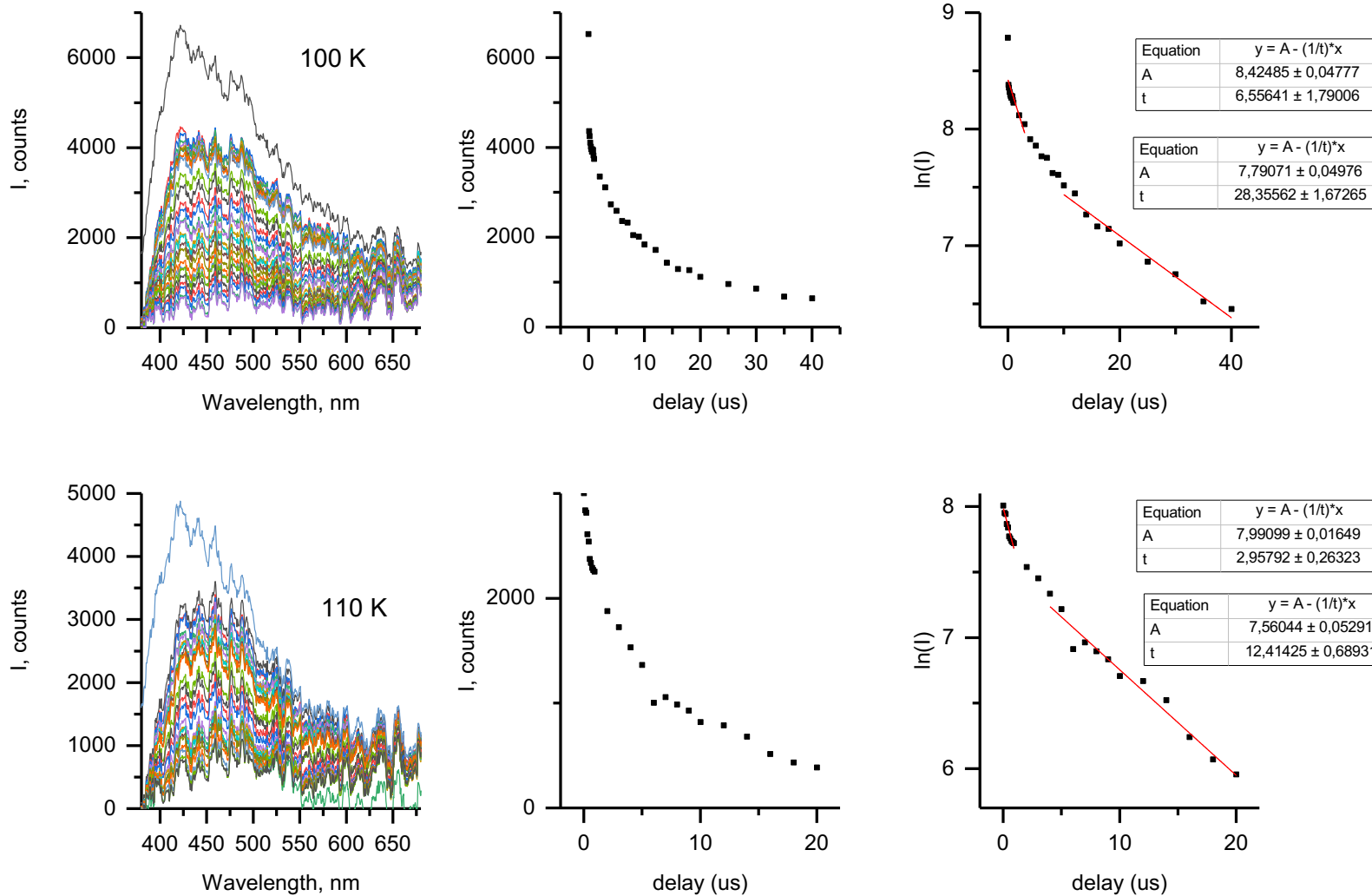


Fig. S11 (continued) Phosphorescence emission spectra at variable delays, emission intensity decays, and $\ln(I)$ vs. delay time plots with fitted linear functions for the fast decaying emission ($\lambda_{\text{em}} = 417$ nm) of **[8]·Br₂** in methanol/ethanol mixture (C = 20 μM) at variable temperatures ($\lambda_{\text{ex}} = 320$ nm, gate = 1 μs).

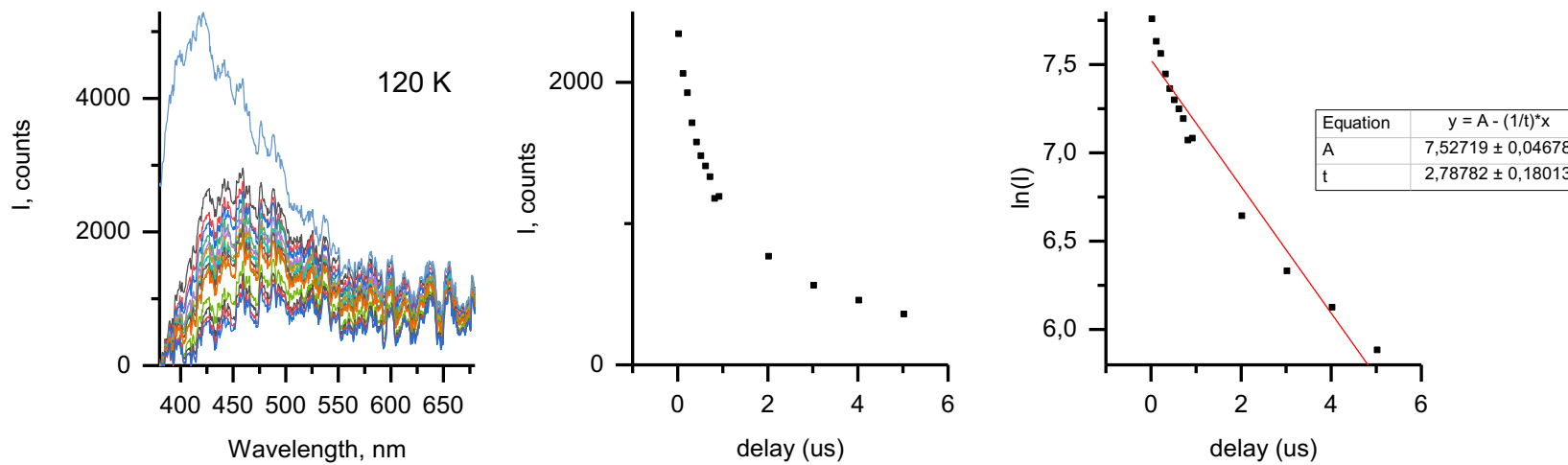


Fig. S11 (continued) Phosphorescence emission spectra at variable delays, emission intensity decays, and $\ln(I)$ vs. delay time plots with fitted linear functions for the fast decaying emission ($\lambda_{\text{em}} = 417$ nm) of **[8]·Br₂** in methanol/ethanol mixture ($C = 20$ μM) at variable temperatures ($\lambda_{\text{ex}} = 320$ nm, gate = 1 μs).

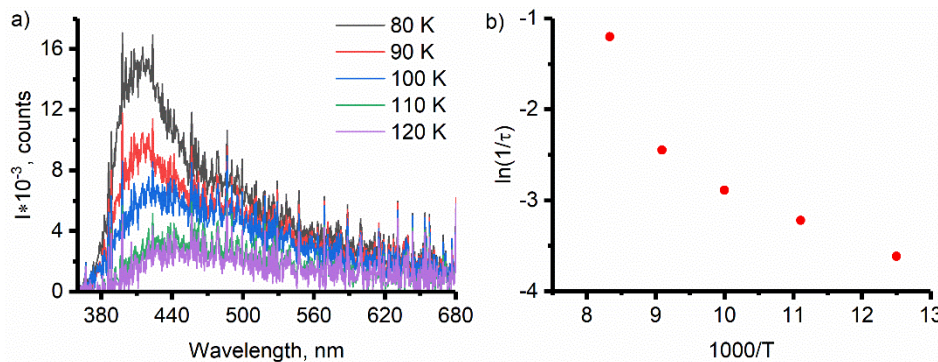


Fig. S12 Phosphorescence emission spectra of **[8]·Br₂** at variable temperatures (delay = 20 ns, gate = 1 μs , a) and Arrhenius plot of $\ln(1/\tau_2)$ vs. $1/T$ for the fast decaying emission ($\lambda_{\text{em}} = 417$ nm, b) in methanol/ethanol mixture ($C = 20$ μM , $\lambda_{\text{ex}} = 320$ nm).

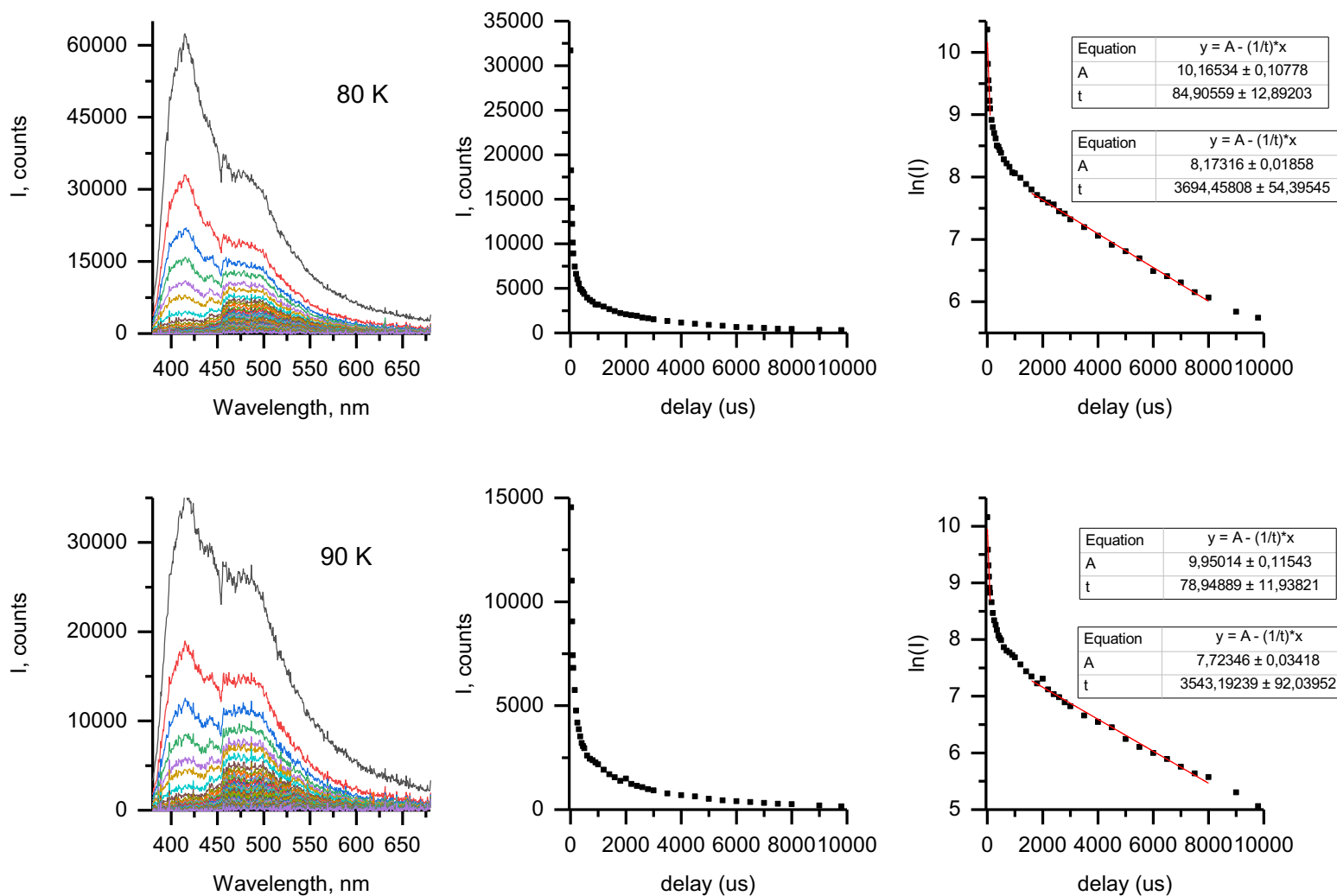


Fig. S13 Phosphorescence emission spectra at variable delays, emission intensity decays, and $\ln(I)$ vs. delay time plots with fitted linear functions for the slow decaying emission ($\lambda_{\text{em}} = 485$ nm) of **[8]·Br₂** in methanol/ethanol mixture (C = 20 μM) at variable temperatures ($\lambda_{\text{ex}} = 320$ nm, gate = 100 μs).

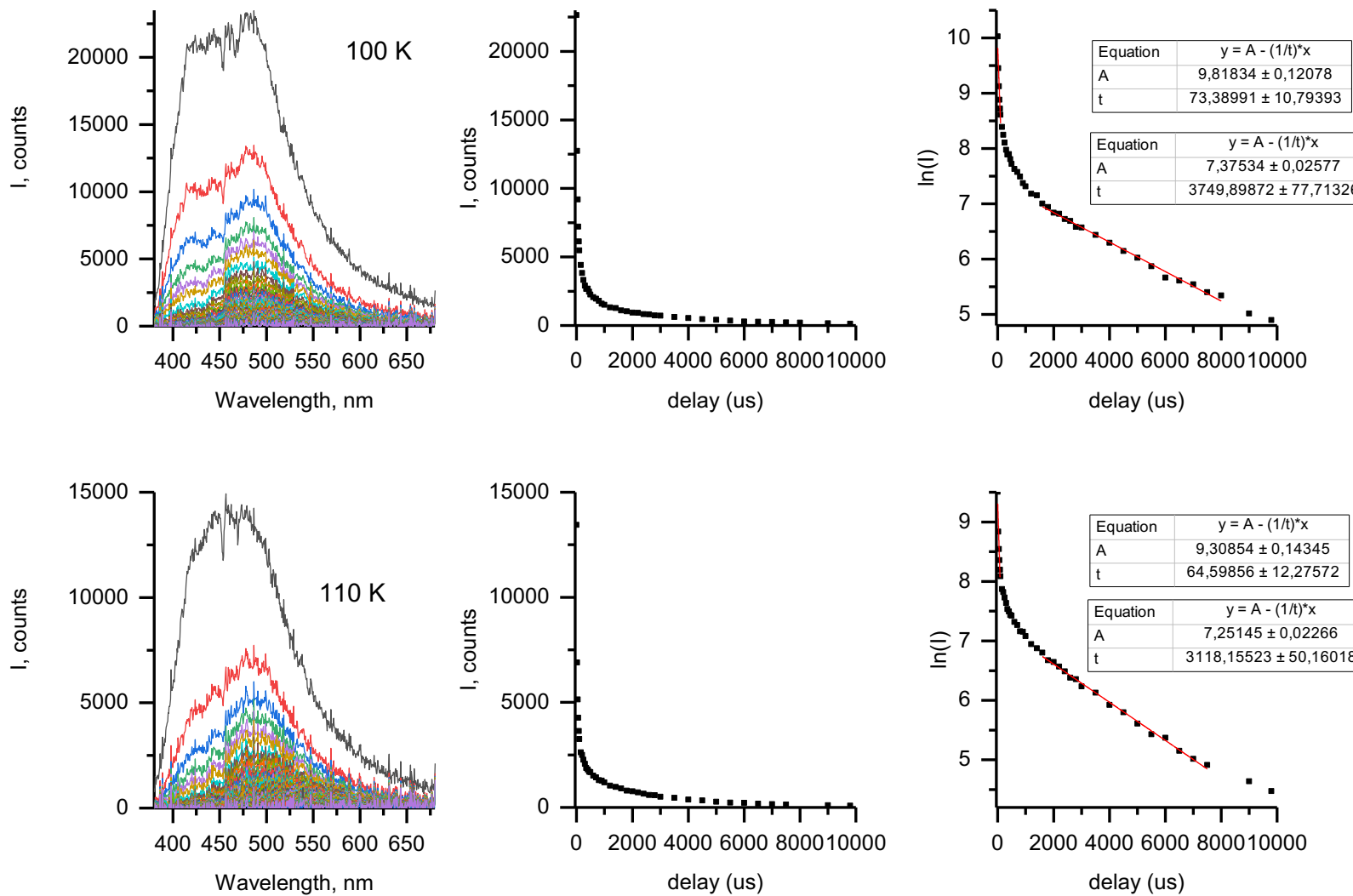


Fig. S13 (continued) Phosphorescence emission spectra at variable delays, emission intensity decays, and $\ln(I)$ vs. delay time plots with fitted linear functions for the slow decaying emission ($\lambda_{\text{em}} = 485$ nm) of $[8]\cdot\text{Br}_2$ in methanol/ethanol mixture ($C = 20$ μM) at variable temperatures ($\lambda_{\text{ex}} = 320$ nm, gate = 100 μs).

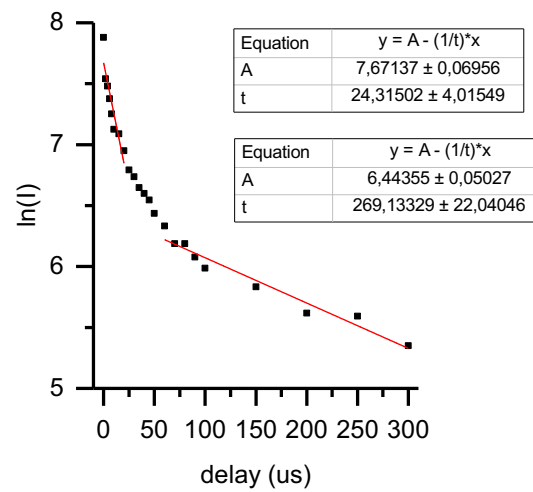
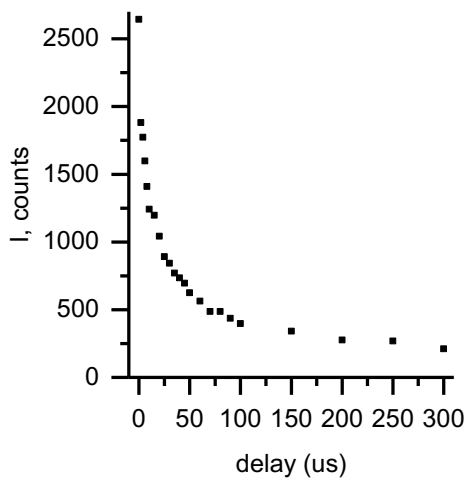
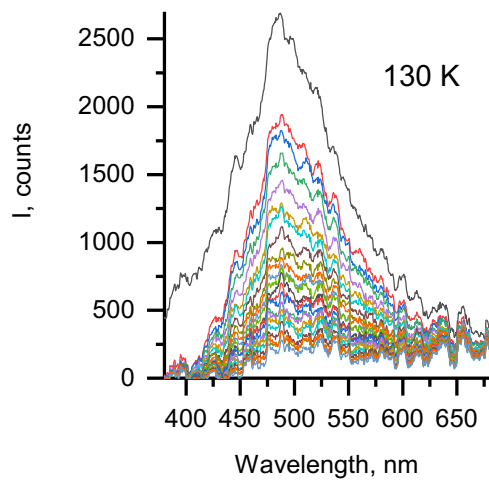
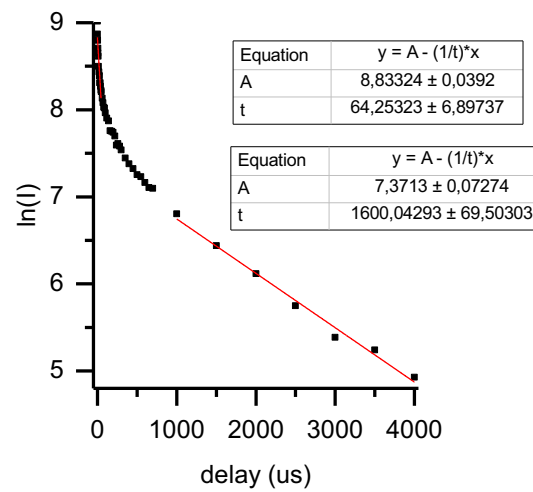
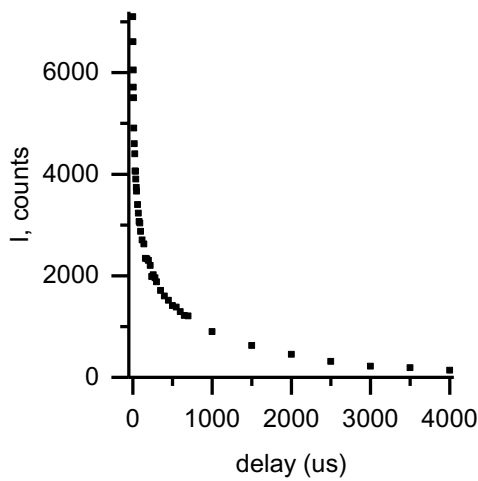
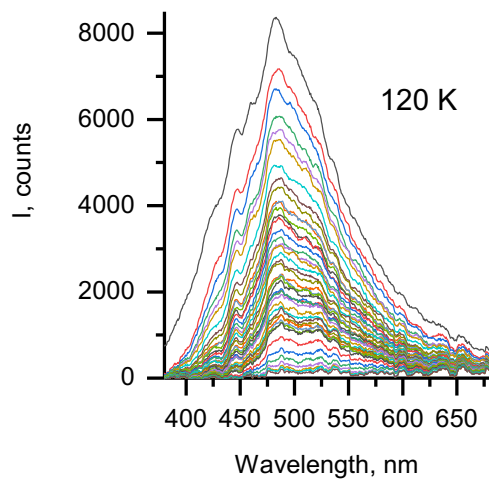


Fig. S13 (continued) Phosphorescence emission spectra at variable delays, emission intensity decays, and $\ln(I)$ vs. delay time plots with fitted linear functions for the slow decaying emission ($\lambda_{\text{em}} = 485$ nm) of $[8]\cdot\text{Br}_2$ in methanol/ethanol mixture ($C = 20$ μM) at variable temperatures ($\lambda_{\text{ex}} = 320$ nm, gate = 100 μs).

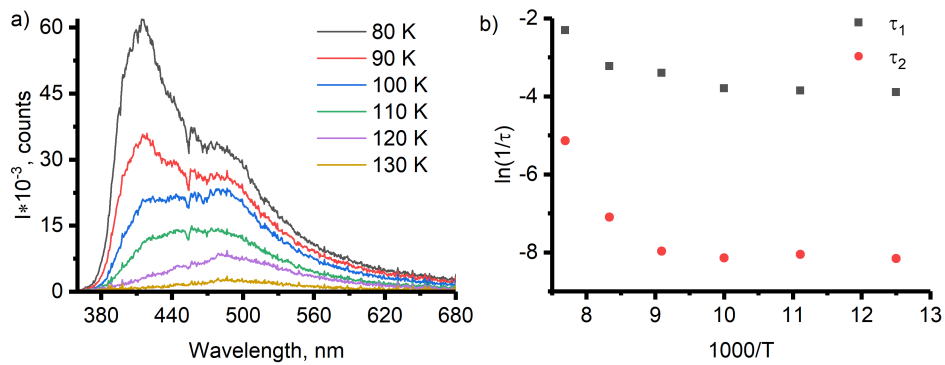


Fig. S14 Phosphorescence emission spectra of **[8]·Br₂** at variable temperatures (delay 20 ns, gate 100 μ s, a) and Arrhenius plots of $\ln(1/\tau)$ vs. $1/T$ for the slow decaying emission ($\lambda_{\text{em}} = 485$ nm, b) in methanol/ethanol mixture ($C = 20$ μ M, $\lambda_{\text{ex}} = 320$ nm).

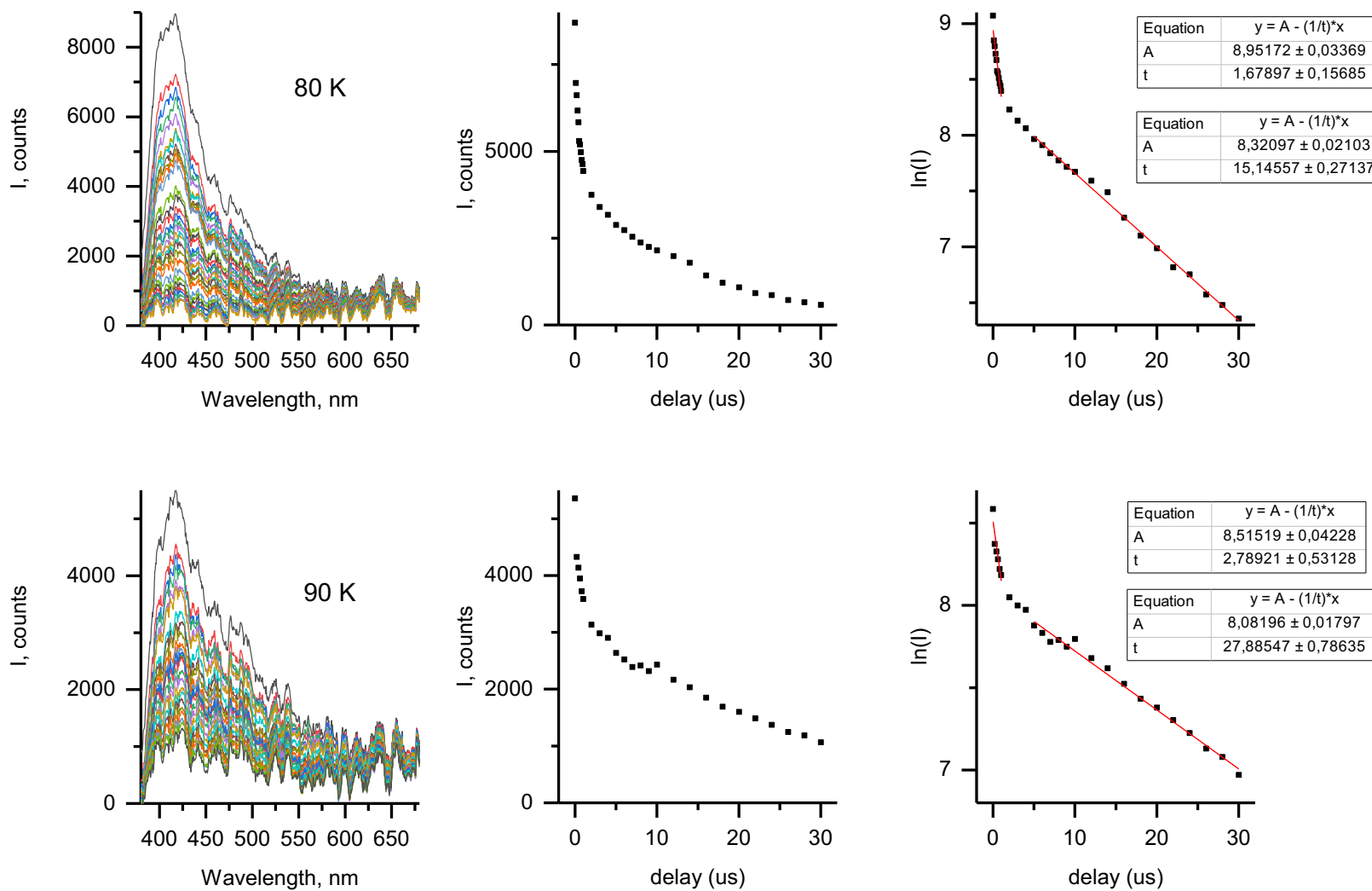


Fig. S15 Phosphorescence emission spectra at variable delays, emission intensity decays, and $\ln(I)$ vs. delay time plots with fitted linear functions for the fast decaying emission ($\lambda_{\text{em}} = 417$ nm) of **[8]·Br₂** in methanol/ethanol mixture (C = 2 μM) at variable temperatures ($\lambda_{\text{ex}} = 320$ nm, gate = 1 μs).

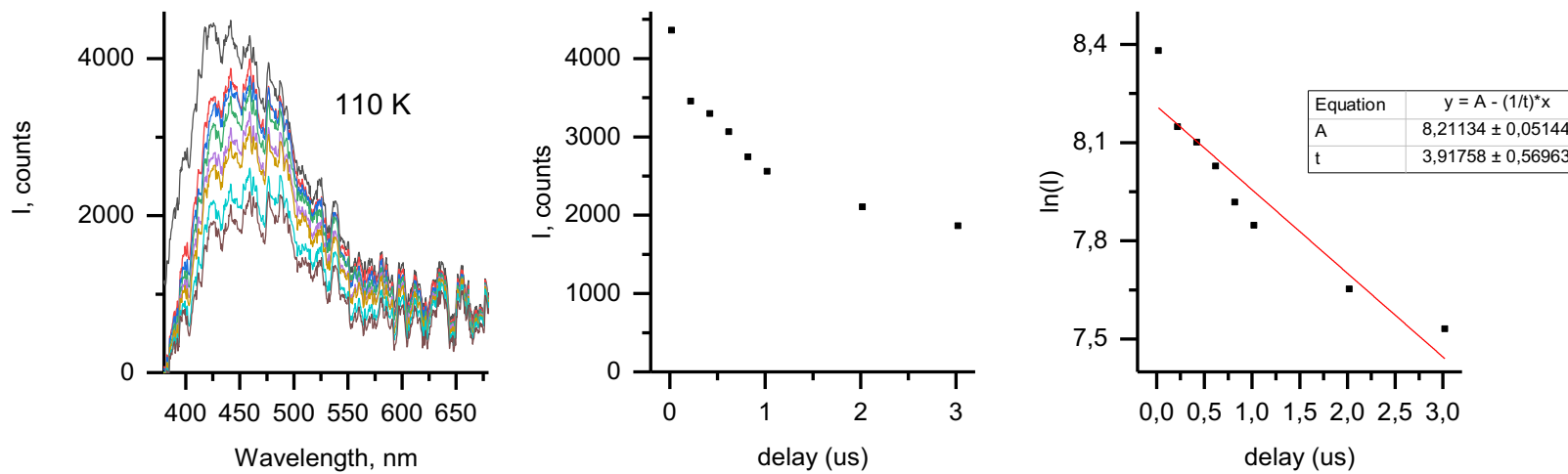


Fig. S15 (continued) Phosphorescence emission spectra at variable delays, emission intensity decays, and $\ln(I)$ vs. delay time plots with fitted linear functions for the fast decaying emission ($\lambda_{\text{em}} = 417$ nm) of **[8]·Br₂** in methanol/ethanol mixture ($C = 2$ μM) at variable temperatures ($\lambda_{\text{ex}} = 320$ nm, gate = 1 μs).

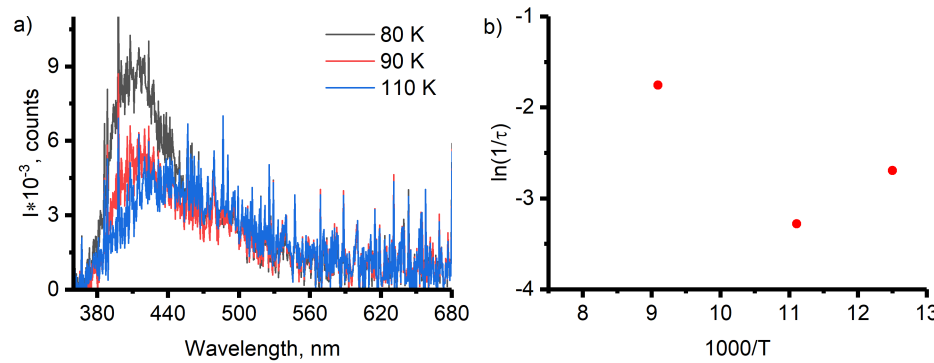


Fig. S16. Phosphorescence emission spectra of **[8]·Br₂** at variable temperatures (delay 20 ns, gate 1 μs , a) and Arrhenius plot of $\ln(1/\tau_2)$ vs. $1/T$ for the fast decaying emission ($\lambda_{\text{em}} = 417$ nm, b) in methanol/ethanol mixture ($C = 2$ μM , $\lambda_{\text{ex}} = 320$ nm).

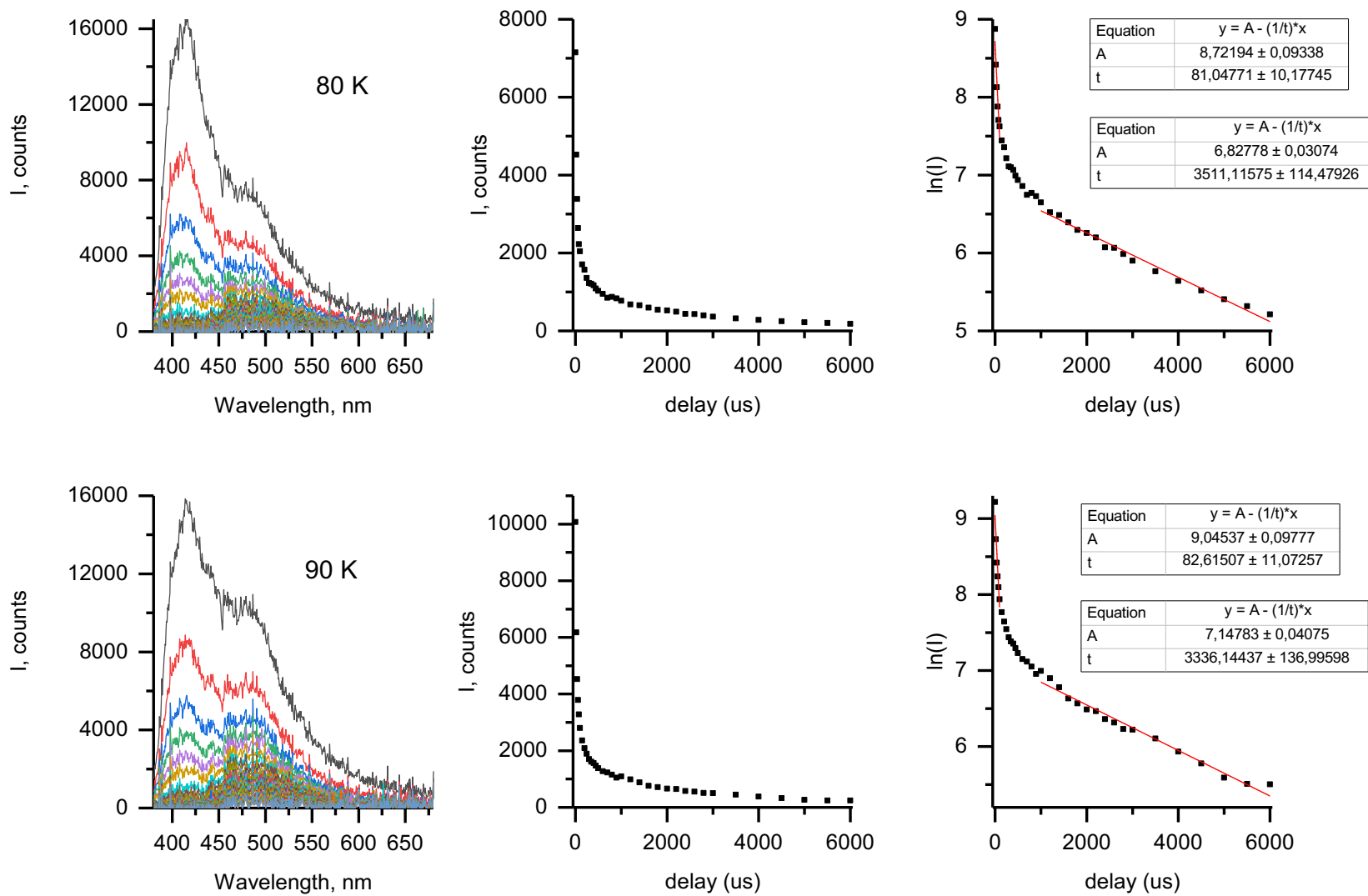


Fig. S17 Phosphorescence emission spectra at variable delays, emission intensity decays, and $\ln(I)$ vs. delay time plots with fitted linear functions for the slow decaying emission ($\lambda_{\text{em}} = 485$ nm) of **[8]·Br₂** in methanol/ethanol mixture (C = 2 μM) at variable temperatures ($\lambda_{\text{ex}} = 320$ nm, gate = 100 μs).

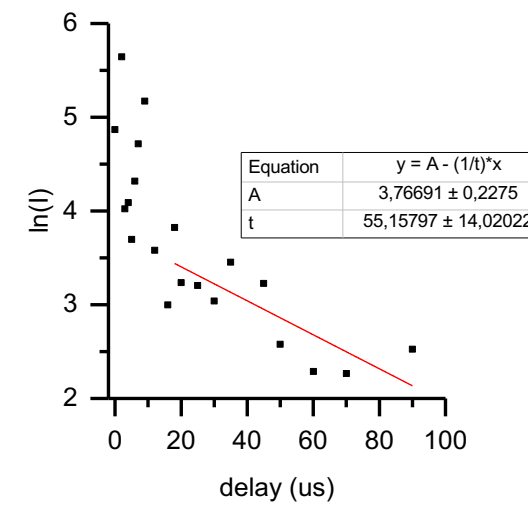
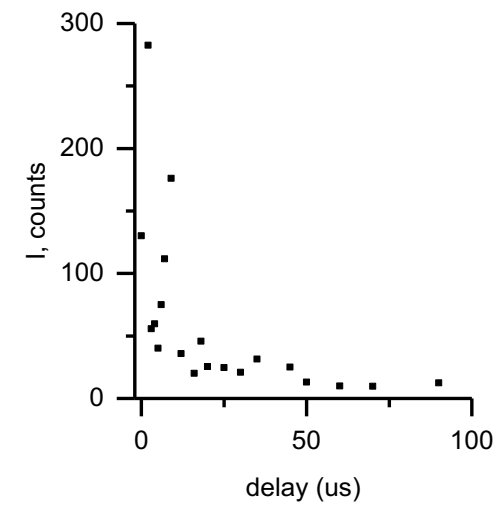
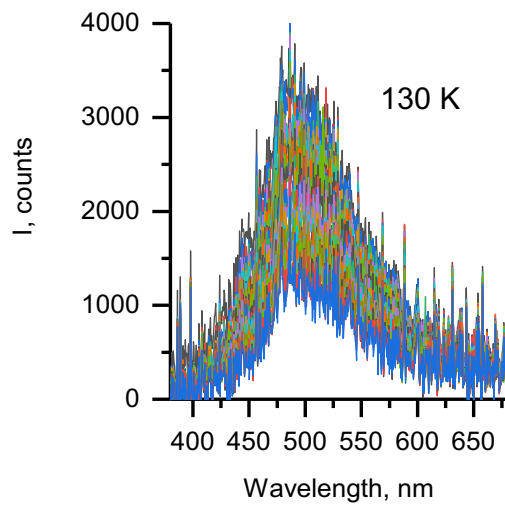
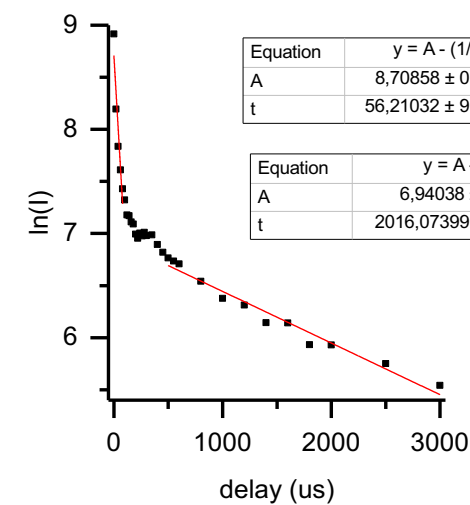
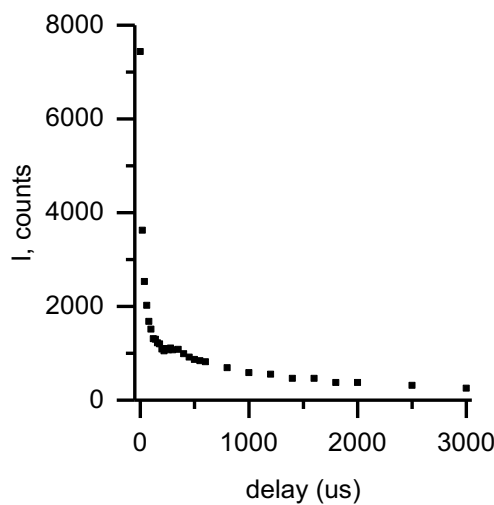
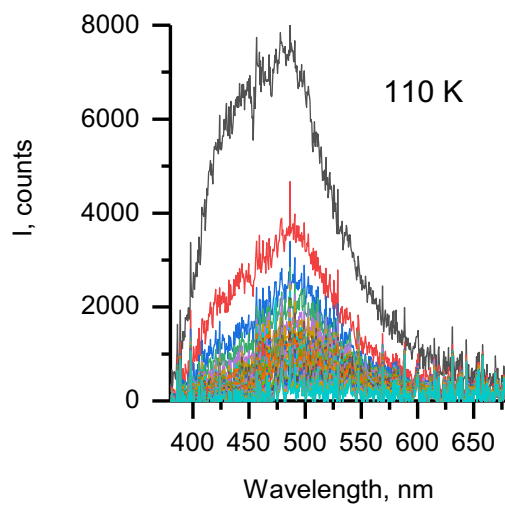


Fig. S17 (continued) Phosphorescence emission spectra at variable delays, emission intensity decays, and $\ln(I)$ vs. delay time plots with fitted linear functions for the slow decaying emission ($\lambda_{\text{em}} = 485$ nm) of **[8]·Br₂** in methanol/ethanol mixture (C = 2 μ M) at variable temperatures ($\lambda_{\text{ex}} = 320$ nm, gate = 100 μ s).

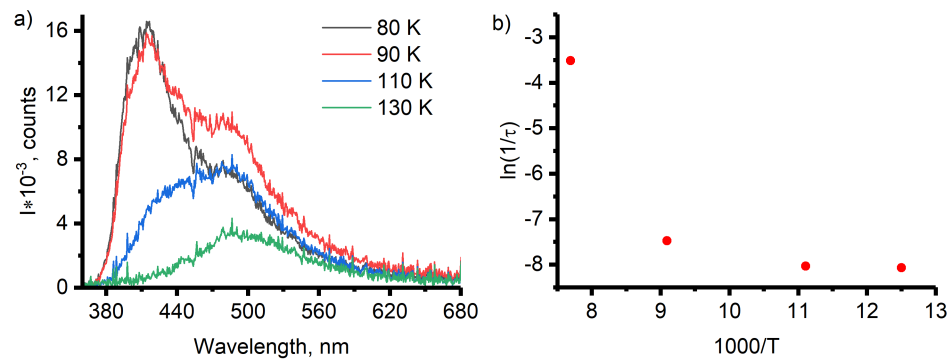


Fig. S18. Phosphorescence emission spectra of **[8]·Br₂** at variable temperatures (delay 20 ns, gate 100 μ s, a) and Arrhenius plot of $\ln(1/\tau_2)$ vs. $1/T$ for the slow decaying emission ($\lambda_{\text{em}} = 485$ nm, b) in methanol/ethanol mixture ($C = 2$ μ M, $\lambda_{\text{ex}} = 320$ nm).

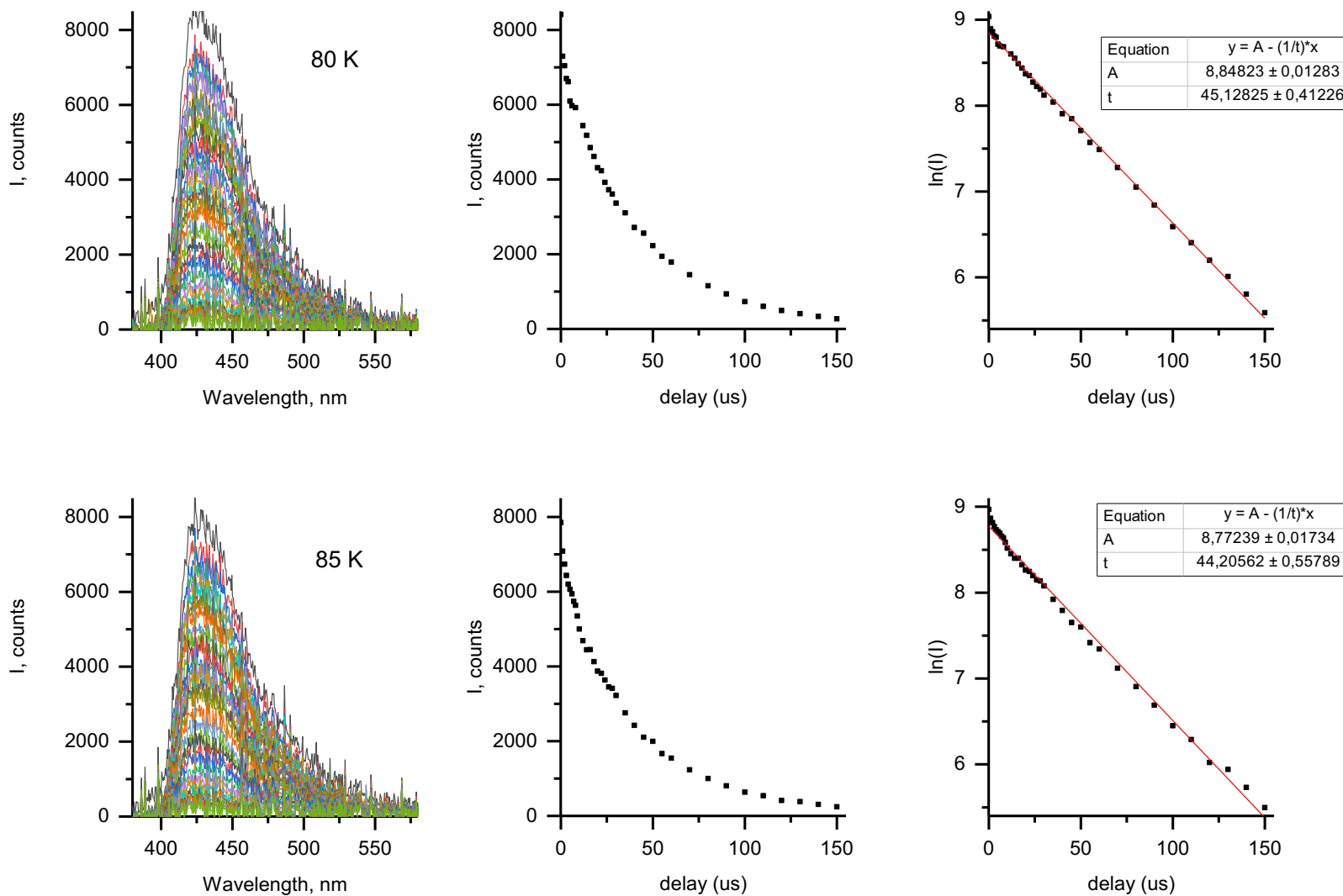


Fig. S19 Phosphorescence emission spectra at variable delays, emission intensity decays, and $\ln(I)$ vs. delay time plots with fitted linear functions for **[9]·Br₂** in methanol/ethanol mixture ($C = 20 \mu\text{M}$) at variable temperatures ($\lambda_{\text{ex}} = 320 \text{ nm}$, gate = 5 μs).

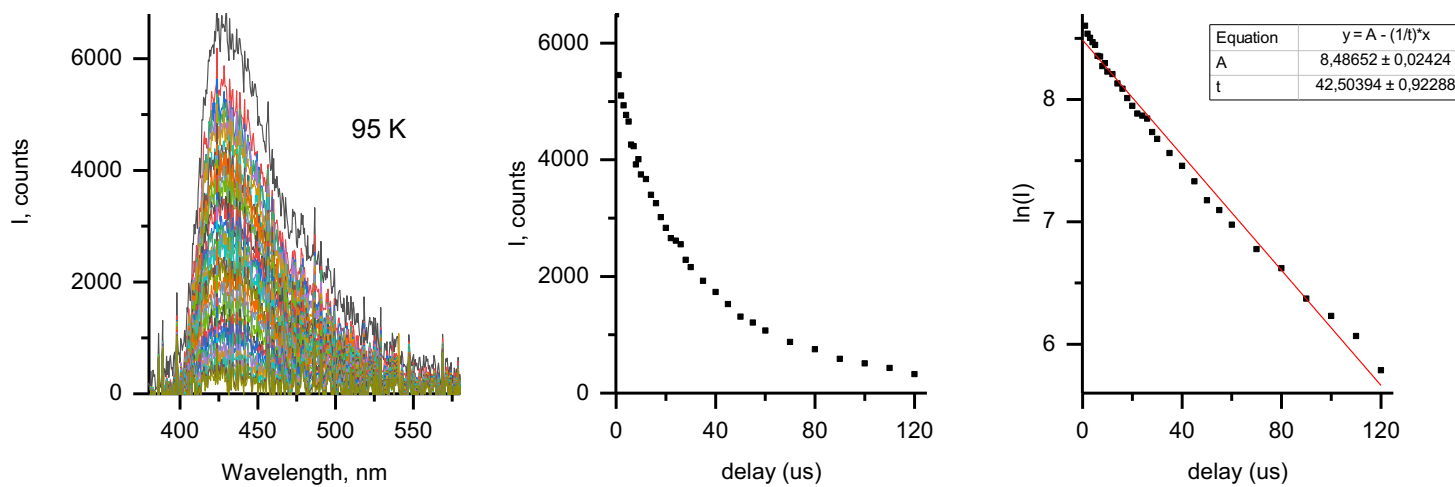
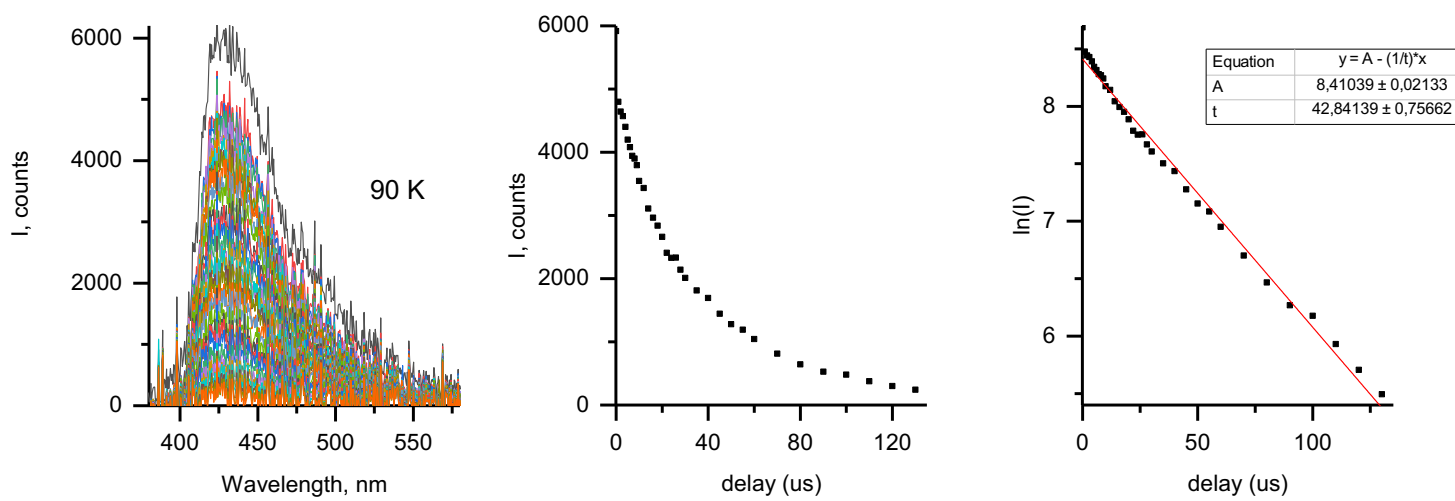


Fig. S19 (continued) Phosphorescence emission spectra at variable delays, emission intensity decays, and $\ln(I)$ vs. delay time plots with fitted linear functions for **[9]·Br₂** in methanol/ethanol mixture ($C = 20 \mu\text{M}$) at variable temperatures ($\lambda_{\text{ex}} = 320 \text{ nm}$, gate = 5 μs).

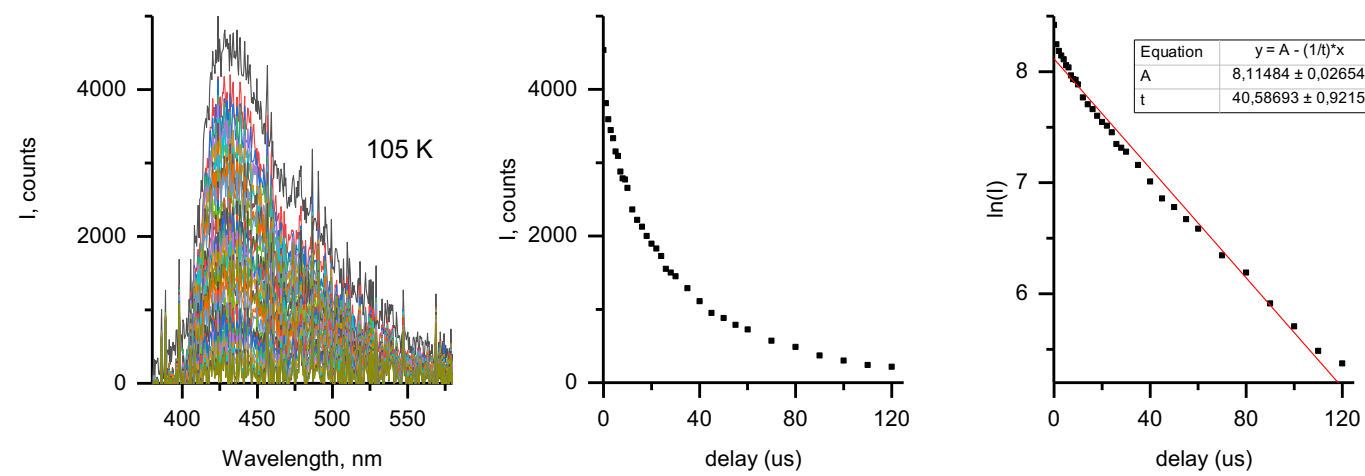
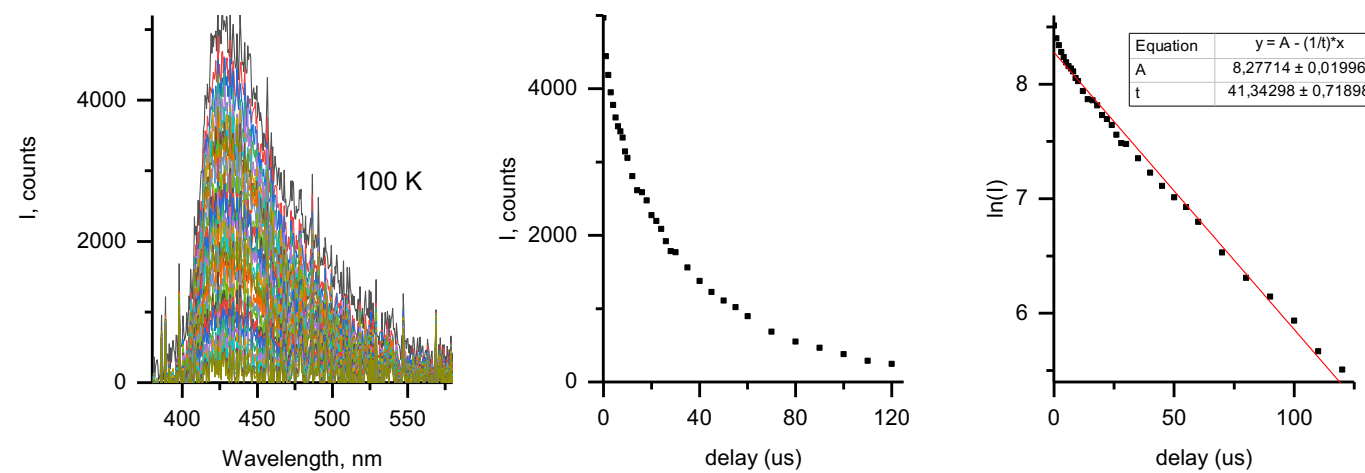


Fig. S19 (continued) Phosphorescence emission spectra at variable delays, emission intensity decays, and $\ln(I)$ vs. delay time plots with fitted linear functions for $[9]\cdot\text{Br}_2$ in methanol/ethanol mixture ($C = 20 \mu\text{M}$) at variable temperatures ($\lambda_{\text{ex}} = 320 \text{ nm}$, gate = 5 μs).

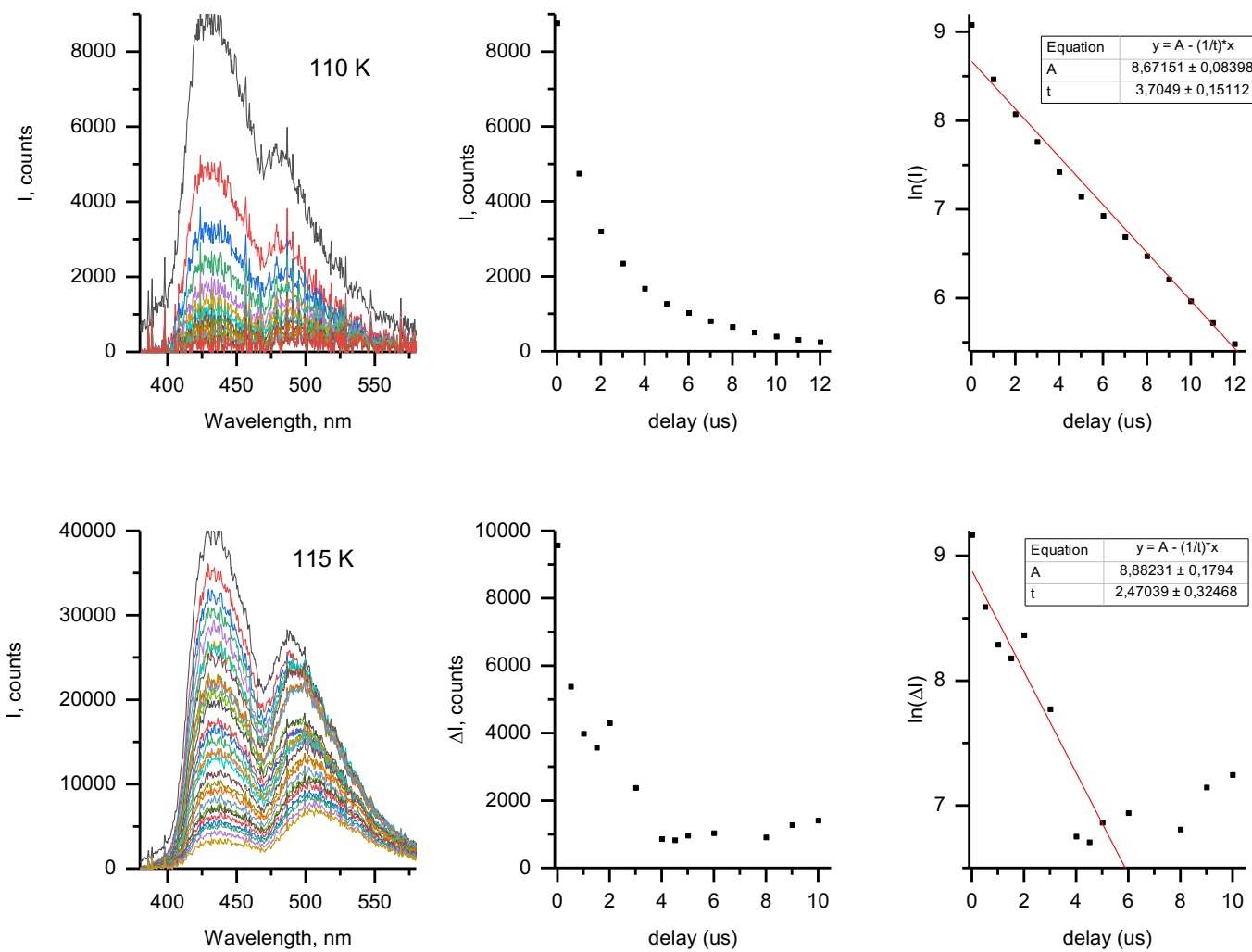


Fig. S19 (continued) Phosphorescence emission spectra at variable delays, emission intensity decays, and $\ln(I)$ vs. delay time plots with fitted linear functions for $[9]\cdot\text{Br}_2$ in methanol/ethanol mixture ($C = 20 \mu\text{M}$) at variable temperatures ($\lambda_{\text{ex}} = 320 \text{ nm}$, gate = 5 μs).

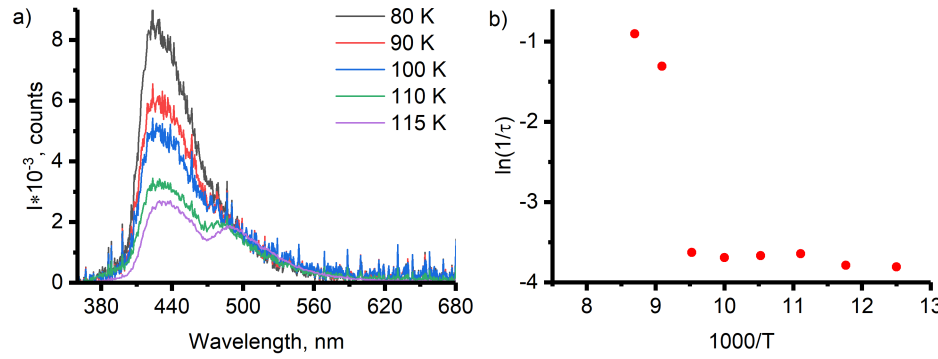


Fig. S20 Phosphorescence emission spectra of **[9]·Br₂** at variable temperatures (delay 20 ns, gate 5 μs, a) and Arrhenius plot of $\ln(1/\tau_2)$ vs. $1/T$ (b) in methanol/ethanol mixture (C = 20 μM, $\lambda_{\text{ex}} = 320$ nm).

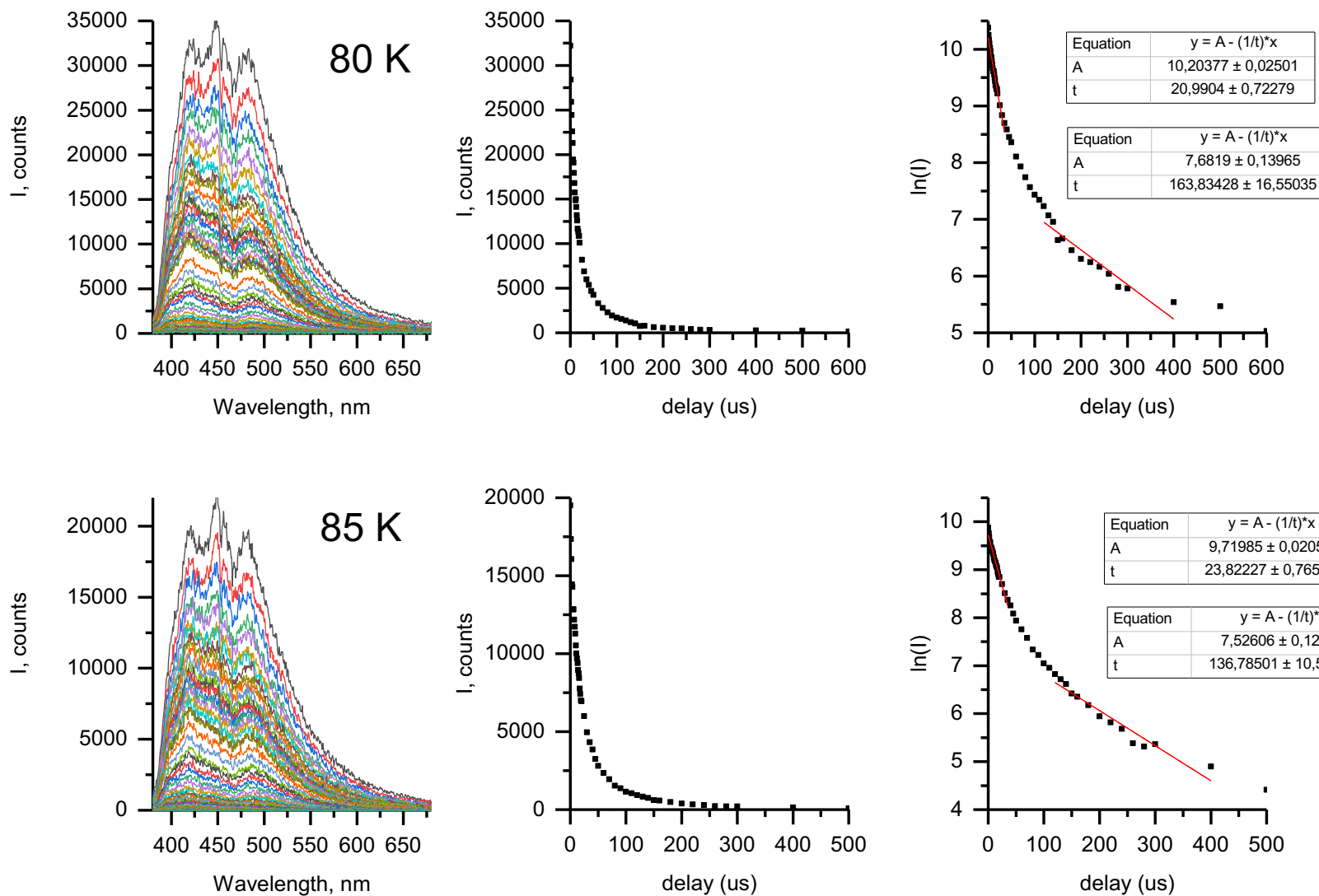


Fig. S21 Phosphorescence emission spectra at variable delays, emission intensity decays, and $\ln(I)$ vs. delay time plots with fitted linear functions for **[10]·Br₂** in methanol/ethanol mixture ($C = 20 \mu\text{M}$) at variable temperatures ($\lambda_{\text{ex}} = 320 \text{ nm}$, gate = 10 μs).

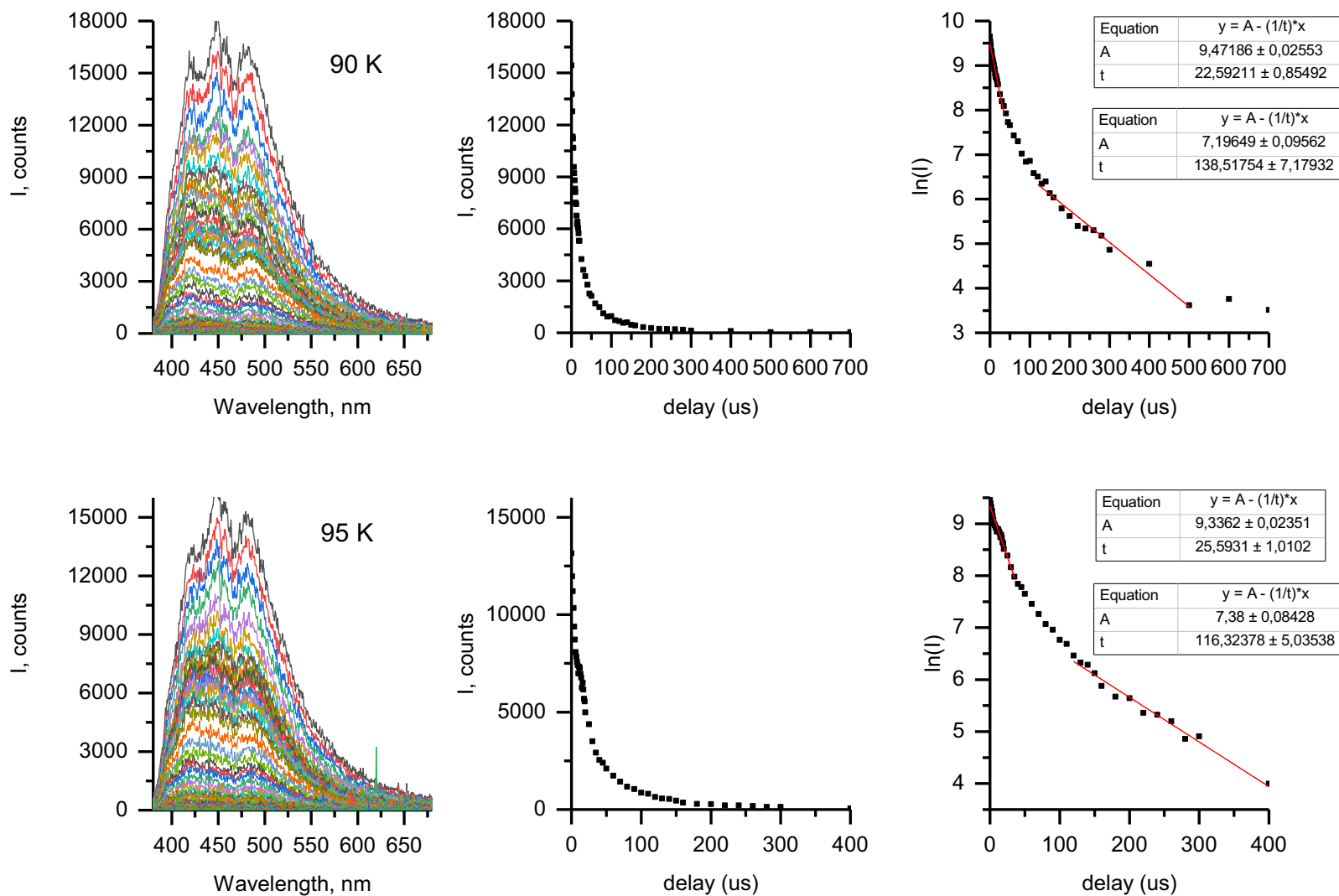


Fig. S21 (continued) Phosphorescence emission spectra at variable delays, emission intensity decays, and $\ln(I)$ vs. delay time plots with fitted linear functions for **[10]·Br₂** in methanol/ethanol mixture ($C = 20 \mu\text{M}$) at variable temperatures ($\lambda_{\text{ex}} = 320 \text{ nm}$, gate = 10 μs).

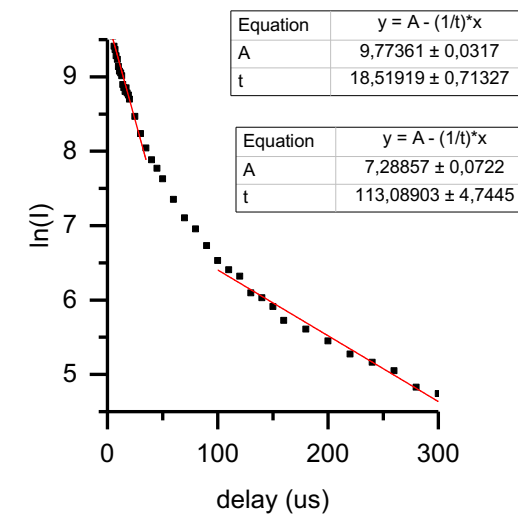
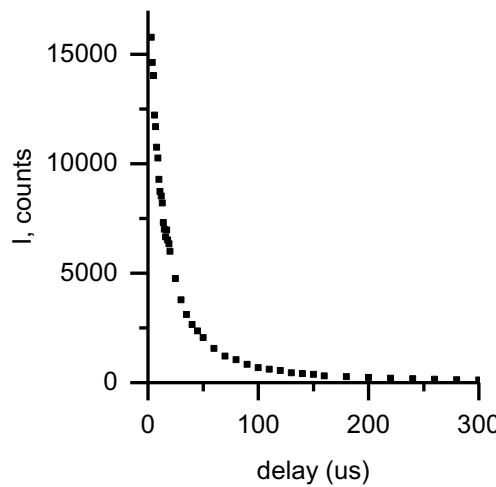
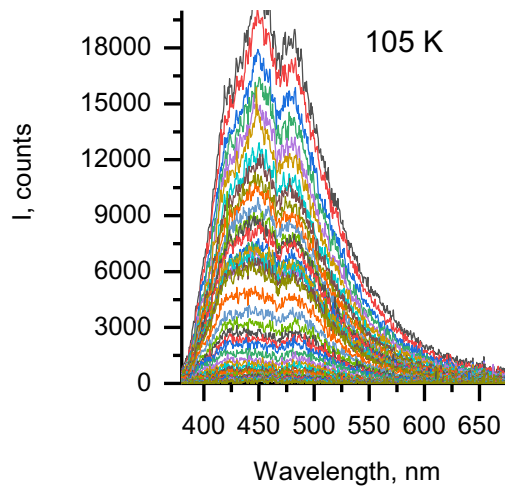
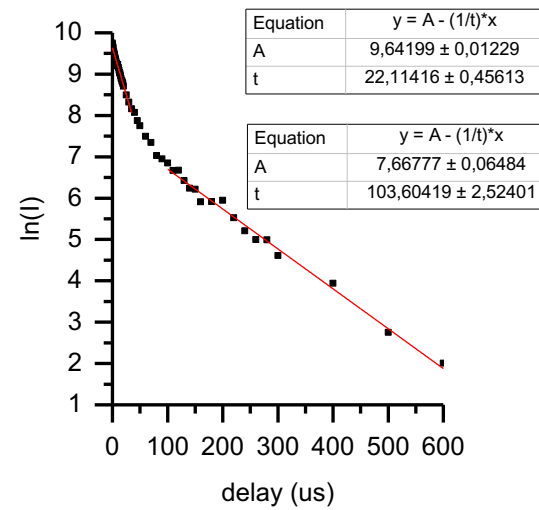
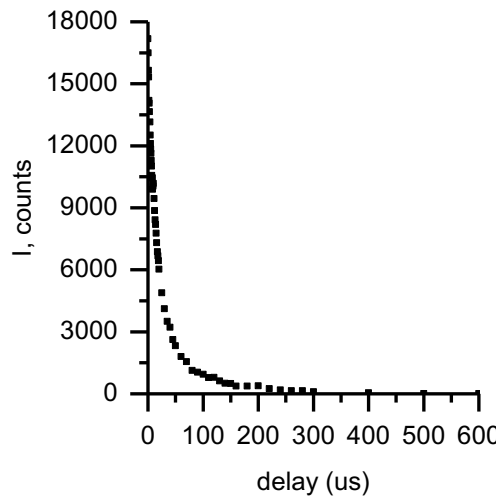
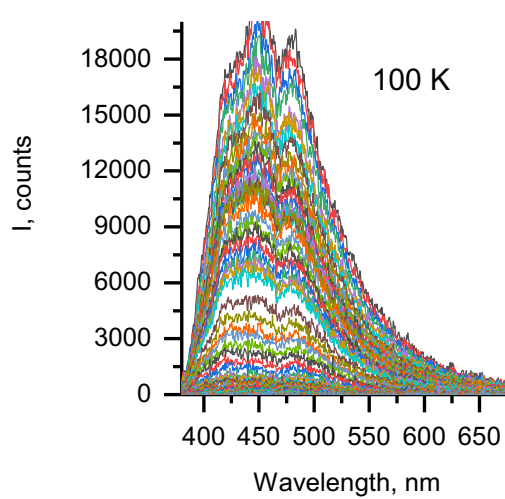


Fig. S21 (continued) Phosphorescence emission spectra at variable delays, emission intensity decays, and $\ln(I)$ vs. delay time plots with fitted linear functions for **[10]·Br₂** in methanol/ethanol mixture (C = 20 μ M) at variable temperatures ($\lambda_{\text{ex}} = 320$ nm, gate = 10 μ s).

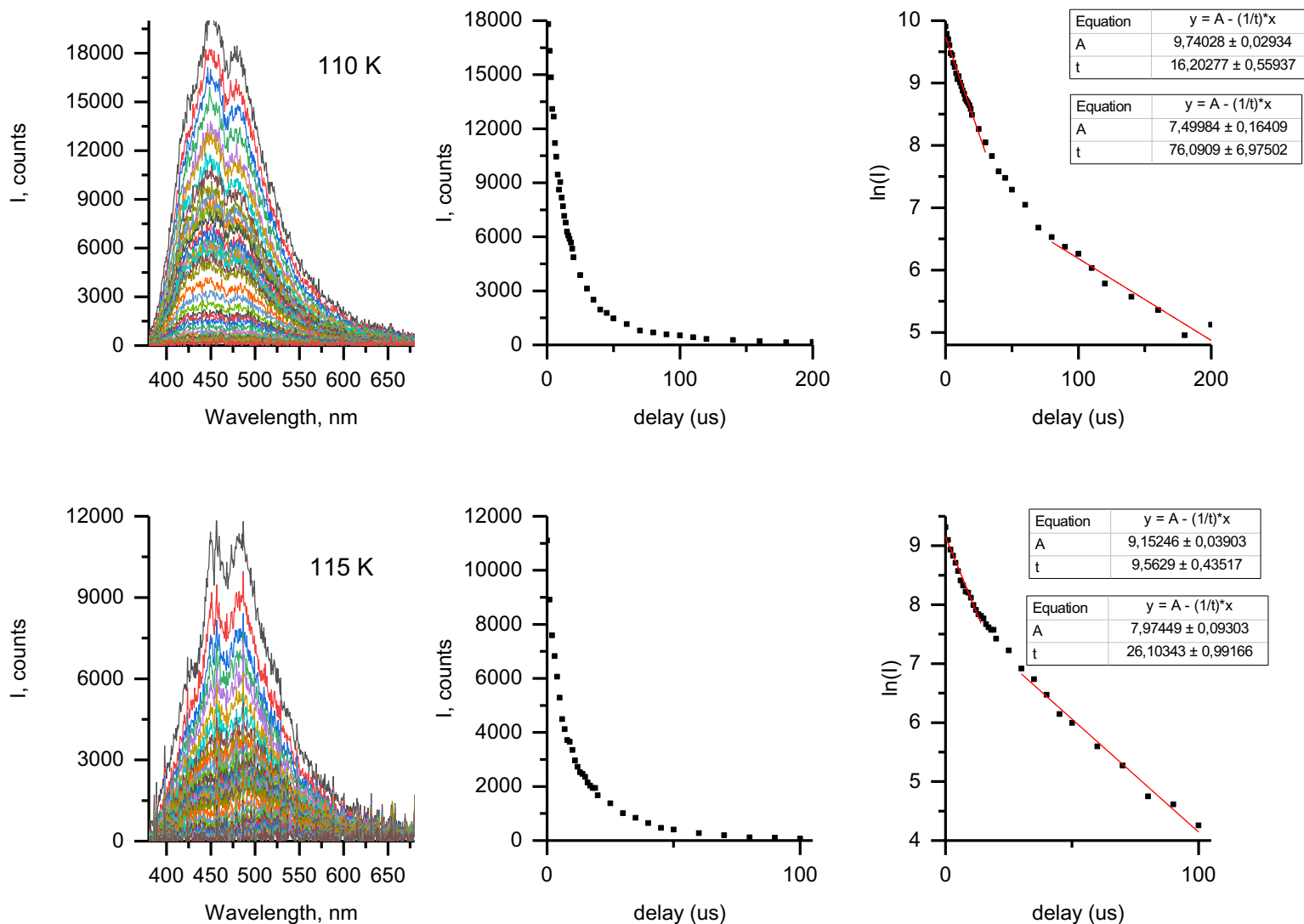


Fig. S21 (continued) Phosphorescence emission spectra at variable delays, emission intensity decays, and $\ln(I)$ vs. delay time plots with fitted linear functions for $[10]\cdot\text{Br}_2$ in methanol/ethanol mixture ($C = 20 \mu\text{M}$) at variable temperatures ($\lambda_{\text{ex}} = 320 \text{ nm}$, gate = $10 \mu\text{s}$).

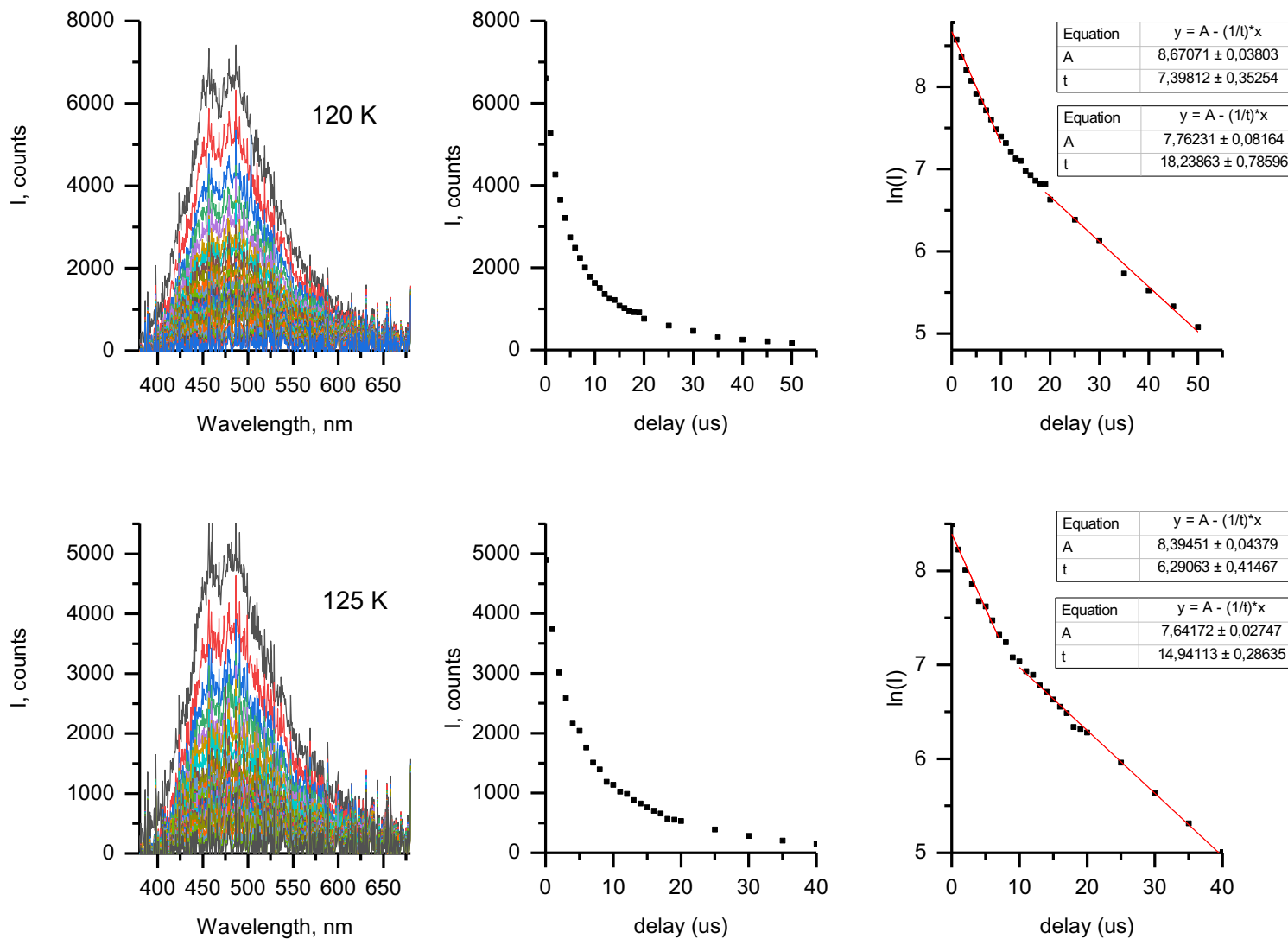


Fig. S21 (continued) Phosphorescence emission spectra at variable delays, emission intensity decays, and $\ln(I)$ vs. delay time plots with fitted linear functions for $[10]\cdot\text{Br}_2$ in methanol/ethanol mixture ($C = 20 \mu\text{M}$) at variable temperatures ($\lambda_{\text{ex}} = 320 \text{ nm}$, gate = 10 μs).

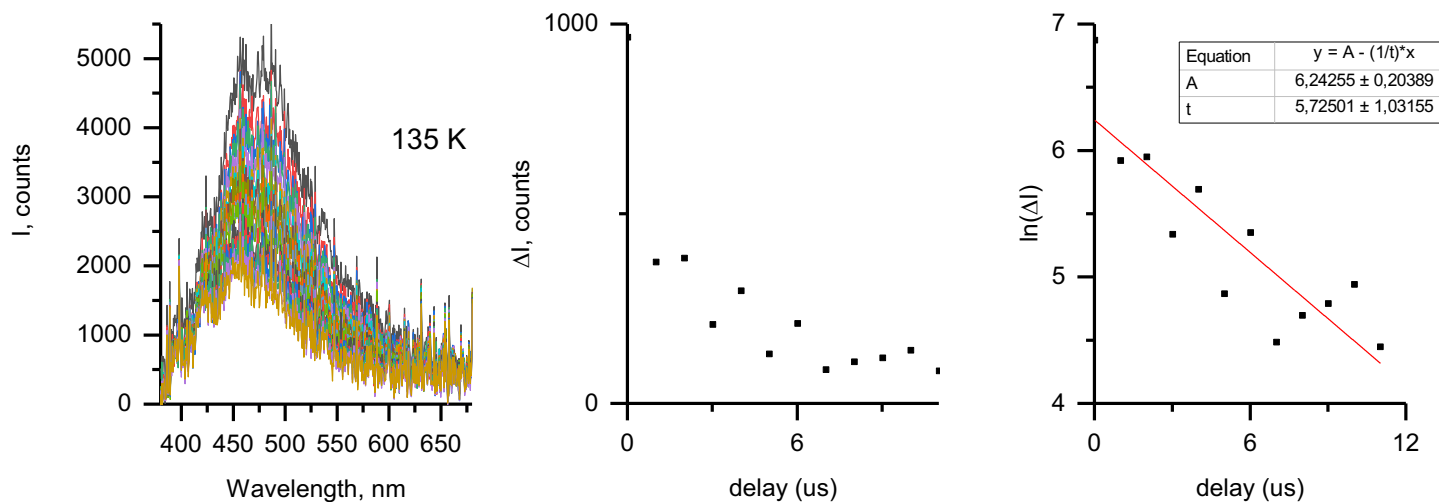
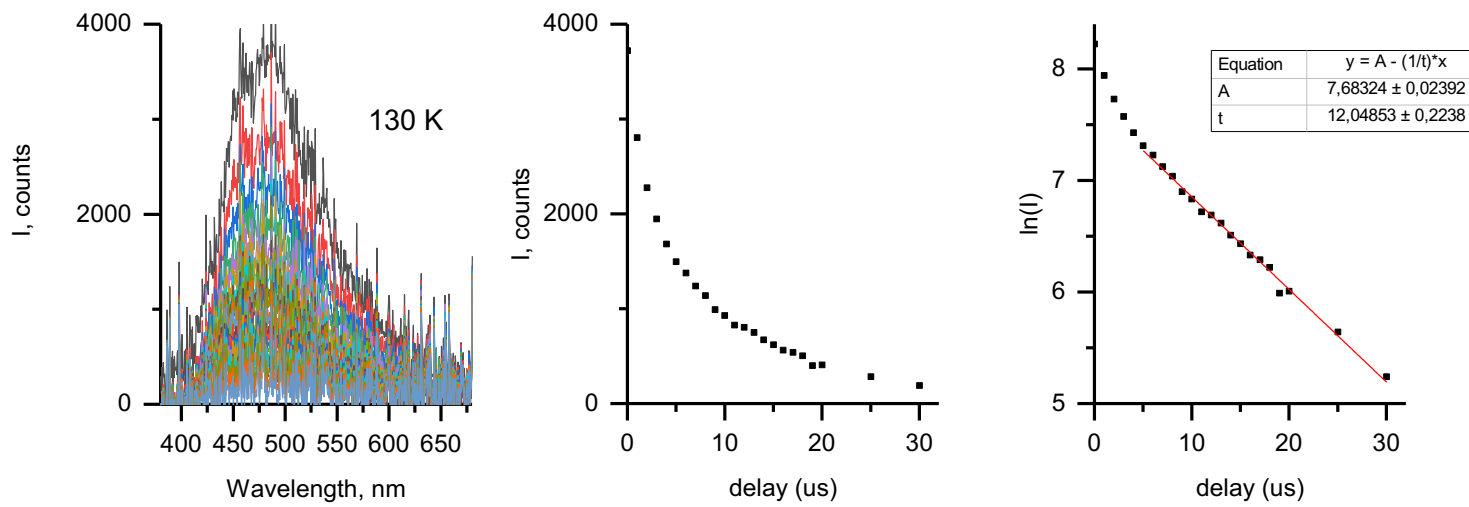


Fig. S21 (continued) Phosphorescence emission spectra at variable delays, emission intensity decays, and $\ln(I)$ vs. delay time plots with fitted linear functions for $[10]\cdot\text{Br}_2$ in methanol/ethanol mixture ($C = 20\text{ }\mu\text{M}$) at variable temperatures ($\lambda_{\text{ex}} = 320\text{ nm}$, gate = $10\text{ }\mu\text{s}$).

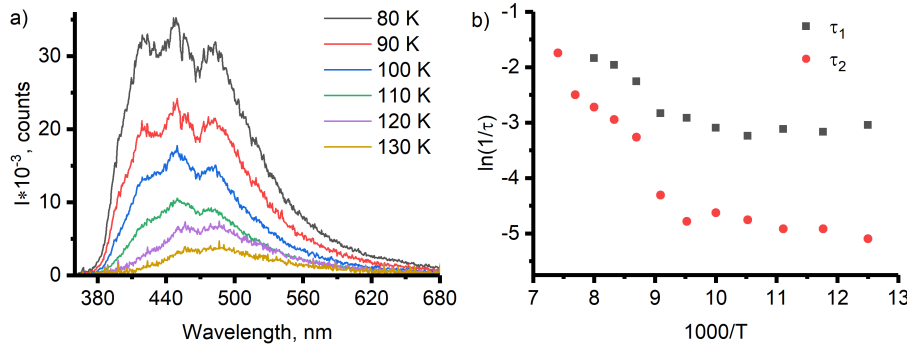


Fig. S22 Phosphorescence emission spectra of **[10]·Br₂** at variable temperatures (delay 20 ns, gate 10 μs, a) and Arrhenius plots of $\ln(1/\tau)$ vs. $1/T$ (b) in methanol/ethanol mixture (C = 20 μM, $\lambda_{\text{ex}} = 320$ nm).

In emission spectra of **[7,9]·Br₂** at temperatures ≥ 120 K, the second emission band ($\lambda_{\text{max}} \approx 500$ nm) appears upon continuous irradiation of the samples, whereas intensity of the first peak diminishes (Fig. S23). After standing in darkness for about 5 minutes, the emission spectrum returns to its original shape.

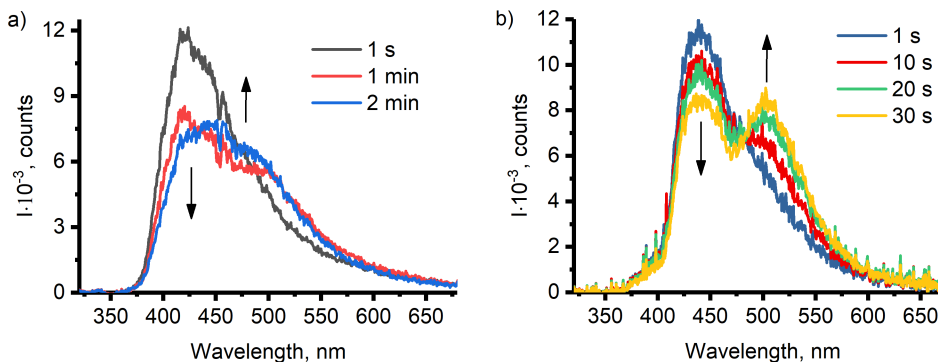
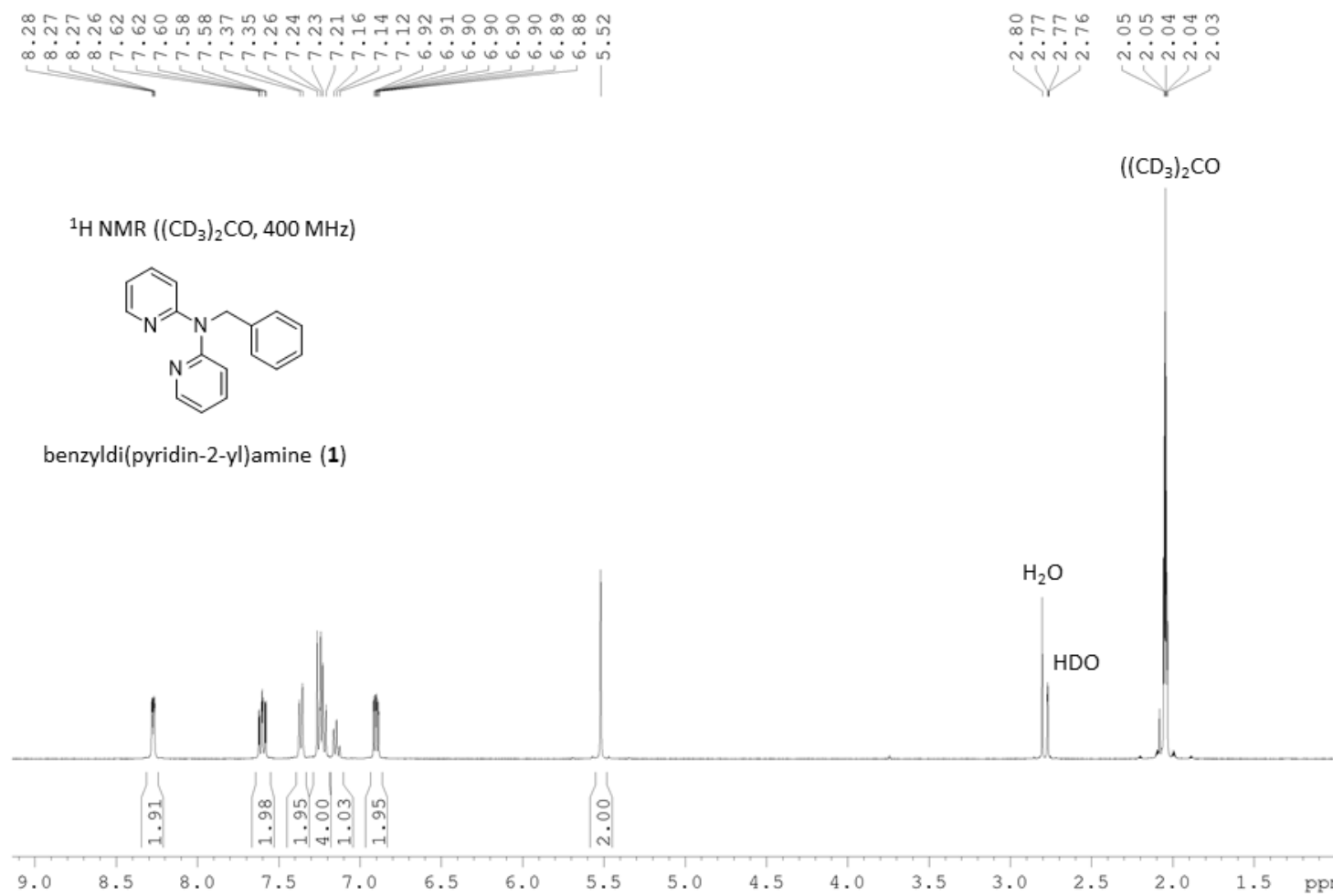


Fig. S23 Phosphorescence emission spectra of **[7]·Br₂** (gate = 1 ms, a) and **[9]·Br₂** (gate = 300 μs, b) in methanol/ethanol solution after continuous irradiation by excitation source for various time (120 K, C = 20 μM, $\lambda_{\text{ex}} = 320$ nm, delay = 20 ns). Arrows indicate changes upon irradiation.

S5. ^1H NMR spectra of 1-10 and S3-S4

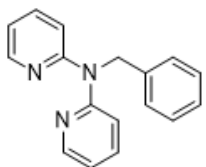


8.28
8.27
8.27
8.26

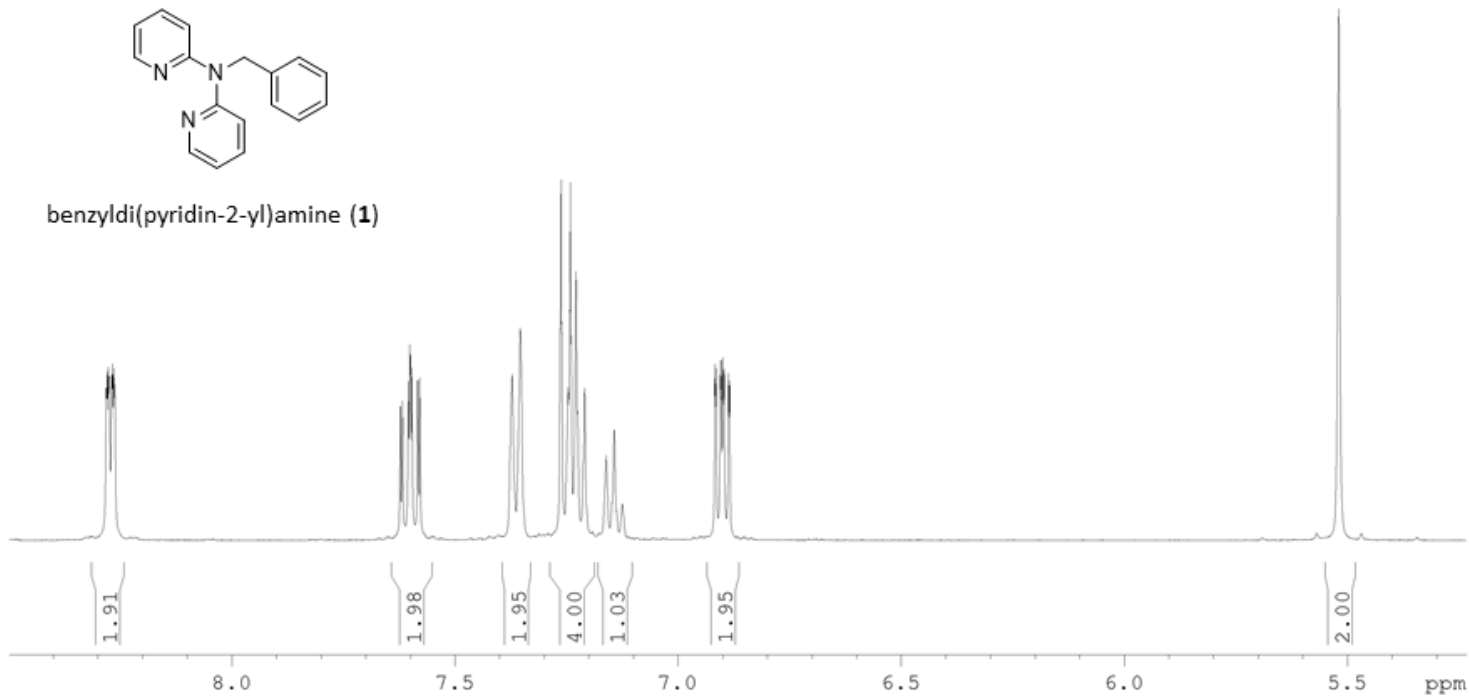
7.62
7.62
7.60
7.58
7.58
7.58
7.37
7.35
7.26
7.24
7.23
7.21
7.16
7.14
7.12
6.92
6.91
6.90
6.90
6.90
6.89
6.88

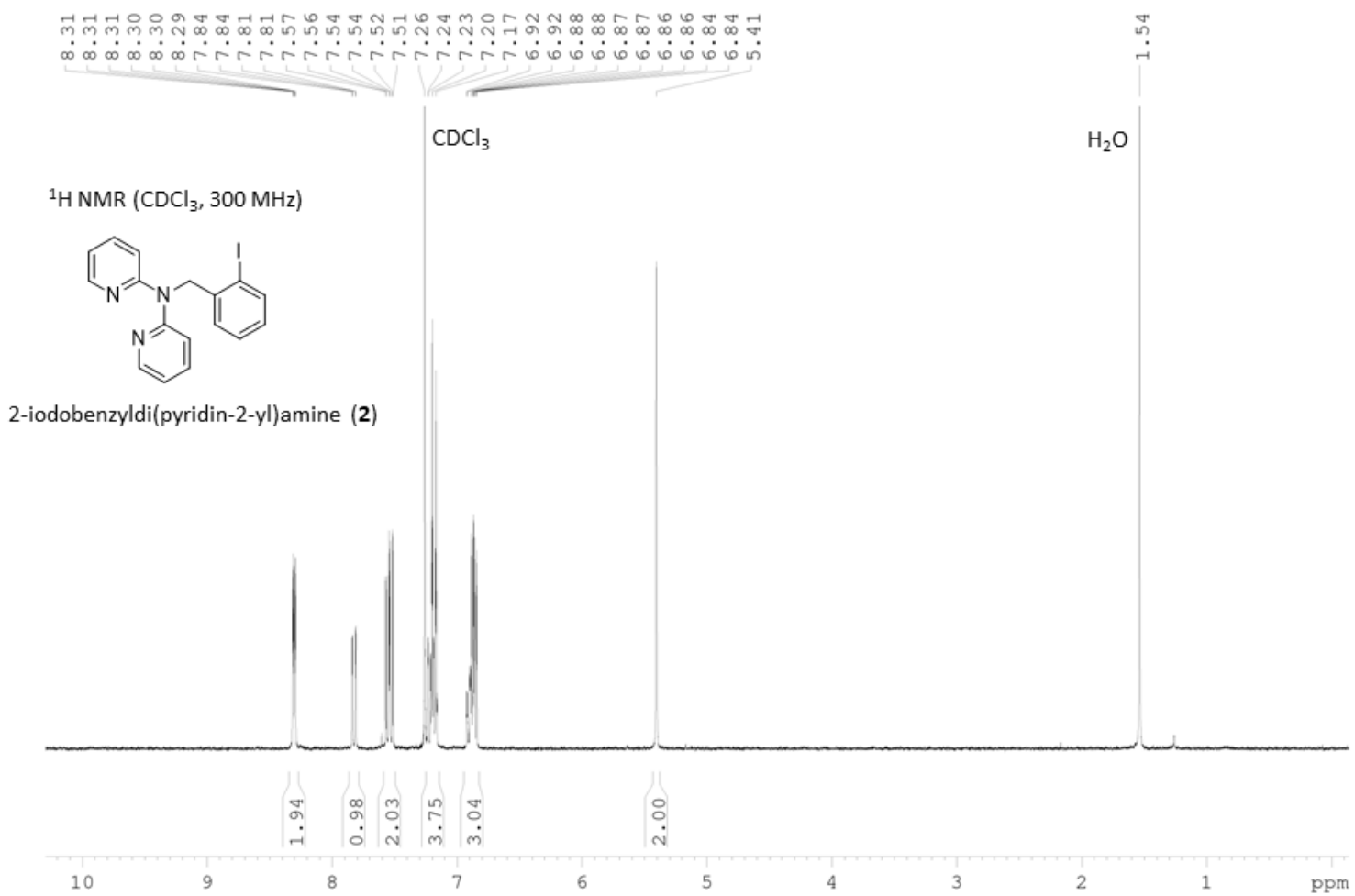
5.52

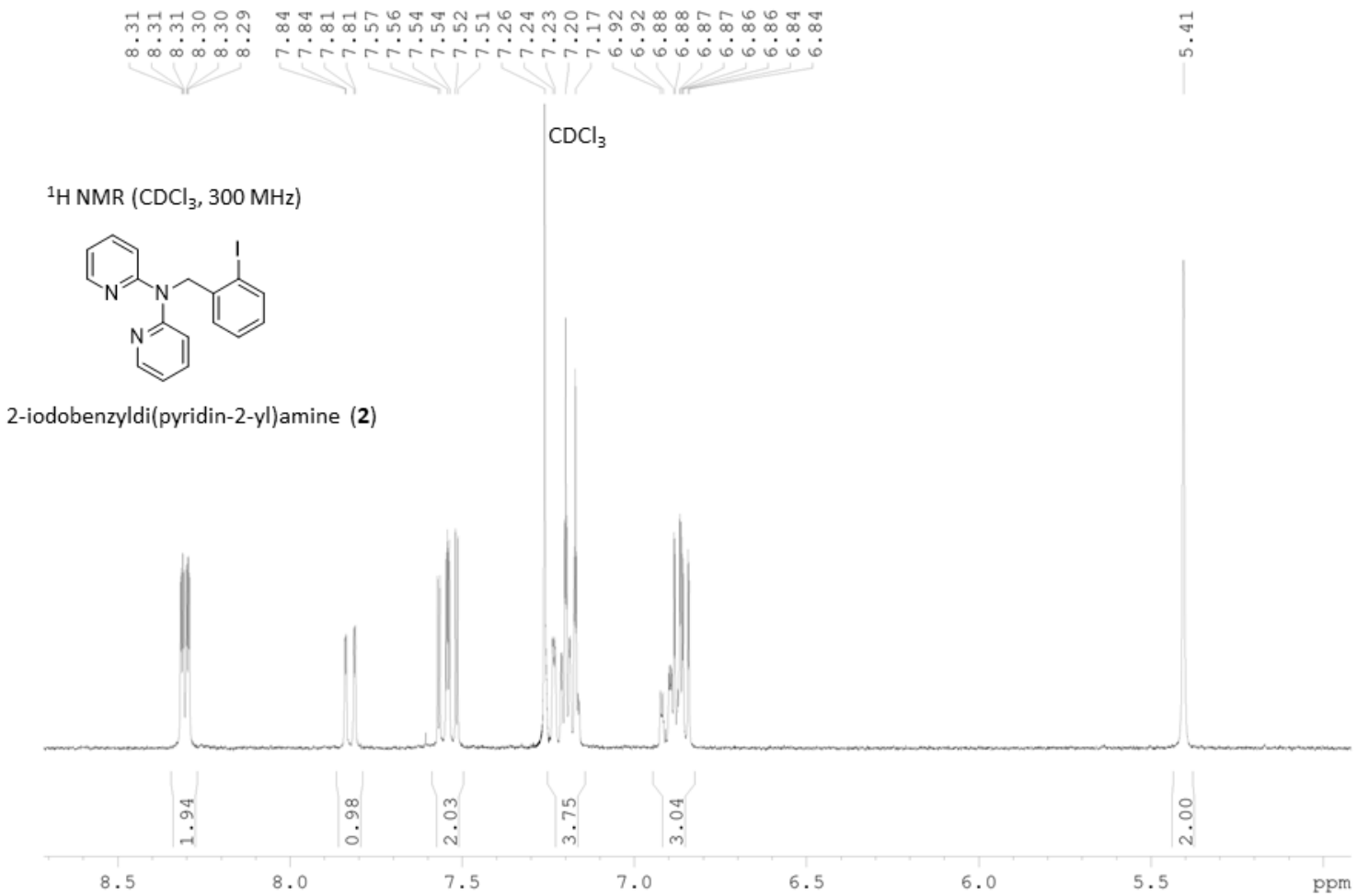
^1H NMR ($(\text{CD}_3)_2\text{CO}$, 400 MHz)

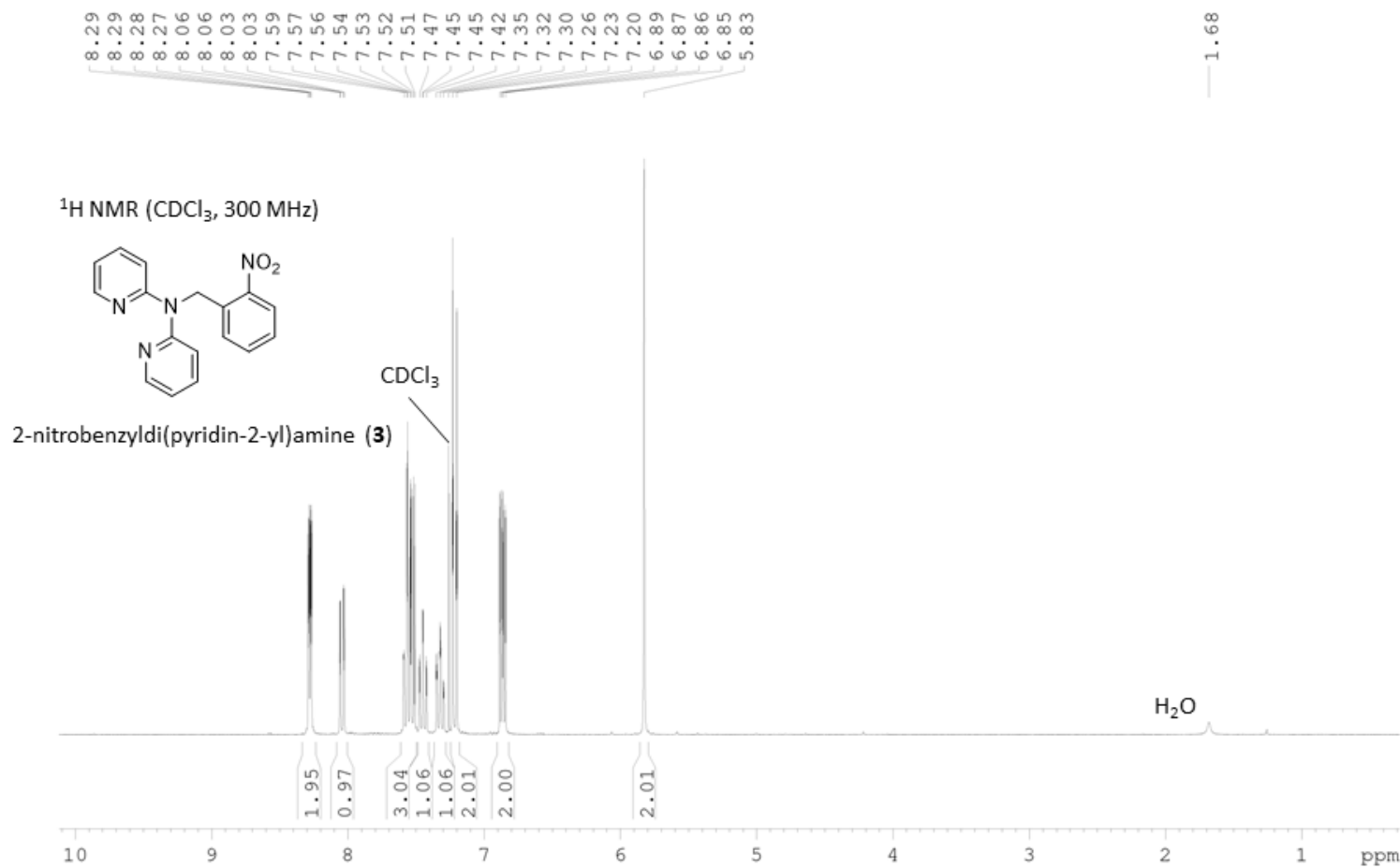


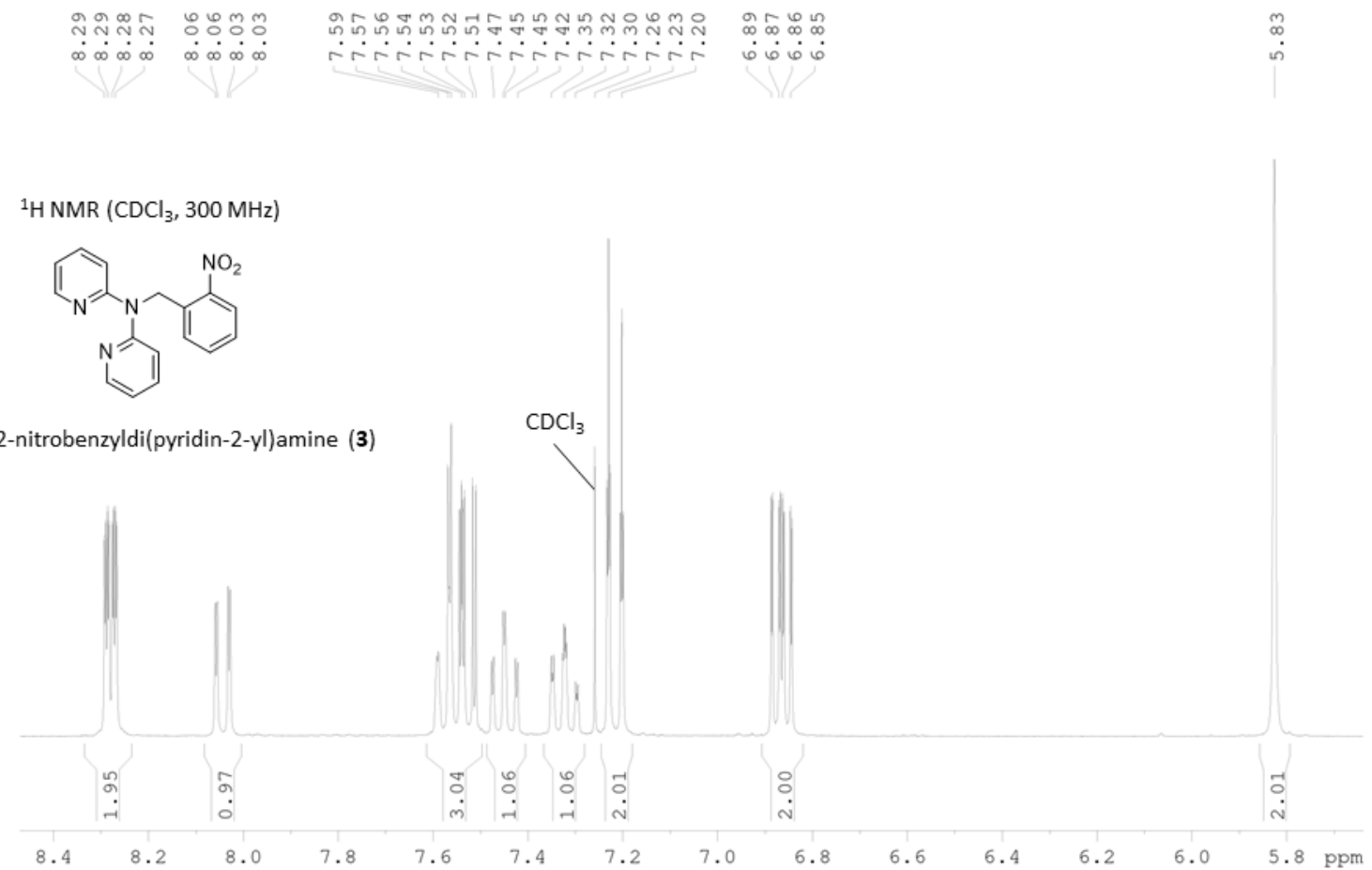
benzylidipyridin-2-ylamine (**1**)

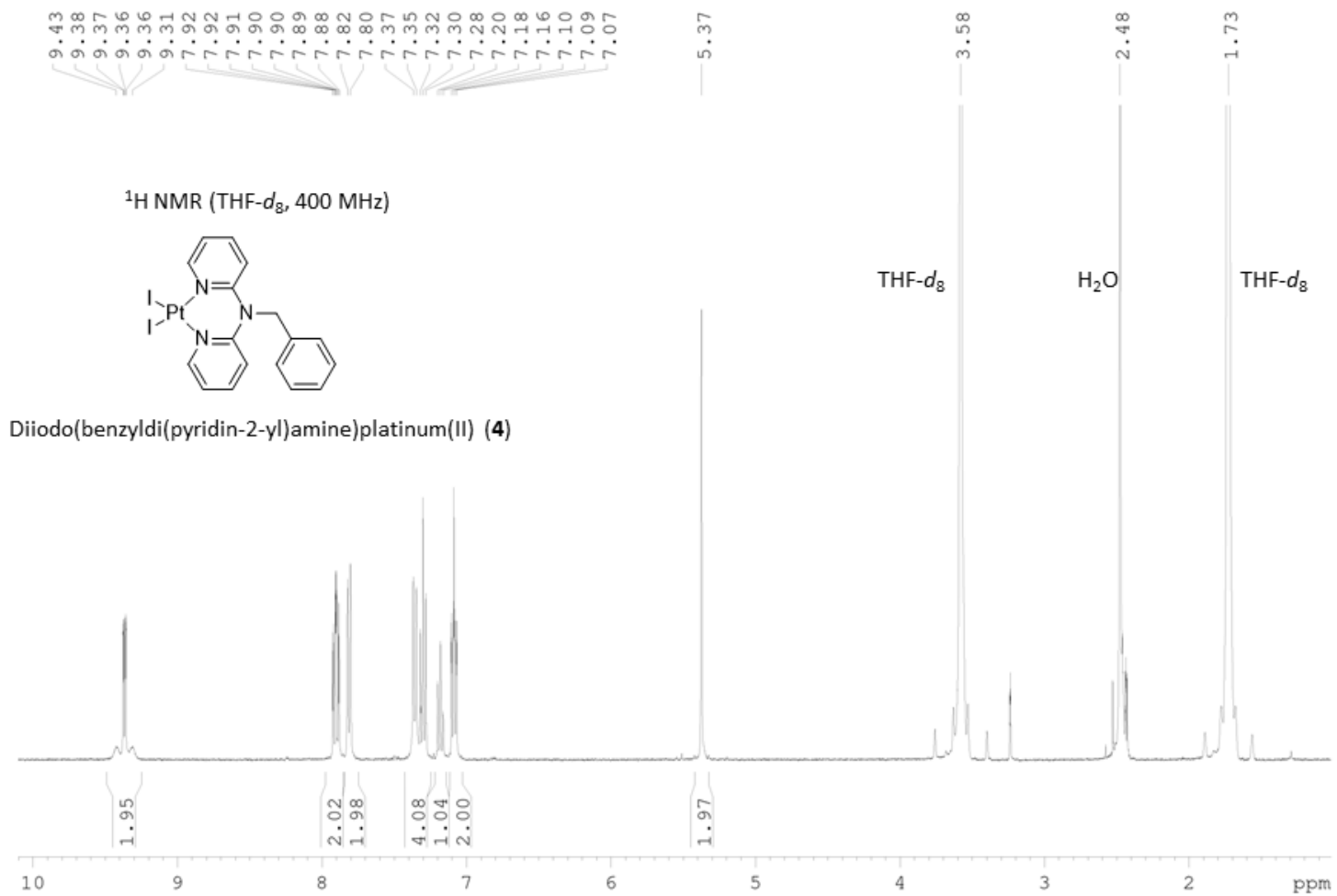


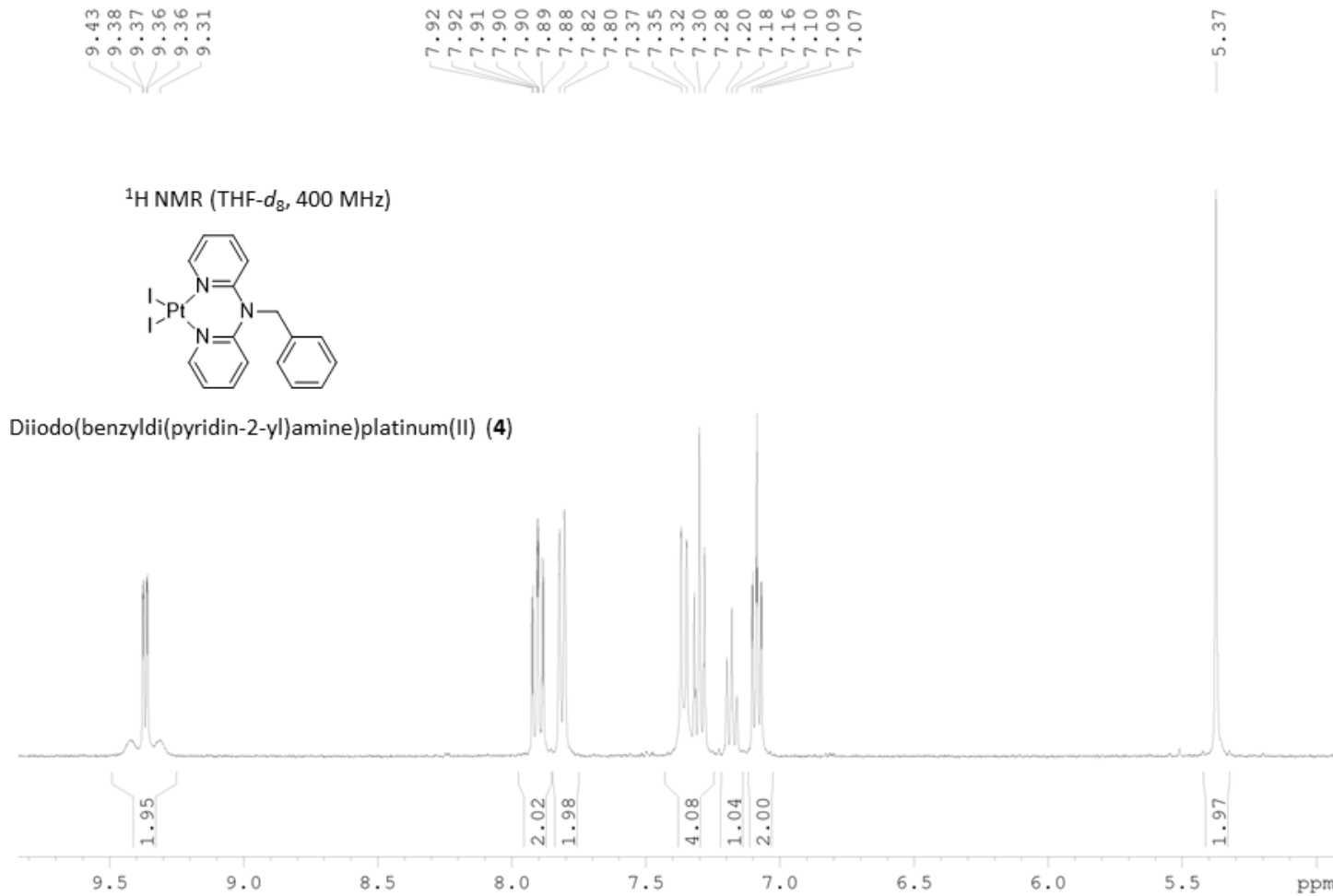


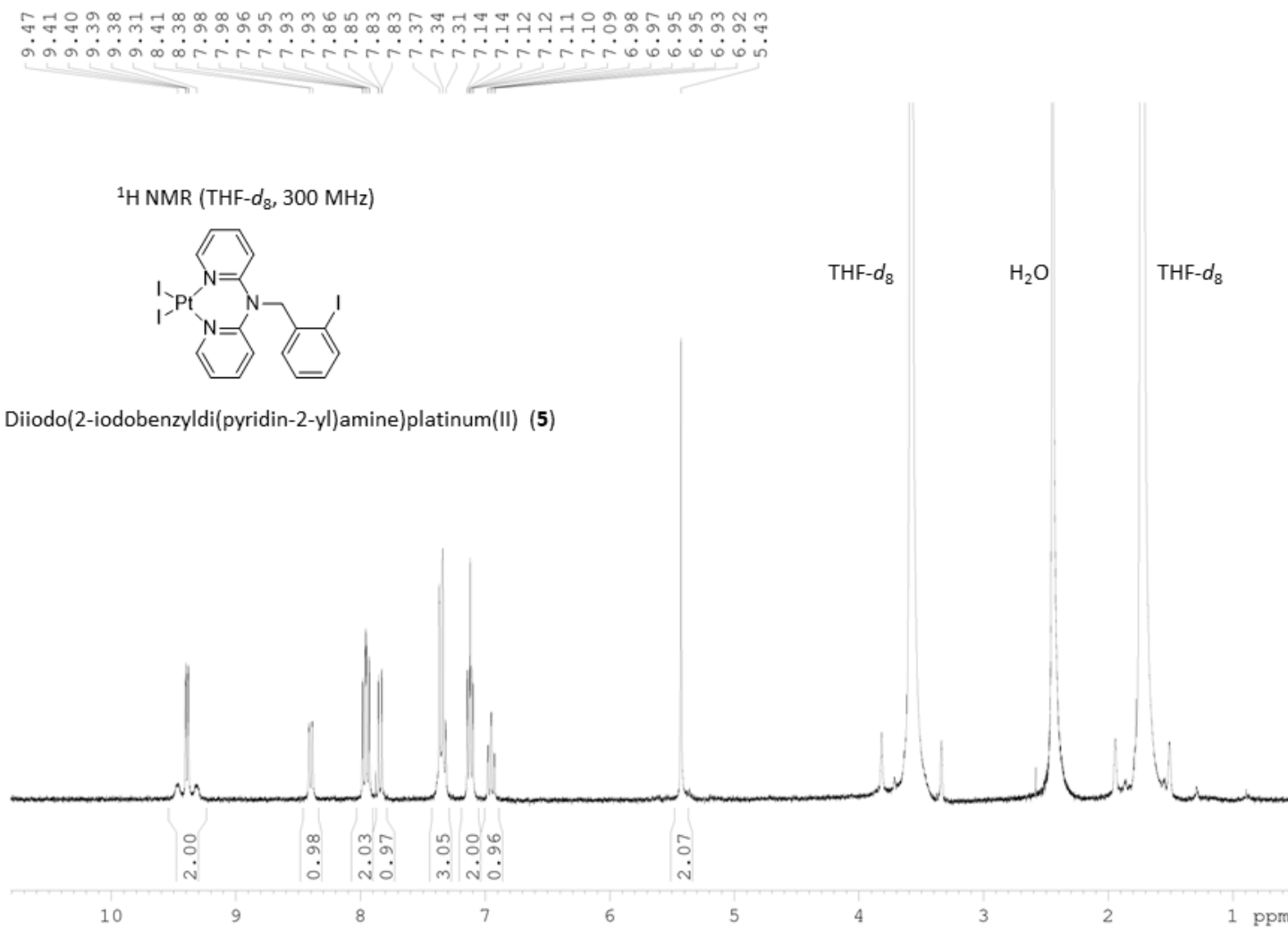










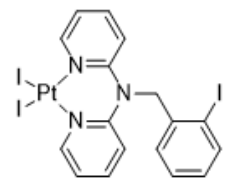


9.47
9.41
9.40
9.39
9.38
9.31

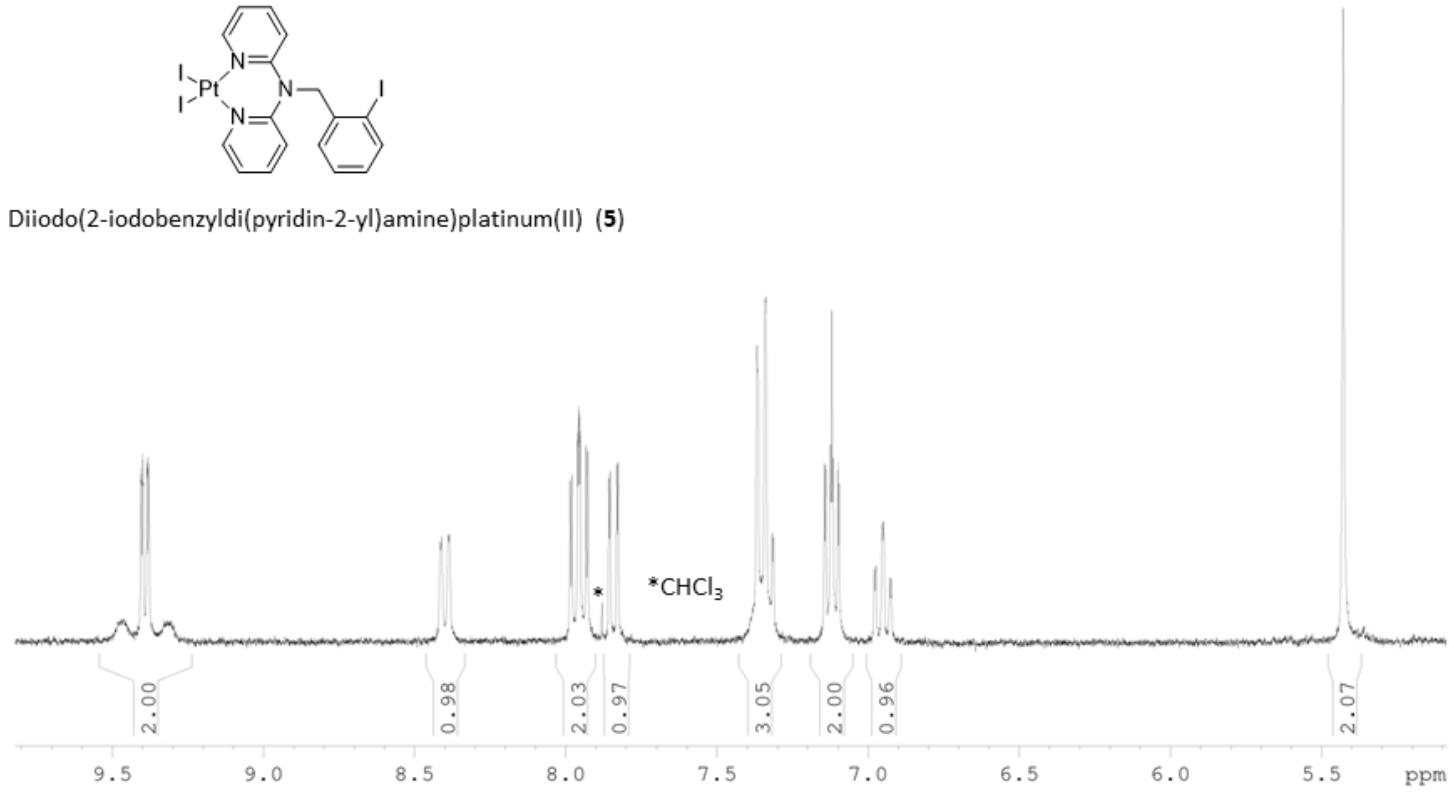
8.41
8.38
7.98
7.98
7.96
7.95
7.93
7.93
7.86
7.85
7.83
7.83
7.37
7.34
7.31
7.14
7.14
7.12
7.12
7.11
7.10
7.09
6.98
6.97
6.95
6.95
6.93
6.92

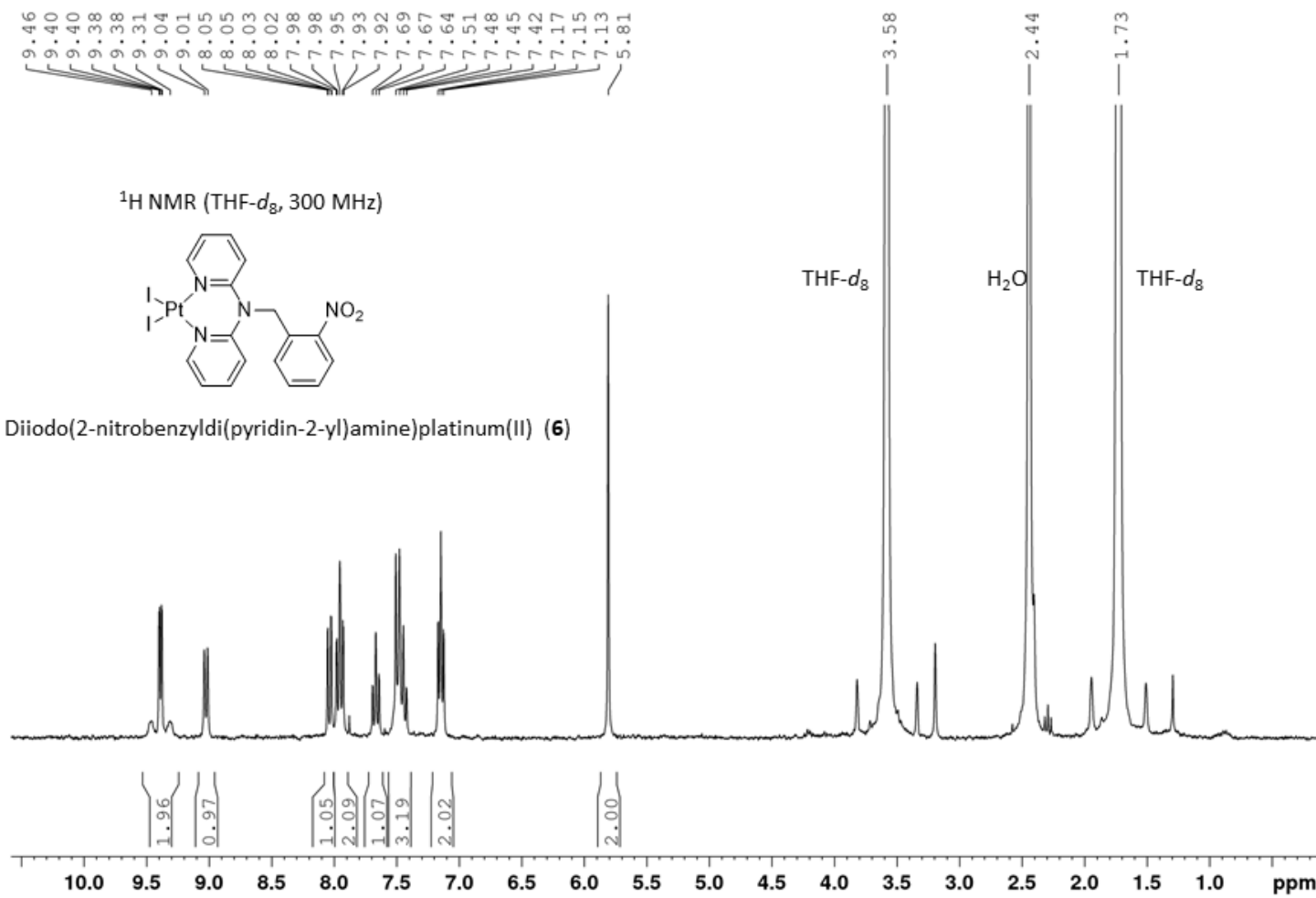
5.43

^1H NMR (THF- d_8 , 300 MHz)



Diiodo(2-iodobenzylidipyridin-2-yl)amineplatinum(II) (**5**)



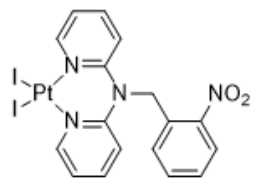


9.46
9.40
9.40
9.38
9.38
9.31
9.04
9.01

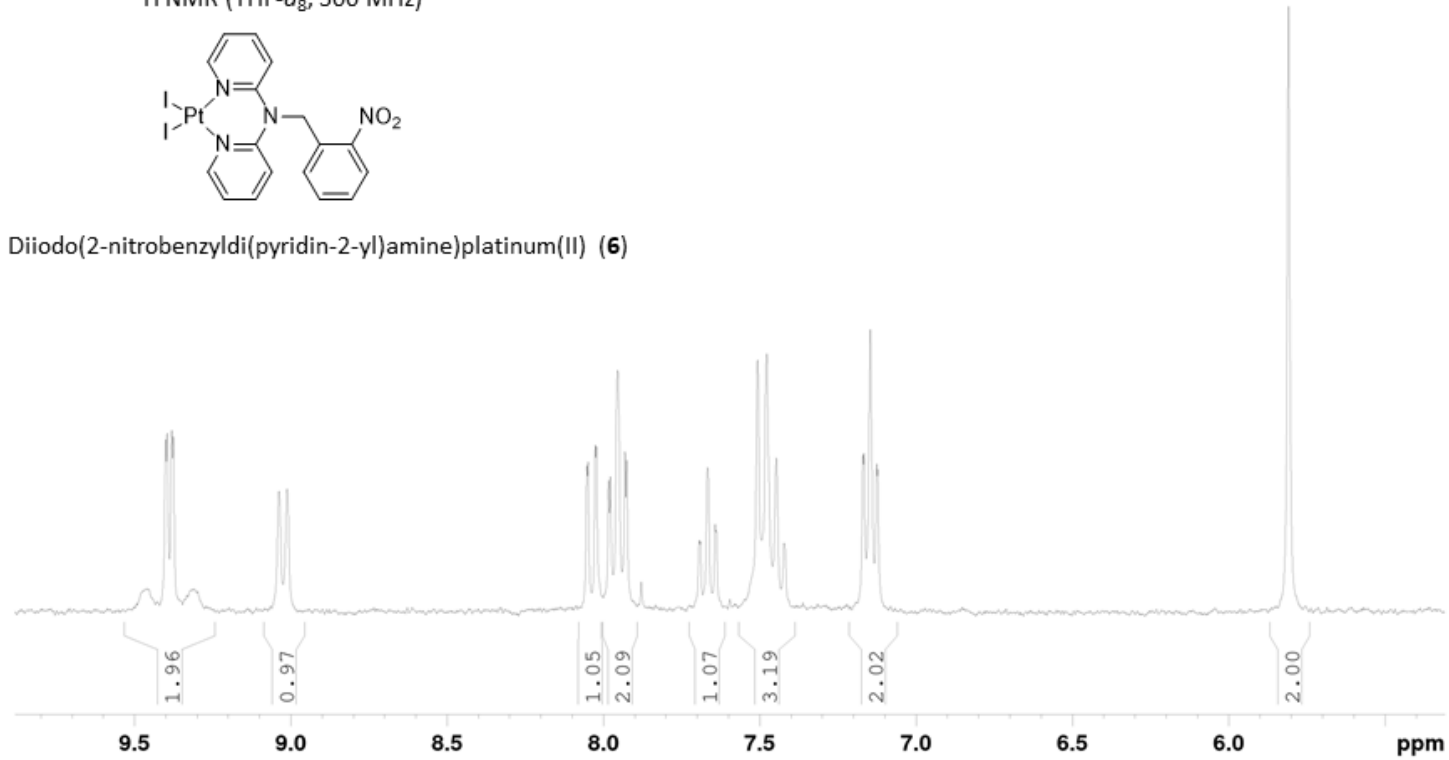
8.05
8.05
8.03
8.02
7.98
7.98
7.95
7.95
7.93
7.92
7.69
7.67
7.64
7.51
7.48
7.45
7.42
7.17
7.15
7.13

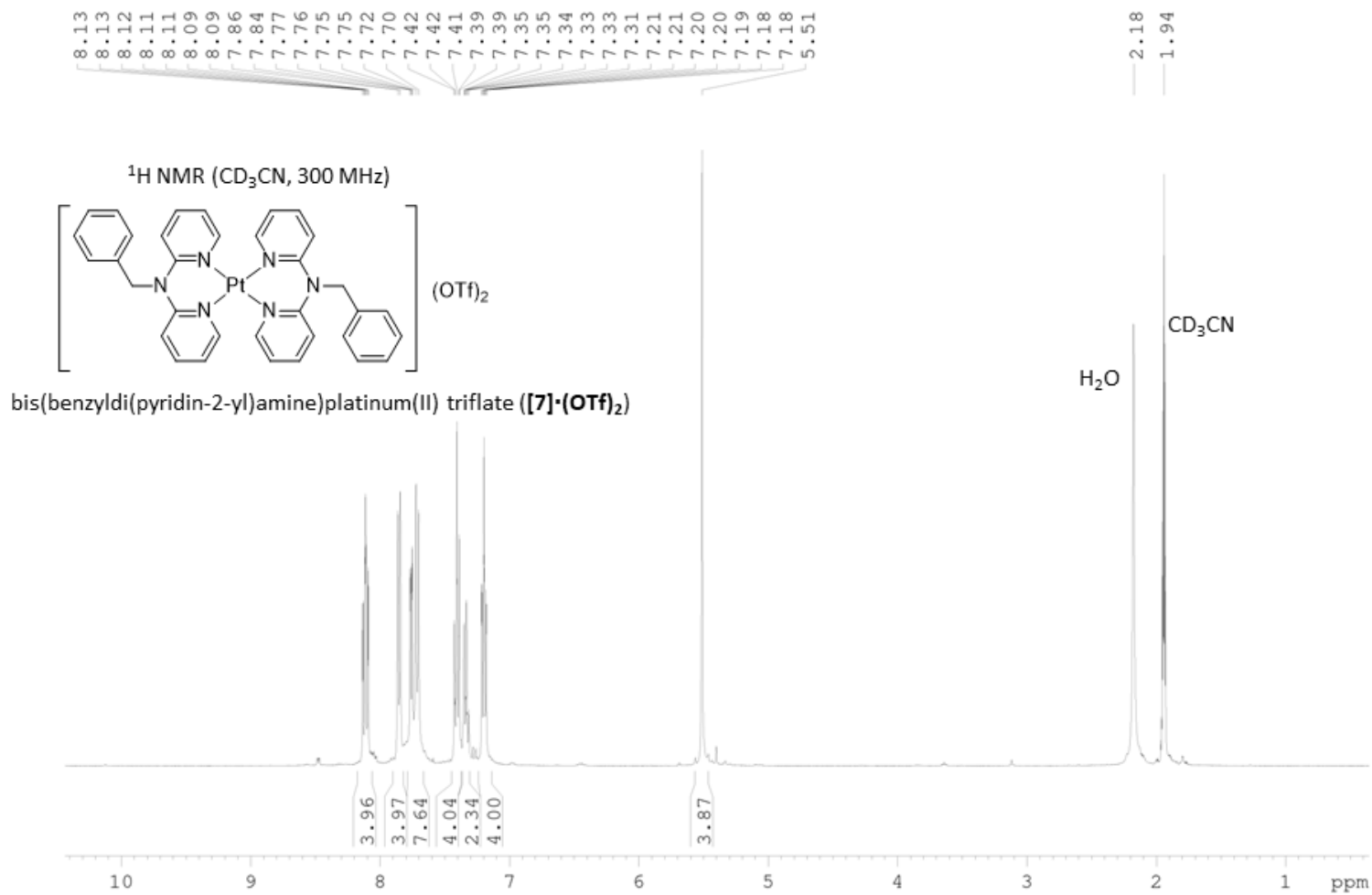
5.81

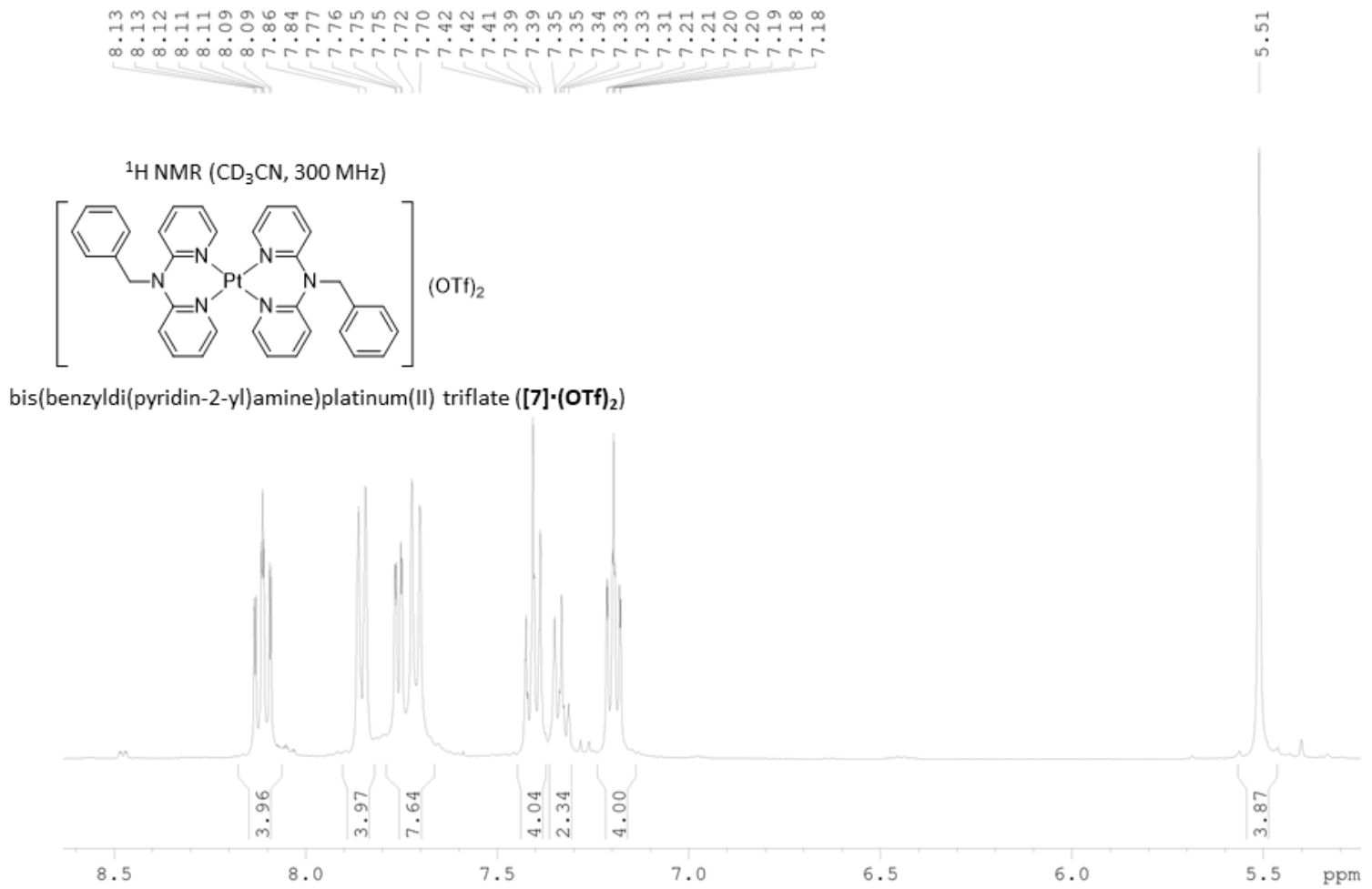
^1H NMR (THF- d_8 , 300 MHz)

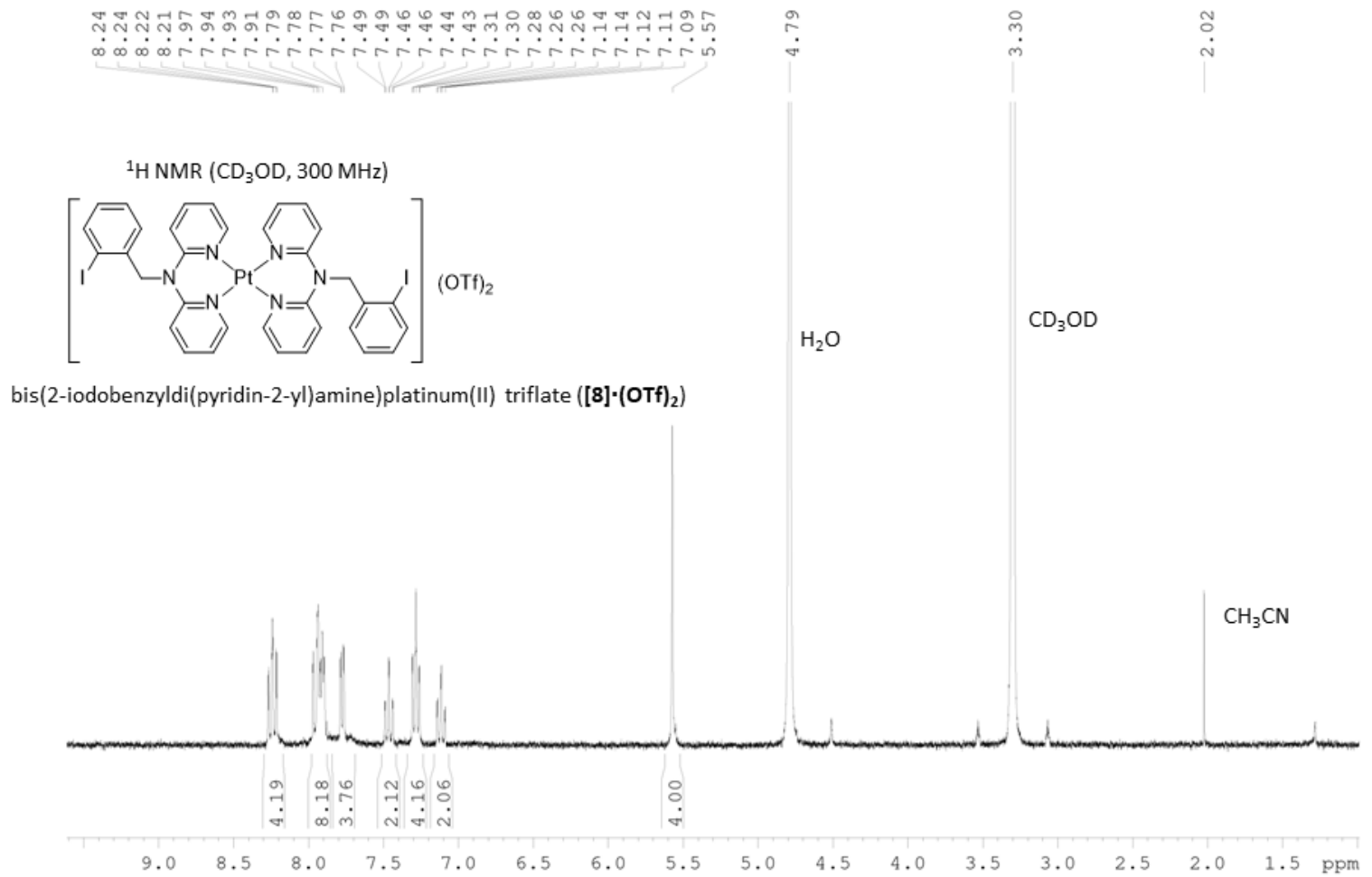


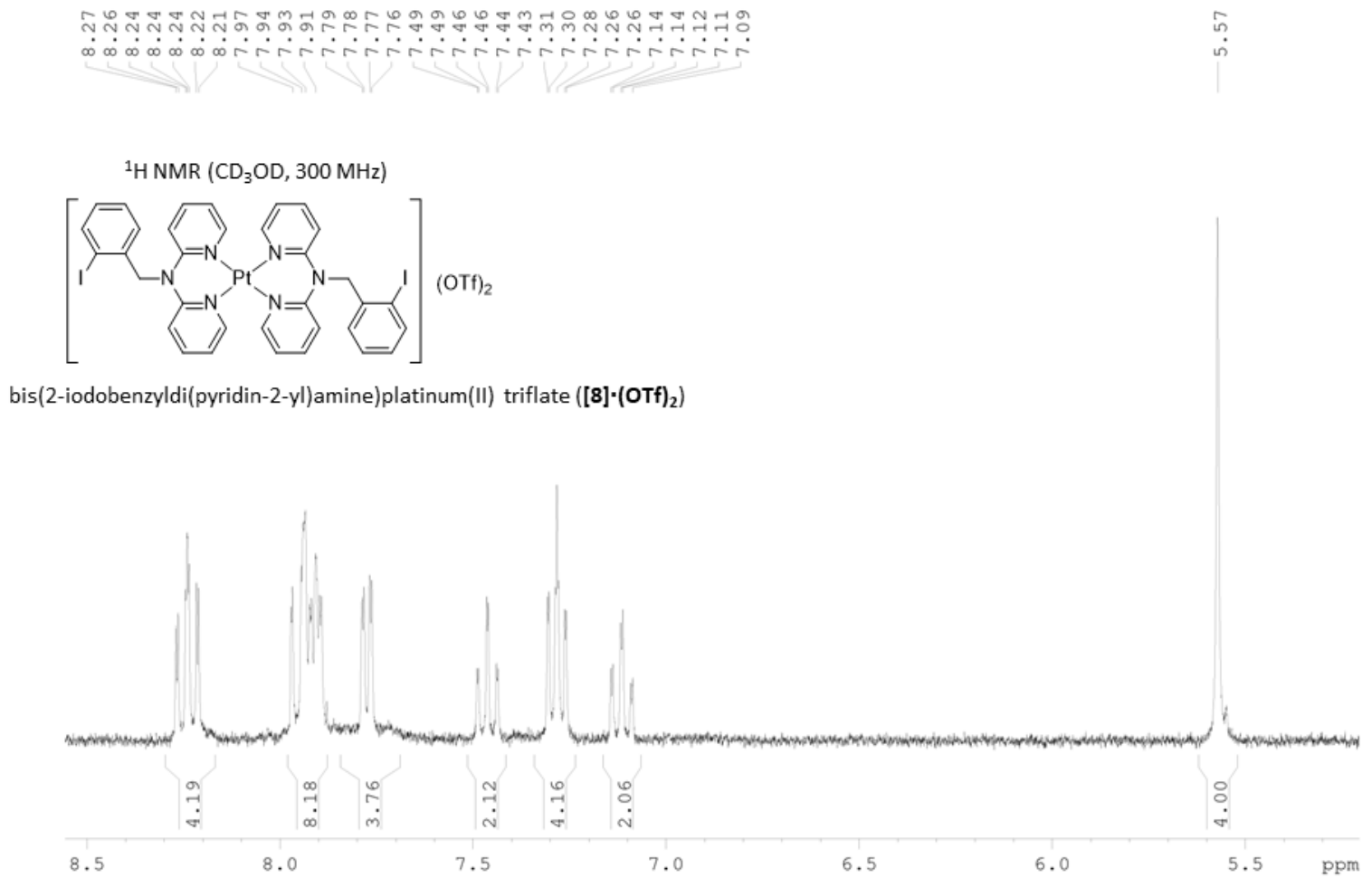
Diiodo(2-nitrobenzylidipyridin-2-yl)amineplatinum(II) (**6**)

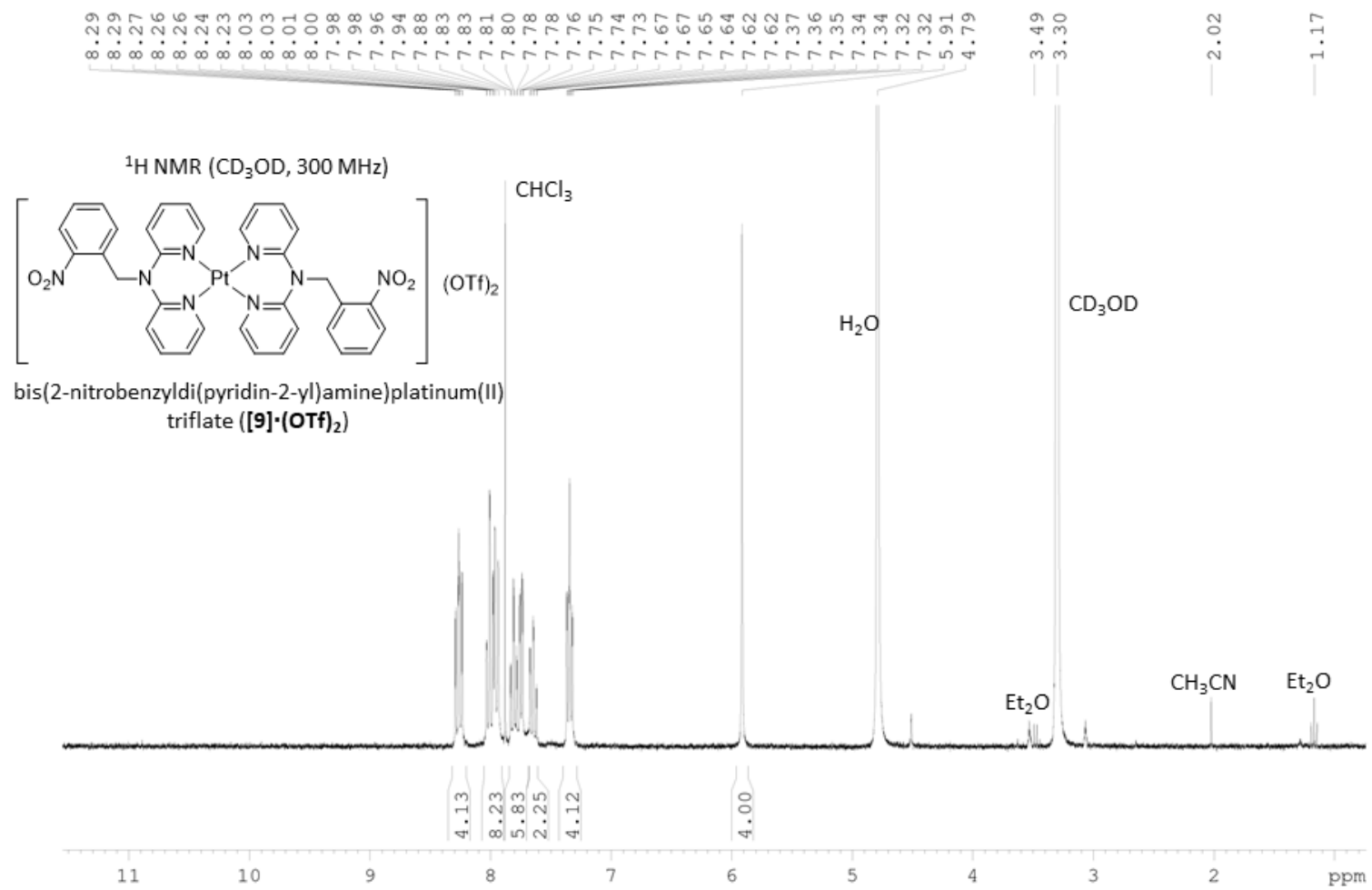


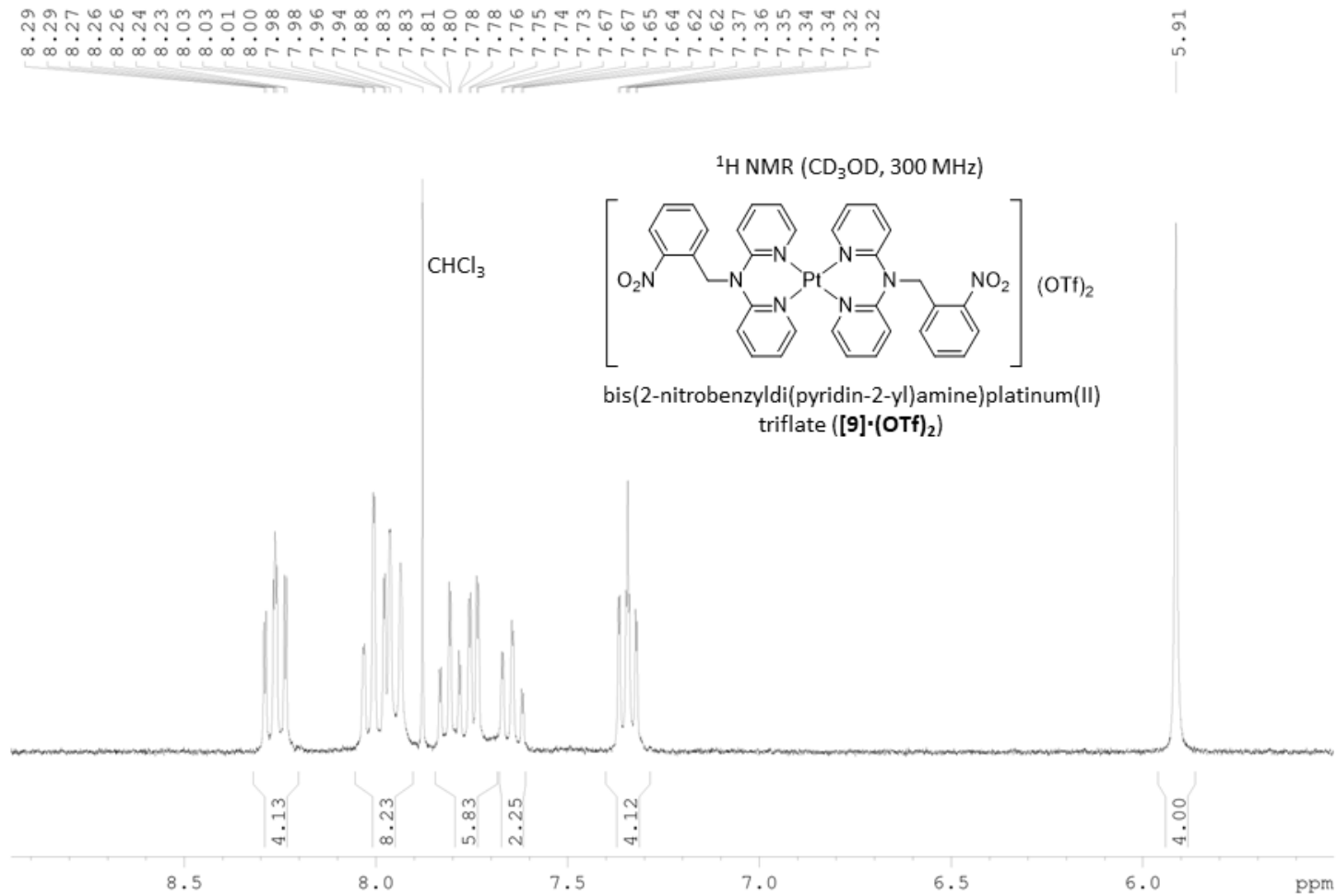


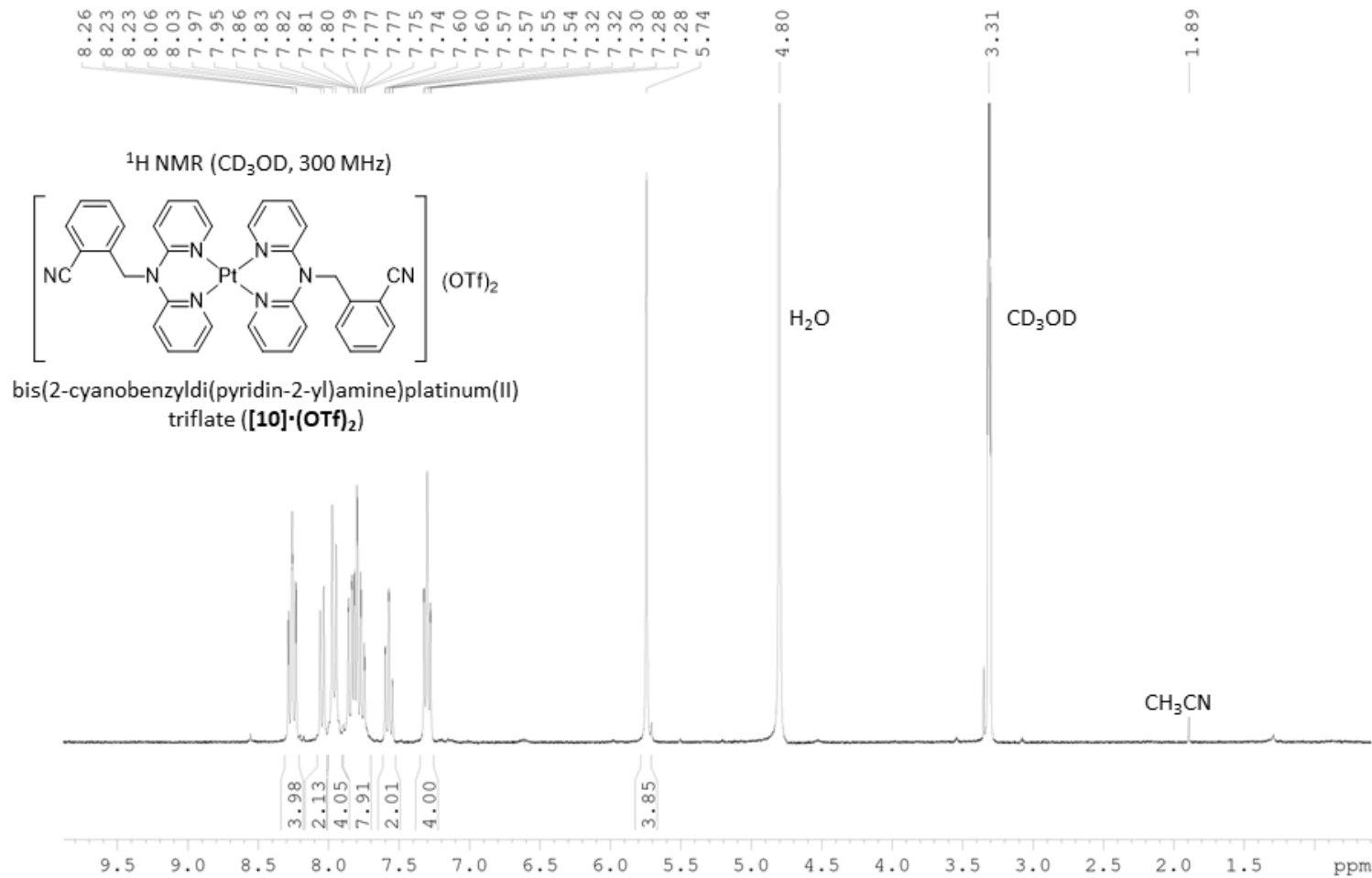


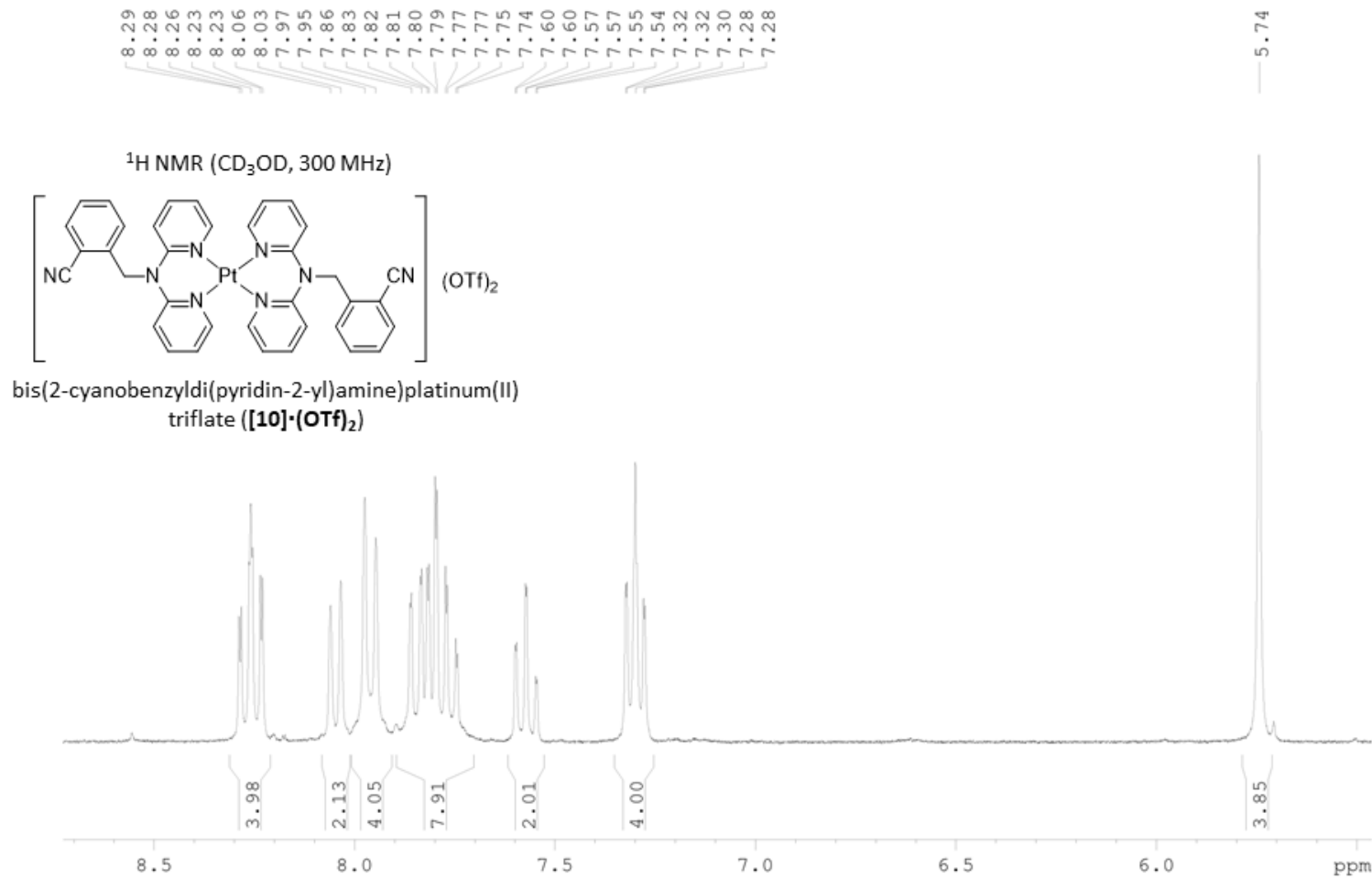


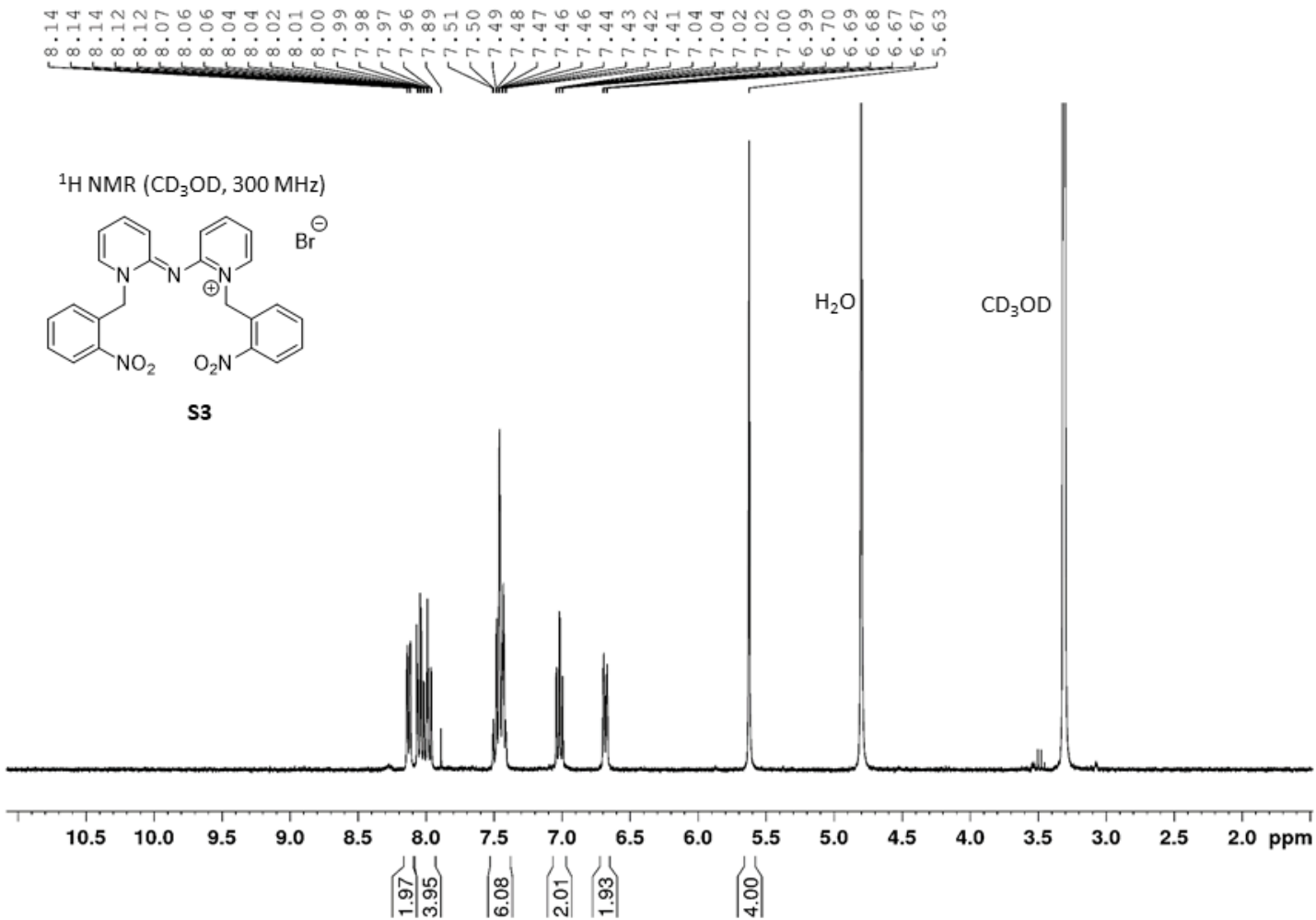


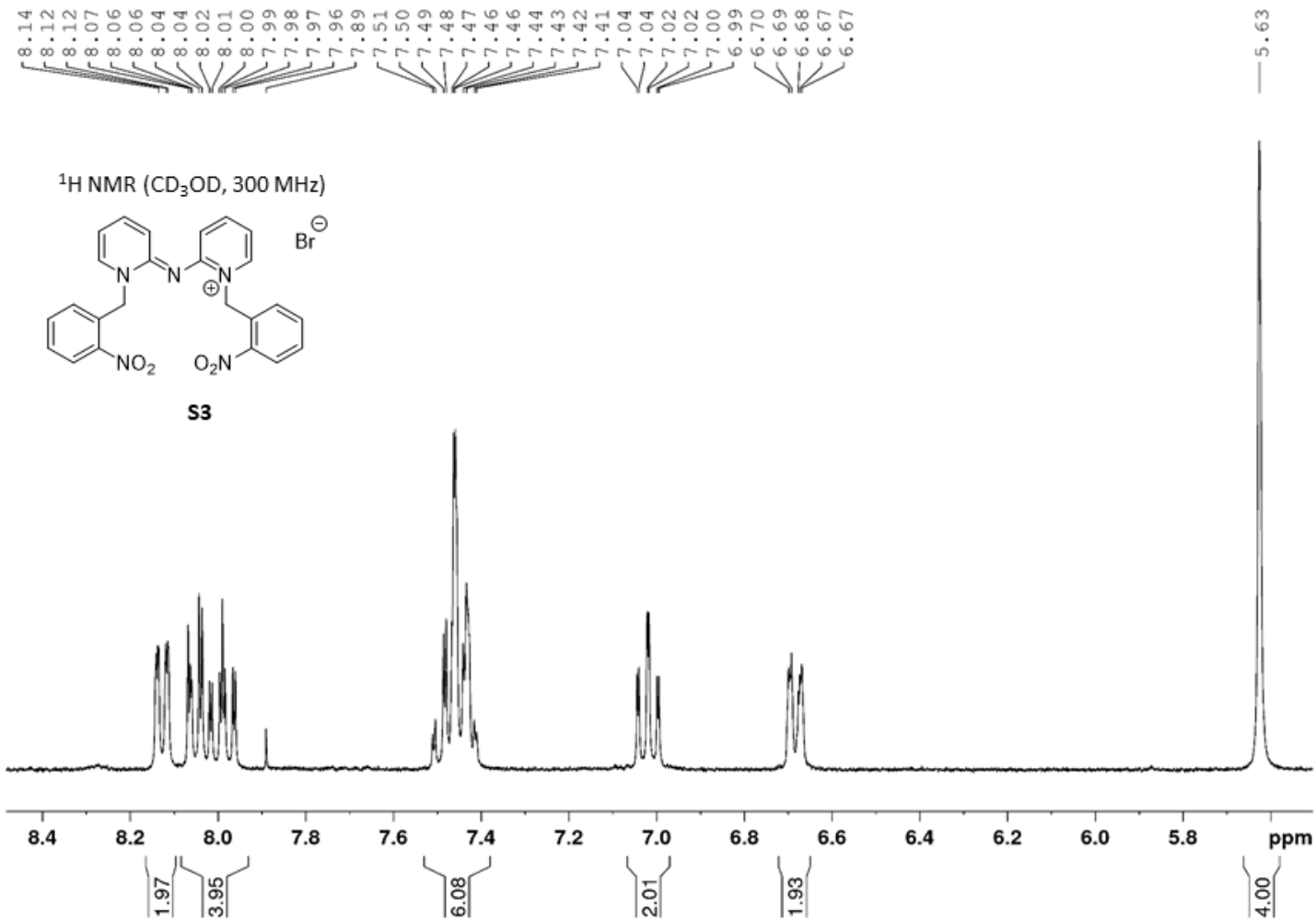


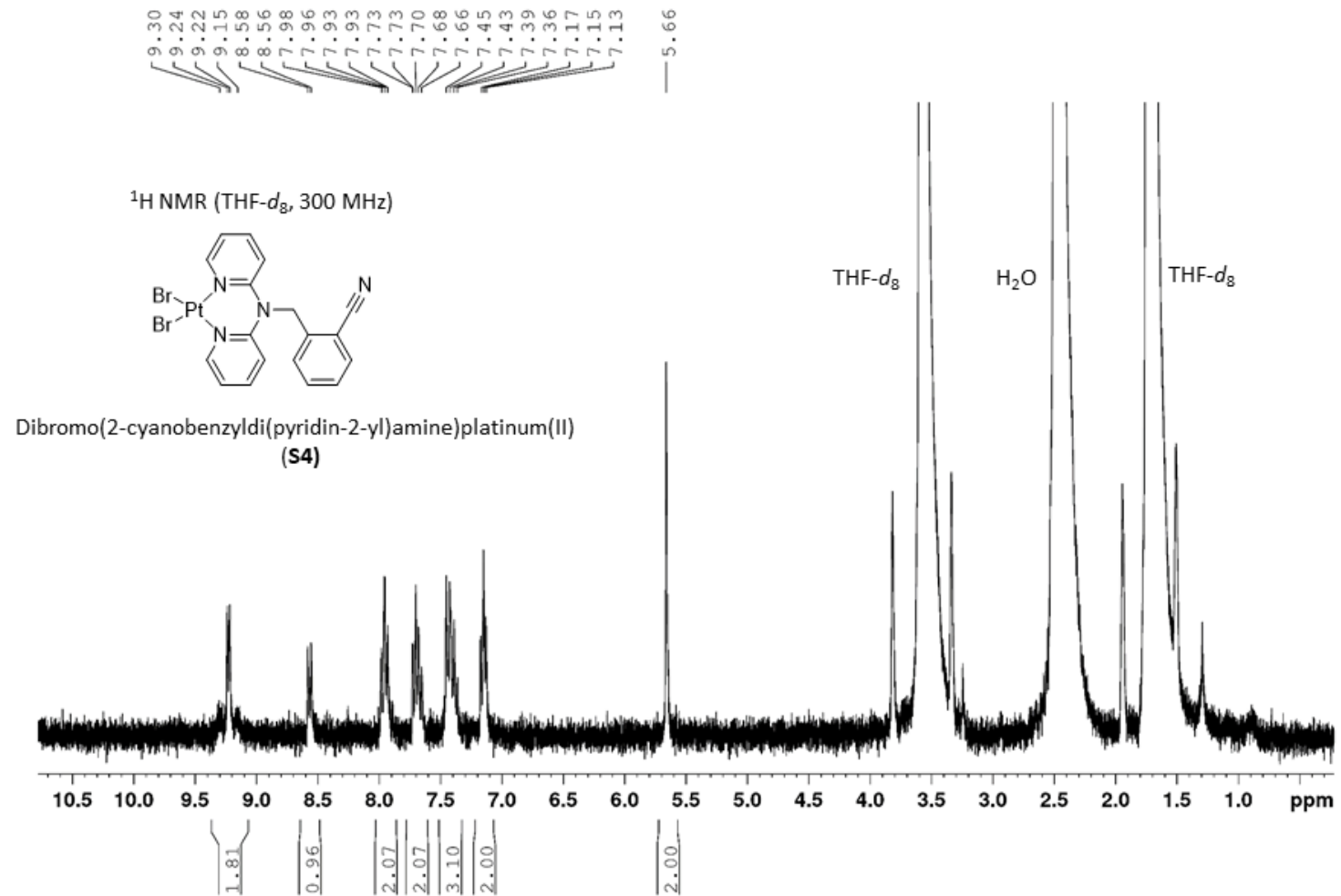












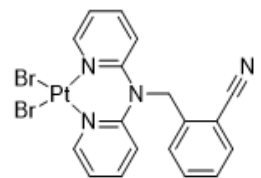
9.30
9.24
9.22
9.15

8.58
8.56

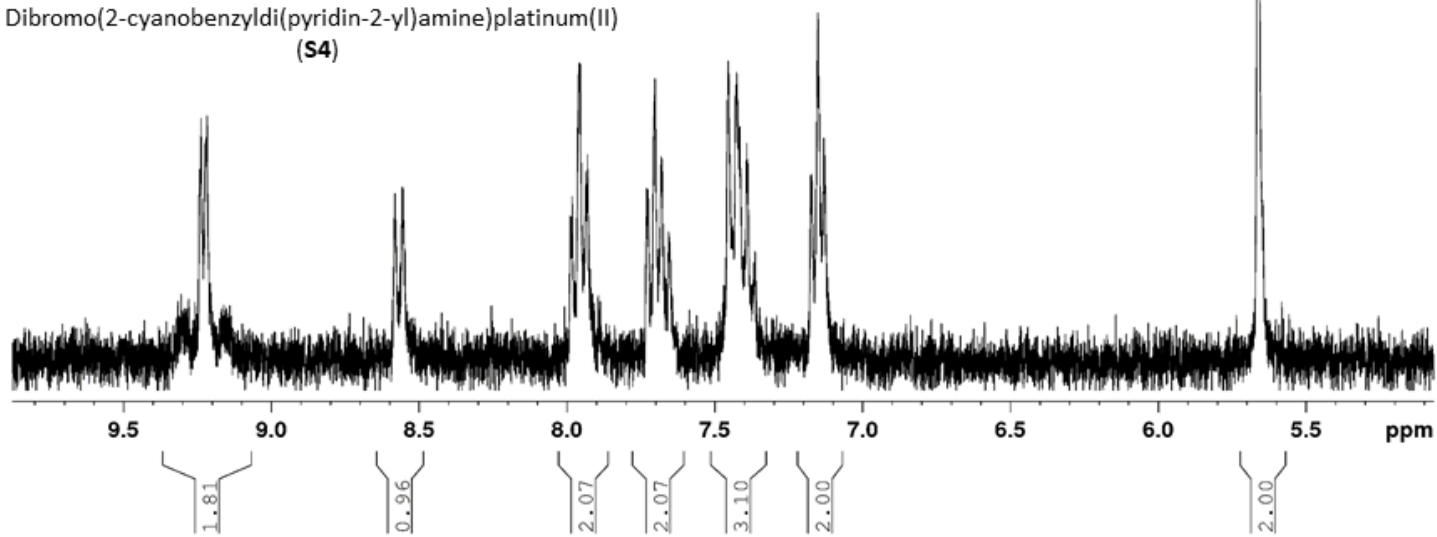
7.98
7.96
7.93
7.93
7.73
7.73
7.70
7.68
7.66
7.45
7.43
7.39
7.36
7.17
7.15
7.13

5.66

¹H NMR (THF-*d*₈, 300 MHz)



Dibromo(2-cyanobenzylidipyridin-2-yl)amineplatinum(II)
(S4)



S6. Crystallographic data for 1-10 and S2-S4

Table S2 Crystal data for 1-10

	1	2	3	4	5	6	[7]·(OTf)₂	[8]·(OTf)₂	[9]·Br₂	[10]·(OTf)₂
empirical formula	C ₁₇ H ₁₅ N ₃	C ₁₇ H ₁₄ IN ₃	C ₁₇ H ₁₄ N ₄ O ₂	C ₁₇ H ₁₅ I ₂ N ₃ Pt	C ₁₇ H ₁₄ I ₃ N ₃ Pt	C ₁₇ H ₁₄ I ₂ N ₄ O ₂ Pt	C ₃₆ H ₃₀ F ₆ N ₆ O ₆ PtS ₂	C ₃₆ H ₂₈ F ₆ I ₂ N ₆ O ₆ PtS ₂	C ₃₄ H ₃₆ Br ₂ N ₈ O ₈ Pt	C ₃₈ H ₃₂ F ₆ N ₈ O ₈ PtS ₂
fw	261.32	387.23	306.32	710.21	836.10	755.21	1015.87	1267.65	1039.62	1101.92
temp (K)	120	170	170	120.0	120.0	120.01(10)	170	170	120.00(10)	170.15
λ (Å)	0.71073	0.71073	0.71073	0.71073	0.71073	0.71073	0.71073	0.71073	0.71073	0.71073
cryst syst	monoclinic	monoclinic	triclinic	triclinic	monoclinic	triclinic	monoclinic	monoclinic	orthorhombic	triclinic
space group	P2 ₁ /n	P2 ₁ /n	P-1	P-1	P2 ₁ /n	P-1	C2/c	C2/c	Pbcn	P-1
<i>a</i> (Å)	8.4032(2)	10.1702(3)	10.4865(3)	9.2074(5)	8.9848(4)	10.2152(7)	23.5841(10)	22.0099(4)	16.6750(10)	8.9668(3)
<i>b</i> (Å)	9.4225(3)	15.1631(7)	11.5093(4)	9.2379(5)	17.1114(8)	10.3480(4)	10.0509(3)	11.6891(2)	14.4166(4)	9.5673(2)
<i>c</i> (Å)	17.6335(5)	10.8990(4)	12.7272(4)	12.4613(8)	13.3644(5)	10.5475(6)	18.4827(7)	18.0292(3)	15.3498(5)	12.7115(4)
<i>α</i> (°)	90	90	106.3640(10)	75.880(4)	90	78.053(4)	90	90	90	70.9280(10)
<i>β</i> (°)	96.235(3)	115.434(2)	90.718(2)	77.716(3)	103.754(4)	73.245(5)	120.9300(10)	120.9270(10)	90	88.4740(10)
<i>γ</i> (°)	90	90	98.779(2)	66.204(3)	90	67.650(5)	90	90	90	76.130(2)
<i>V</i> (Å ³)	1387.95(7)	1517.86(10)	1454.08(8)	932.68(10)	1995.77(15)	981.42(10)	3758.1(2)	3978.99(12)	3690.0(3)	999.00(5)
<i>Z</i>	4	4	4	2	4	2	4	4	4	1
ρ _{calc} (Mg/m ³)	1.251	1.694	1.399	2.529	2.783	2.556	1.795	2.116	1.871	1.832
μ(Kα) (mm ⁻¹)	0.076	2.106	0.096	10.834	11.675	38.238	3.929	5.265	6.030	3.708
No. reflns.	7077	16275	18033	11251	19229	10871	16911	27241	8462	20912
Unique reflns.	3753	4418	6617	4222	5606	4124	4475	5155	3964	5845
GOOF (F ²)	1.070	1.115	1.036	1.072	1.177	1.032	1.067	1.167	1.049	1.071
R _{int}	0.0216	0.0316	0.0346	0.0300	0.0363	0.0477	0.0443	0.0411	0.0328	0.0268
R1 ^a (<i>I</i> ≥ 2σ)	0.0504	0.0369	0.0576	0.0275	0.0443	0.0385	0.0353	0.0346	0.0349	0.0193
wR2 ^b (<i>I</i> ≥ 2σ)	0.1238	0.0783	0.1251	0.0571	0.0808	0.0958	0.0669	0.0637	0.0663	0.0451
CCDC number	1868987	1868988	1868989	1868990	1868993	1868999	1868991	1868994	1868992	1868996

^a R1 = Σ||*F*_o|| - ||*F*_c||/Σ|*F*_o|. ^b wR2 = [Σ[w(*F*_o² - *F*_c²)²]/Σ[w(*F*_o²)²]]^{1/2}.

Table S3 Selected bond lengths and angles for **1-10**

	1	2	3	4	5	6	[7]·(OTf)₂	[8]·(OTf)₂	[9]·Br₂	[10]·(OTf)₂
d(N3-C1) (Å)	1.4043(17)	1.402(4)	1.403(2)	1.418(6)	1.406(10)	1.408(10)	1.401(5)	1.398(5)	1.413(7)	1.408(2)
d(N3-C6) (Å)	1.4021(18)	1.400(4)	1.404(2)	1.388(6)	1.404(10)	1.392(11)	1.392(5)	1.415(5)	1.417(6)	1.409(2)
d(Pt1-N1) (Å)				2.039(4)	2.036(7)	2.047(6)	2.023(4)	2.010(3)	2.024(4)	2.0136(15)
d(Pt1-N2) (Å)				2.058(4)	2.044(6)	2.026(6)	2.014(4)	2.015(3)	2.011(4)	2.0135(15)
d(Pt1-I1) (Å)				2.5801(4)	2.5893(6)	2.5830(5)				
d(Pt1-I2) (Å)				2.5971(4)	2.5970(7)	2.5880(6)				
∠(C1-N3-C6) (°)	123.73(11)	123.6(2)	124.30(16)	119.4(4)	118.0(6)	119.1(7)	121.7(4)	119.5(3)	117.3(4)	117.73(15)
∠(N1-Pt1-N2) (°)				85.31(16)	85.2(3)	84.9(2)	85.81(14)	85.91(14)	86.67(17)	85.35(6)
∠(I1-Pt1-I2) (°)				91.811(14)	90.98(2)	91.878(19)				
∠(Py1-Py2) ^a (°)				50.9(2)	50.6(3)	53.5(3)	46.03(17)	52.86(15)	53.05(16)	55.66(6)

^a ∠(Py1-Py2) = dihedral angle between mean planes of the two pyridine rings of dpa ligands in platinum(II) complexes.

Table S4 Crystal data for **S2-S4**

	S2	S3	S4
empirical formula	C ₁₄ H ₁₀ N ₂ O ₄	C ₂₄ H ₂₀ BrN ₅ O ₄	C ₁₈ H ₁₄ Br ₂ N ₄ Pt
fw	270.24	522.36	641.24
temp (K)	123.00(10)	123.01(10)	120.00(10)
λ (Å)	0.71073	1.54184	0.71073
cryst syst	monoclinic	monoclinic	orthorhombic
space group	P2 ₁ /n	P2 ₁ /c	Pbca
<i>a</i> (Å)	3.6845(2)	8.23630(4)	13.1641(6)
<i>b</i> (Å)	14.3789(7)	14.82926(10)	15.8672(7)
<i>c</i> (Å)	11.4290(5)	18.24598(11)	17.2994(7)
α (°)	90	90	90
β (°)	95.990(5)	91.5826(5)	90
γ (°)	90	90	90
<i>V</i> (Å ³)	602.20(5)	2227.68(2)	3613.5(3)
<i>Z</i>	2	4	8
ρ_{calc} (Mg/m ³)	1.490	1.557	2.357
μ (K α) (mm ⁻¹)	0.939	2.882	12.198
No. reflns.	2797	31951	8088
Unique reflns.	1262	4685	3414
GOOF (F ²)	1.090	1.047	0.980
R _{int}	0.0241	0.0223	0.0366
R1 ^a ($I \geq 2\sigma$)	0.0445	0.0253	0.0289
wR2 ^b ($I \geq 2\sigma$)	0.1142	0.0655	0.0411
CCDC number	1868998	1868997	1868995

^a R1 = $\sum ||F_o| - |F_c|| / \sum |F_o|$. ^b wR2 = $[\sum [w(F_o^2 - F_c^2)^2] / \sum [w(F_o^2)^2]]^{1/2}$.

S7. Cited literature

- 1 B. Antonioli, D. J. Bray, J. K. Clegg, K. Gloe, K. Gloe, O. Kataeva, L. F. Lindoy, J. C. McMurtrie, P. J. Steel, C. J. Sumby and M. Wenzel, *Dalton Trans.*, 2006, 4783–4794.
- 2 L. Shi, Y. Liu, Q. Liu, B. Wei and G. Zhang, *Green Chem.*, 2012, **14**, 1372–1375.
- 3 A. Blanc and C. G. Bochet, *J. Org. Chem.*, 2003, **68**, 1138–1141.
- 4 S. Licciulli, I. Thapa, K. Albahily, I. Korobkov, S. Gambarotta, R. Duchateau, R. Chevalier and K. Schuhem, *Angew. Chem. Int. Ed.*, 2010, **49**, 9225–9228.
- 5 J. H. D. Bowen, E. J.; Eland, *Proc. Chem. Soc.*, 1963, **0**, 202.
- 6 V. M. Clark, A. Cox and E. J. Herbert, *J. Chem. Soc. C*, 1968, 831–833.
- 7 J. D. Cocker, G. I. Gregory and G. B. Webb, Br. Pat., GB 1262864, 1972.